ROCKETDYNE
A DIVISION OF NORTH AMERICAN AVIATION, INC
6633 CANOGA AVENUE, CANOGA PARK, CALIFORNIA

R-6288

# AN INSTRUMENTATION SYSTEM TO STUDY ROCKET EXHAUST PLUME RADIATIVE PROCESSES

FINAL REPORT

Contract NAS8-11261
G.O. 8620

**PREPARED BY**
Physics Group
Rocketdyne Research

**APPROVED BY**
J. E. Witherspoon
Chief
Physics, Mathematics & Measurements

NO OF PAGES 125 plus vii **REVISIONS** DATE 27 August 1965

| DATE | REV BY | PAGES AFFECTED | REMARKS |
|---|---|---|---|
| | | | |
| | | | |
| | | | |

FORM R18-G REV. 4-64

## FOREWORD

This final report was prepared by W. F. Herget, P. E. Schumacher, J. D. Enloe, B. P. Levin, and E. Suarez-Alfonso of the Radiation Physics Group of the Rocketdyne Research Department in fulfillment of the requirements of contract number NAS8-11261. The authors wish to acknowledge the assistance of A. G. DeBell, C. I. Bright, Q. S. Anderson, R. K. Hales, V. F. Olson, and B. Rosen in this program.

## ABSTRACT

The research, development, and modification of an instrumentation system to study processes affecting radiative heat transfer from the exhaust plumes of rockets utilizing $LO_2$/RP-1 propellants is reported. The instrumentation system is applicable to the study of the formation and distribution of carbonaceous radiative emitters and the location and progress of the exhaust afterburning. The principal components of the system are the model rocket motor with its associated hardware and instrumentation, the specially modified infrared spatially scanning spectroradiometer, the exhaust plume sampling probe, and the ultraviolet instrumentation, which includes the ultraviolet photographic pyrometer and the telespectrograph. The description of each of the major components of the system is accompanied by a discussion of the principles of their operation, an evaluation of their performance, examples of the results obtained, and recommendations for improvement. Applications of the instrumentation system to the study of radiative processes in rocket exhausts are discussed.

TABLE OF CONTENTS

# ILLUSTRATIONS

# INTRODUCTION

An important requirement in the design of space vehicles is the prediction of the thermal radiation from the rocket exhaust plume to external missile components.

The most accurate method for estimating the thermal radiation from the rocket exhaust plume considers the thermodynamic states and radiative properties of the several emitting species as a function of position in the plume. Consequently, for an accurate calculation of plume radiation the contribution from every infinitesimal volume of gas in the exhaust plume must be taken into consideration. This requires knowledge of the spatial distribution of pressure, temperature, and concentration of species throughout the plume, and the radiative properties of the emitting species, such as the spectral absorption coefficients.

The principal emitters in the exhaust of rocket engines utilizing liquid oxygen/RP-1 propellants, such as the F-1 engine, are water vapor, carbon dioxide, and carbon particles (Ref. 1). Of these emitters, carbon is the most important from the standpoint of thermal radiation. The radiation from carbon particles is an intense continuum, in contrast to the discrete band radiation from gaseous emitters; this is demonstrated in Figures 1 and 2, (Ref. 2) which show the spectral radiance from the gaseous exhaust of a 1000-pound-thrust rocket engine burning liquid oxygen/ethanol and from the two-phase exhaust of the same engine burning liquid oxygen/RP-1. The difference in level between the two curves (Fig. 1 and 2) can be attributed almost exclusively to the carbon particle radiation.

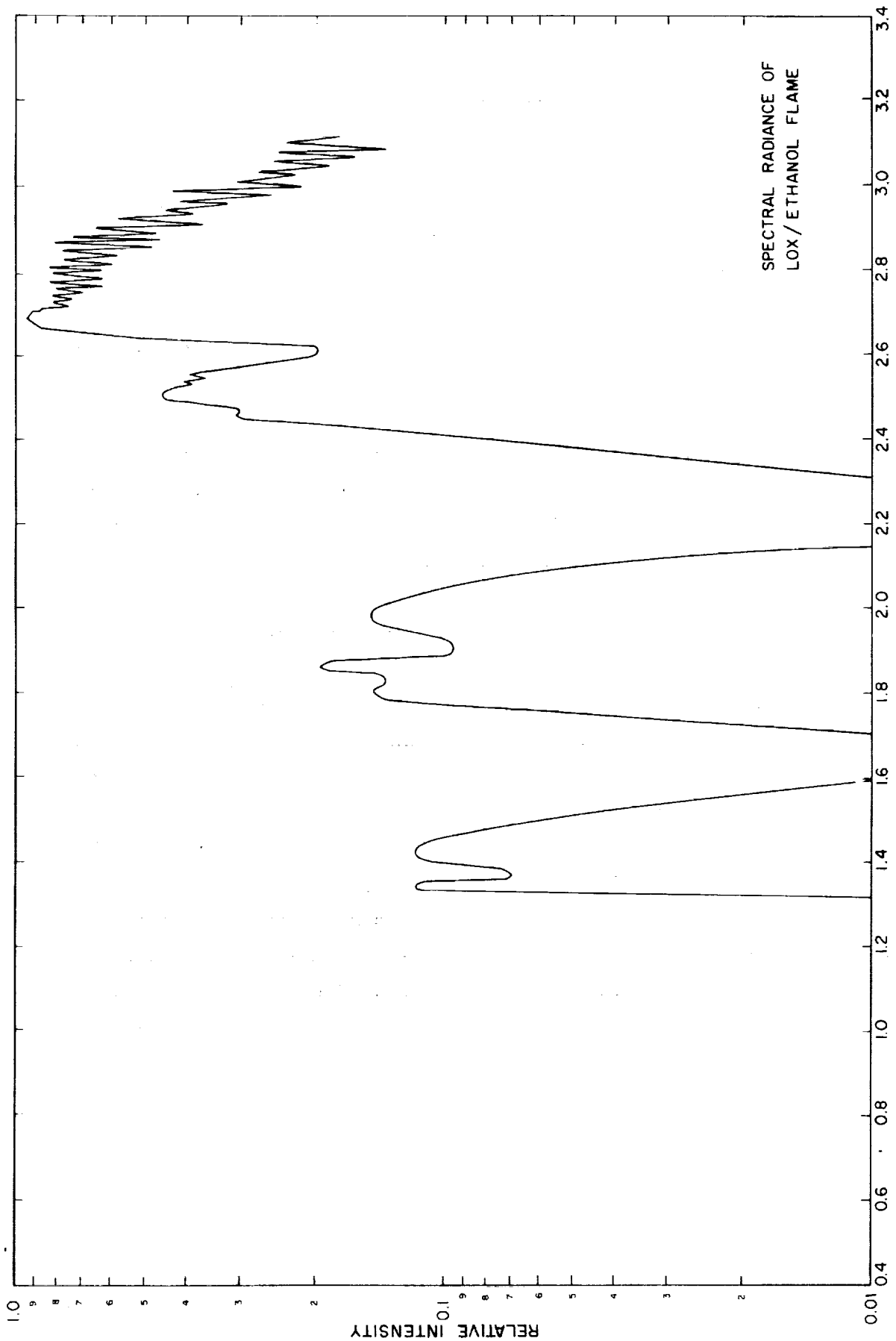


Figure 1. Spectral Radiance of $LO_2$/Ethanol Flame

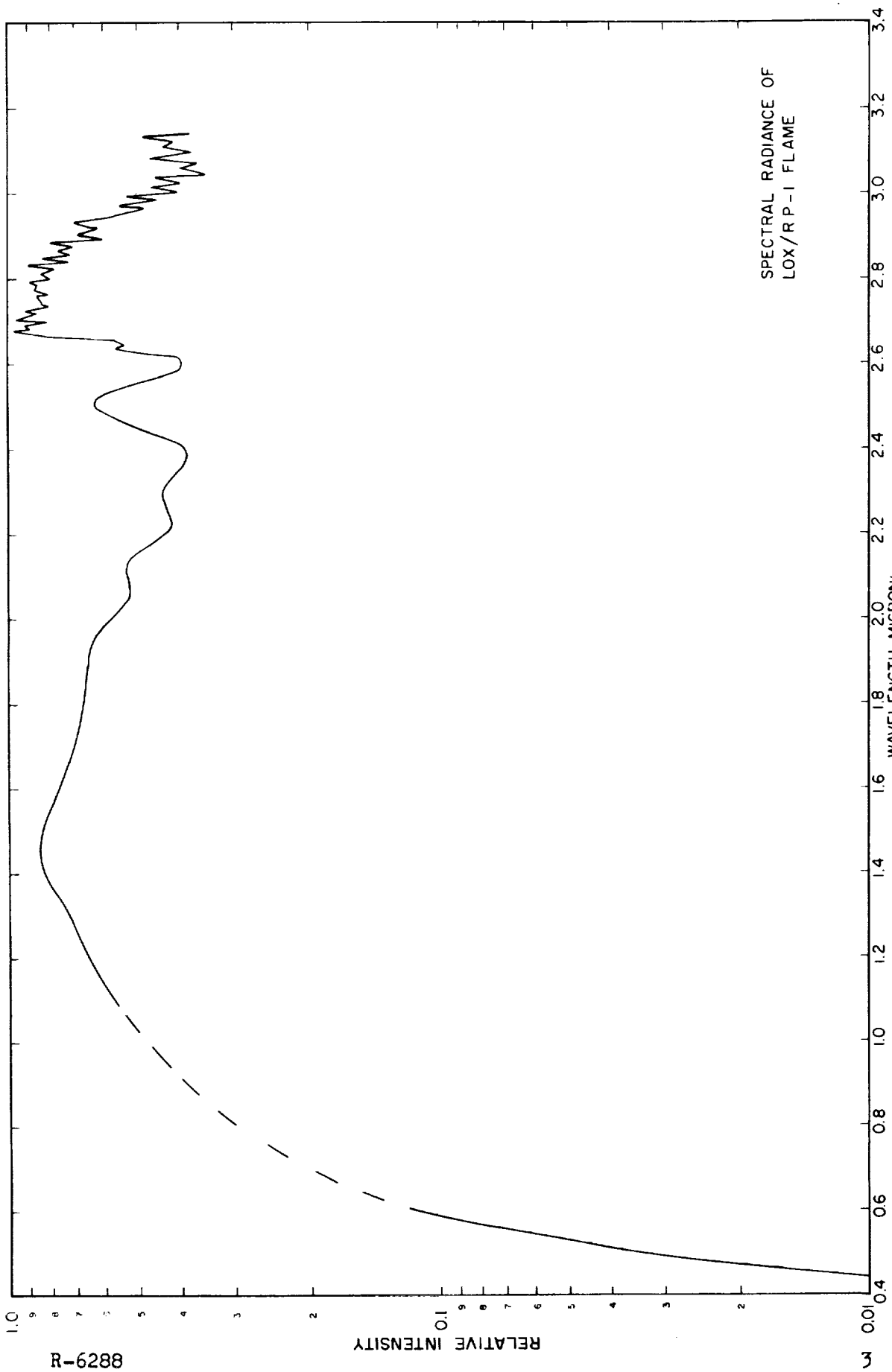


Figure 2. Spectral Radiance of $LO_2$/RP-1 Flame

In the lower altitude regimes, where atmospheric oxygen is plentiful, a vigorous afterburning of the combustible reaction products results in a mantle which surrounds the plume and is approximately 400°K hotter than the exhaust core. Experimental studies (Refs. 2, 3) have demonstrated that this mantle is responsible for most of the radiant flux from single exhaust plumes. As the vehicle ascends and the ambient pressure decreases, the expansion of the plume results in an increase in the configuration factor for the transfer from the afterburning mantle to the base plate. At higher altitudes the afterburning contributes significantly to the thermal environment of the base plate owing to the enormous solid angle through which the base plate is irradiated.

The Physics Group of Rocketdyne Research is presently engaged in a continuing experimental investigation of the properties of carbonaceous radiative emitters and the afterburning phenomena in the exhausts of rocket engines utilizing liquid oxygen/RP-1 propellants.

The objective of this program is to study, assess, and understand the role of carbon as a thermal radiator and the geometry, location, and progress of afterburning phenomena in the exhaust plume of rocket engines, such as the F-1.

The investigation of the afterburning and the radiative properties of carbon in rocket exhausts can be conveniently organized into the following chronological sequence:

1. The design and development of instrumentation including radiometric equipment, exhaust sampling system, and rocket motor testing apparatus.
2. Rocket motor test firings to acquire radiometric and sampling

data on the exhaust radiative properties.

3. Analysis and tabulation of the radiative properties obtained from the data and the testing of these radiative properties in a heat transfer prediction model.
4. Continued work on the design and performance of new experiments as required by the knowledge gained in the preceding phases.

This report describes the preliminary effort of this combined study, that is, the development and construction and checkout of the instrumentation system which is to be used in the main, scientific part of the program. In addition some of the radiometric techniques which are to be used in the scientific study are described.

## FUNCTIONS OF THE INSTRUMENTATION SYSTEM

Although the exact mechanism for the formation of carbon is not understood, in general, it is agreed that the carbon is generated in the degradation of vaporized fuel pockets. In the case of typical rocket engines which use a fuel-rich region near the chamber walls for cooling purposes, it is postulated that most of the carbon is generated near the chamber wall. The quantity of carbon generated in the combustion of liquid oxygen/RP-1 propellants is expected to depend on the overall propellant mixture ratio, the distribution of the propellant mixture ratio across the face of the injector, and the atomizing and mixing efficiency of the injector. Some controversy exists as to the mechanism involved in establishing the particle size; however, it is expected that this is determined mainly by the chamber pressure and possibly by the chamber "stay time", L*.

In view of these considerations the instrumentation system has included a complete capability to operate a model F-1 thrust chamber at actual chamber pressures and provisions for varying significant motor operating parameters. With this arrangement the effect of the various motor operating parameters on both the afterburning and the carbon formation and distribution can be studied.

In addition to operating the model motor, the remaining functions of the instrumentation system consist of the following:

1. To determine the radial temperature and emissivity gradients in the exhaust of the F-1 model motor. This is to be accomplished by radiation measurements along parallel chordal

optical paths in various planes parallel to the nozzle exit plane. Such radiation measurements offer the only means of examining plume structure with no perturbation of the flow field by the measuring apparatus.

2. To determine, by direct sampling of the exhaust, the number density, particle size distribution, and relative mass concentration of the carbon particles in the exhaust of the F-1 model motor.
3. To study the location, geometry, and progress of the afterburning by monitoring the ultraviolet emission from the OH molecule in the exhaust. This involves both photographic pyrometry and high-resolution spectrographic techniques.

# DESCRIPTION AND EVALUATION OF INSTRUMENTATION SYSTEM

## ROCKET MOTOR AND ASSOCIATED SYSTEMS

The extensive instrumentation system designed for this program includes rocket motors capable of operating at F-1 chamber pressures. Among the associated rocket motor control systems are high-pressure fuel, oxidizer, and coolant systems; pneumatic systems; electronic sensing, recording and control systems; and the necessary test and calibration systems. Since most of these systems were located at Rocketdyne's Plume Studies Laboratory, it was decided to modify this laboratory for the specific requirements of this program. This required the installation of high-pressure fuel and oxidizer systems, the modification of an existing coolant system for operation at higher pressures, and minor modifications to the existing electronic and pneumatic systems.

The arrangement of the propellant and pneumatic systems is shown in Figs. 3-6, Rocketdyne drawings 5409-3 through -6, respectively. It consists basically of two oxidizer systems, two fuel systems, a coolant system, and the necessary pneumatic systems to control laboratory operations, including the various purges to spectroscopic equipment. Each system is fully instrumented, not only to establish the operation of the rocket motor and associated hardware, but also to detect any system fluctuations which may affect the recorded spectroscopic and gas sampling data. The required modifications to the Plume Studies Laboratory were completed and the rocket motor and associated systems were evaluated prior to firing to gather spectroscopic and gas sampling data.

F1

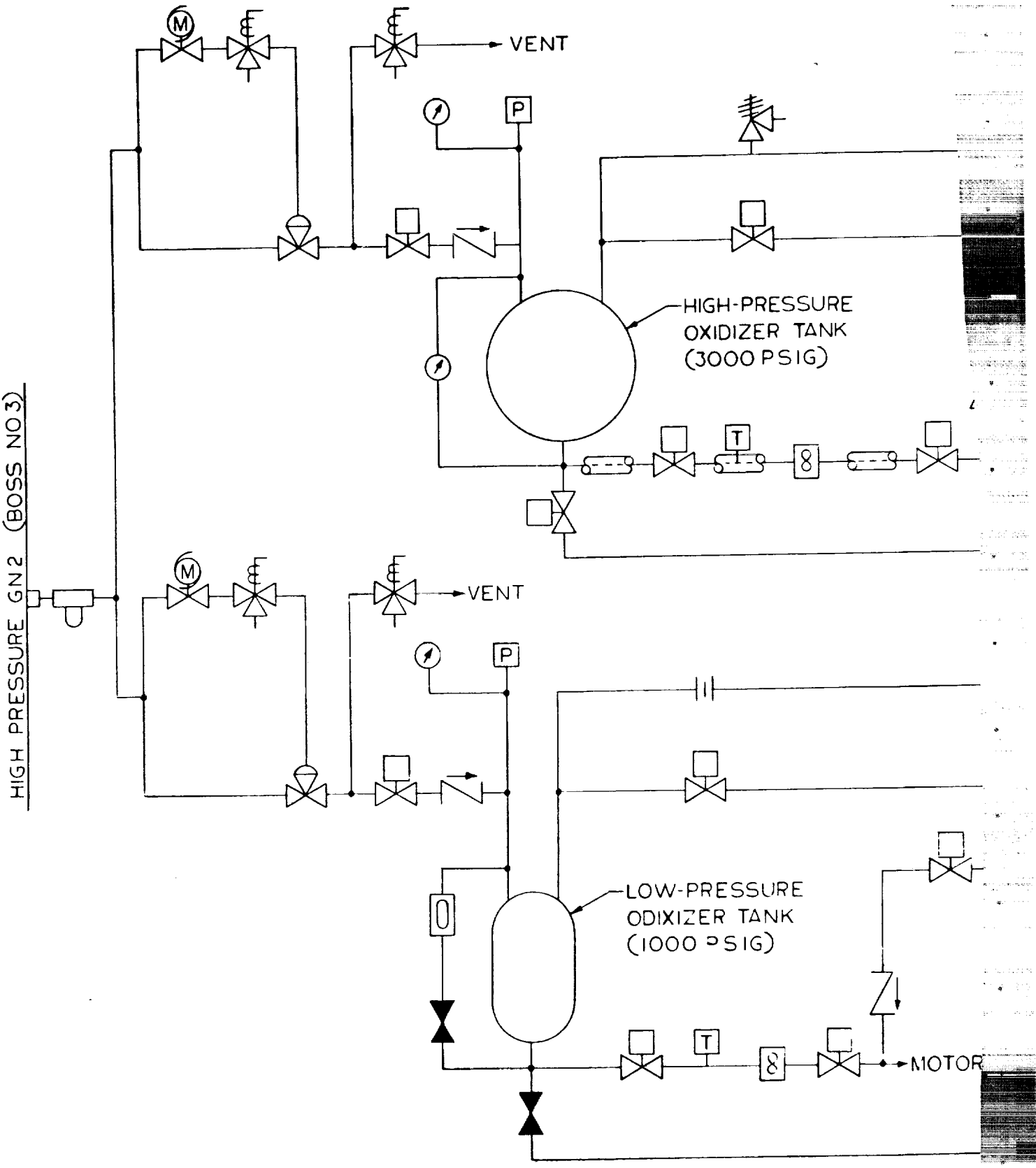
VENT
P
HIGH-PRESSURE
OXIDIZER TANK
(3000 PSIG)
T
HIGH PRESSURE GN2 (BOSS NO 3)
VENT
P
LOW-PRESSURE
ODIXIZER TANK
(1000 PSIG)
T
MOTOR

F2

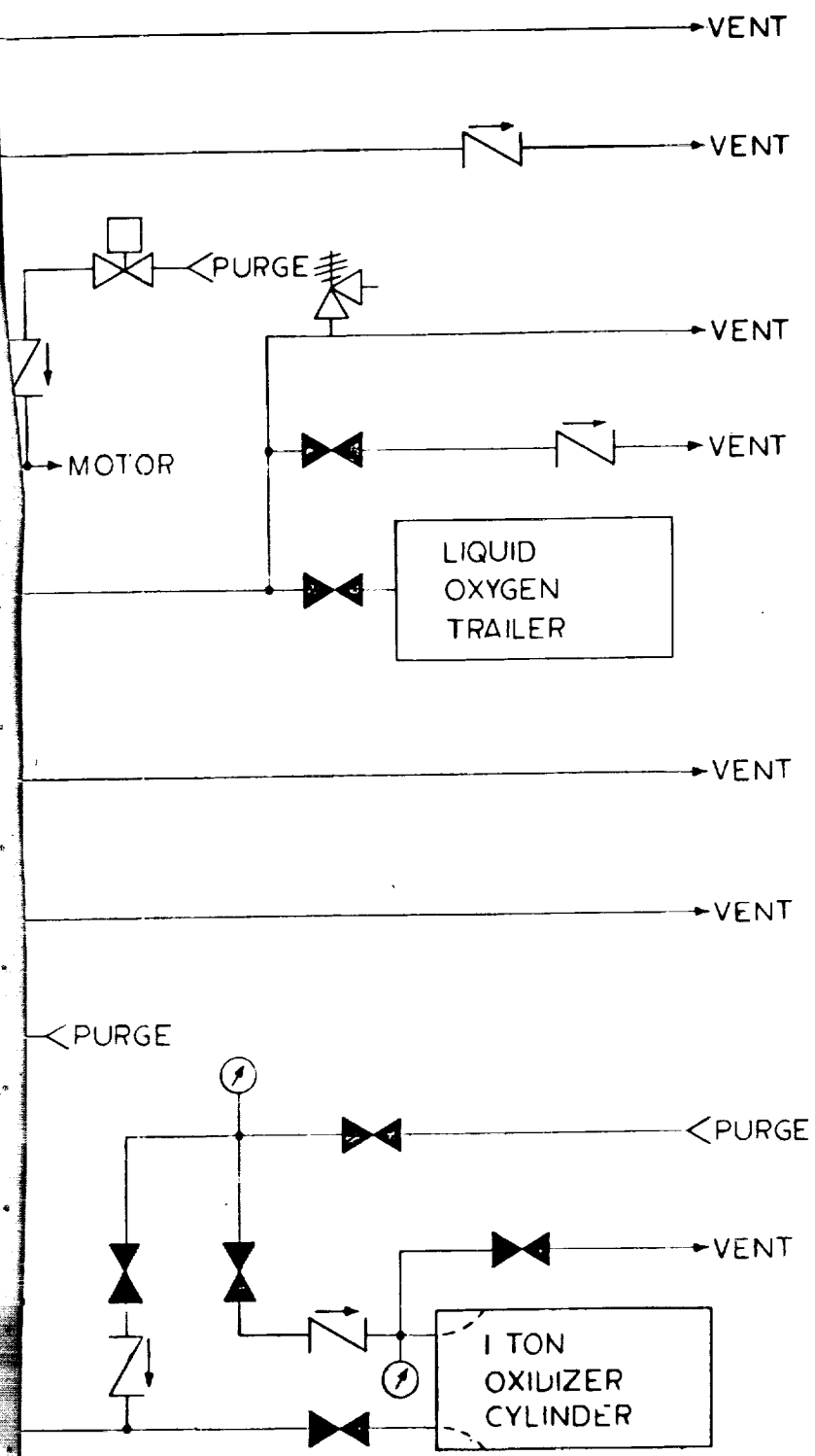


LEGEND

- SERVO VALVE
- HAND REGULATOR
- BUTTERFLY VALVE
- BALL VALVE, MANUAL
- NEEDLE VALVE, MANUAL
- GATE VALVE, MANUAL
- GLOBE VALVE, MANUAL
- PRESSURE REGULATING VALVE
- COCK OR PLUG VALVE
- SLEEVE VALVE
- CYLINDER-OPERATED VALVE
- MOTOR OPERATED VALVE
- SOLENOID VALVE
- CHECK VALVE, BALL, SWING OR LIFT
- RELIEF VALVE
- THREE-WAY VALVE (HAND LEVER SH
- FOUR-WAY VALVE (SOLENOID SHOWI
- HOSE VALVE
- SCREWED CAP
- LINE STRAINER, 50 MESH AND LARGE
- FILTER, 300 MICRON OR LESS (INLINE, T,
- EXPANSION JOINT, SLIDING TYPE
- BELLOWS JOINT, EXPANSION, HINGED OR I
- FLEXIBLE HOSE
- BURST DISC
- ORIFICE FLANGE
- PUMP CENTRIFUGAL
- HEAT EXCHANGER
- GAUGE
- BLIND FLANGE
- CROSSING LINES
- CONNECTING LINES
- FLOWMETER, TURBINE
- FLOW STRAIGHTENER
- JACKETED LINE
- INSULATED LINE
- BOSS, A.N.D.
- BOSS, SPECIAL PURPOSE
- "FRANTZ" TYPE SCREEN
- FLOWMETER, INDICATE TYPE
- PUMP, PISTON (INDICATE "VACUUM" IF APPL
- PUMP ROTARY (INDICATE "VACUUM" IF APP
- SIGHT GLASS

| | | |
|---|---|---|
| DFMN | GUTHRIE | 9-27-64 |
| CK | E. SUAREZ | 10/5/64 |
| DES | E SUAREZ | 10/5/64 |
| SUP | [illegible] | 10-5-64 |

ROCKETDYNE
A DIVISION OF NORTH AMERICAN AVIATION, I
CANOGA PARK, CALIFORNIA

FIELD LABORATORY SCHEMATIC

FLAME STUDY LABORAT
OXIDIZER SYSTEMS

| CODE IDENT NO. | SIZE | |
|---|---|---|
| FIG. 3 | D | 5409-3 |
| SCALE | | SHEET 1 |

FOLDOUT FRAME 2

L UNLESS OTHERWISE SPECIFIED

F2

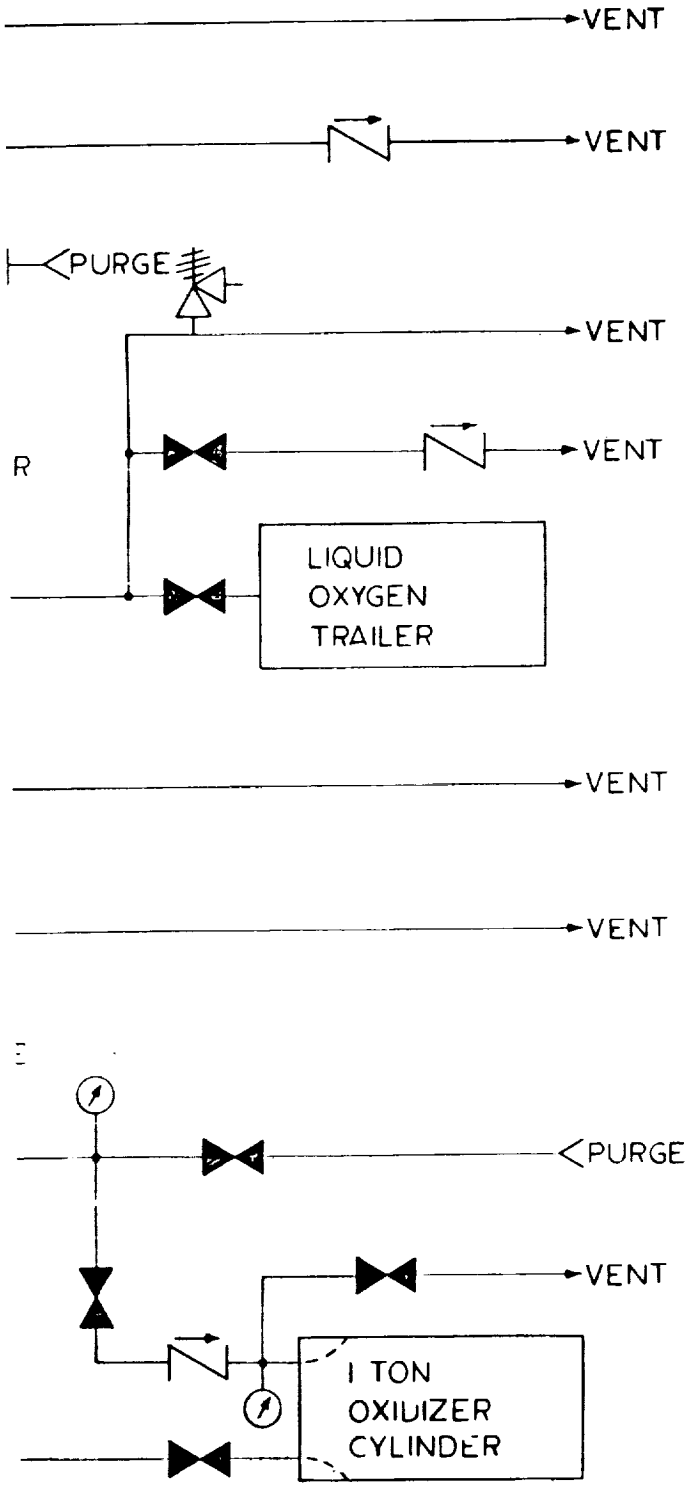


LEGEND

- SERVO VALVE
- HAND REGULATOR
- BUTTERFLY VALVE
- BALL VALVE, MANUAL
- NEEDLE VALVE, MANUAL
- GATE VALVE, MANUAL
- GLOBE VALVE, MANUAL
- PRESSURE REGULATING VALVE
- COCK OR PLUG VALVE
- SLEEVE VALVE
- CYLINDER-OPERATED VALVE
- MOTOR OPERATED VALVE
- SOLENOID VALVE
- CHECK VALVE, BALL, SWING OR LIFT
- RELIEF VALVE
- THREE-WAY VALVE (HAND LEVER SHOWN)
- FOUR-WAY VALVE (SOLENOID SHOWN)
- HOSE VALVE
- SCREWED CAP
- LINE STRAINER, 50 MESH AND LARGER
- FILTER, 300 MICRON OR LESS (INLINE, T, OR OFFSET)
- EXPANSION JOINT, SLIDING TYPE
- BELLOWS JOINT, EXPANSION, HINGED OR BELLOWS
- FLEXIBLE HOSE
- BURST DISC
- ORIFICE FLANGE
- PUMP CENTRIFUGAL
- HEAT EXCHANGER
- GAUGE
- BF BLIND FLANGE
- CROSSING LINES
- CONNECTING LINES
- FLOWMETER, TURBINE
- FLOW STRAIGHTENER
- JACKETED LINE
- INSULATED LINE
- BOSS, A.N.D.
- BOSS, SPECIAL PURPOSE
- "FRANTZ" TYPE SCREEN
- F/M FLOWMETER, INDICATE TYPE
- PUMP, PISTON (INDICATE "VACUUM" IF APPLICABLE)
- PUMP ROTARY (INDICATE "VACUUM" IF APPLICABLE)
- SIGHT GLASS

| | | |
|---|---|---|
| DFMN | GUTHRIE | 9-27-64 |
| CK | E. SUAREZ | 10/5/64 |
| DES | E SUAREZ | 10/5/64 |
| SUP | [illegible] | 10-5-64 |

ROCKETDYNE
A DIVISION OF NORTH AMERICAN AVIATION, INC.
CANOGA PARK, CALIFORNIA

FIELD LABORATORY SCHEMATIC

FLAME STUDY LABORATORY
OXIDIZER SYSTEMS

| CODE IDENT NO. | SIZE | |
|---|---|---|
| FIG. 3 | D | 5409-3 |

SCALE | SHEET 1 OF 4

FOLDOUT FRAME 3

IF SPECIFIED

FORM 606-A-21 NEW 8-6

5409-3

B1

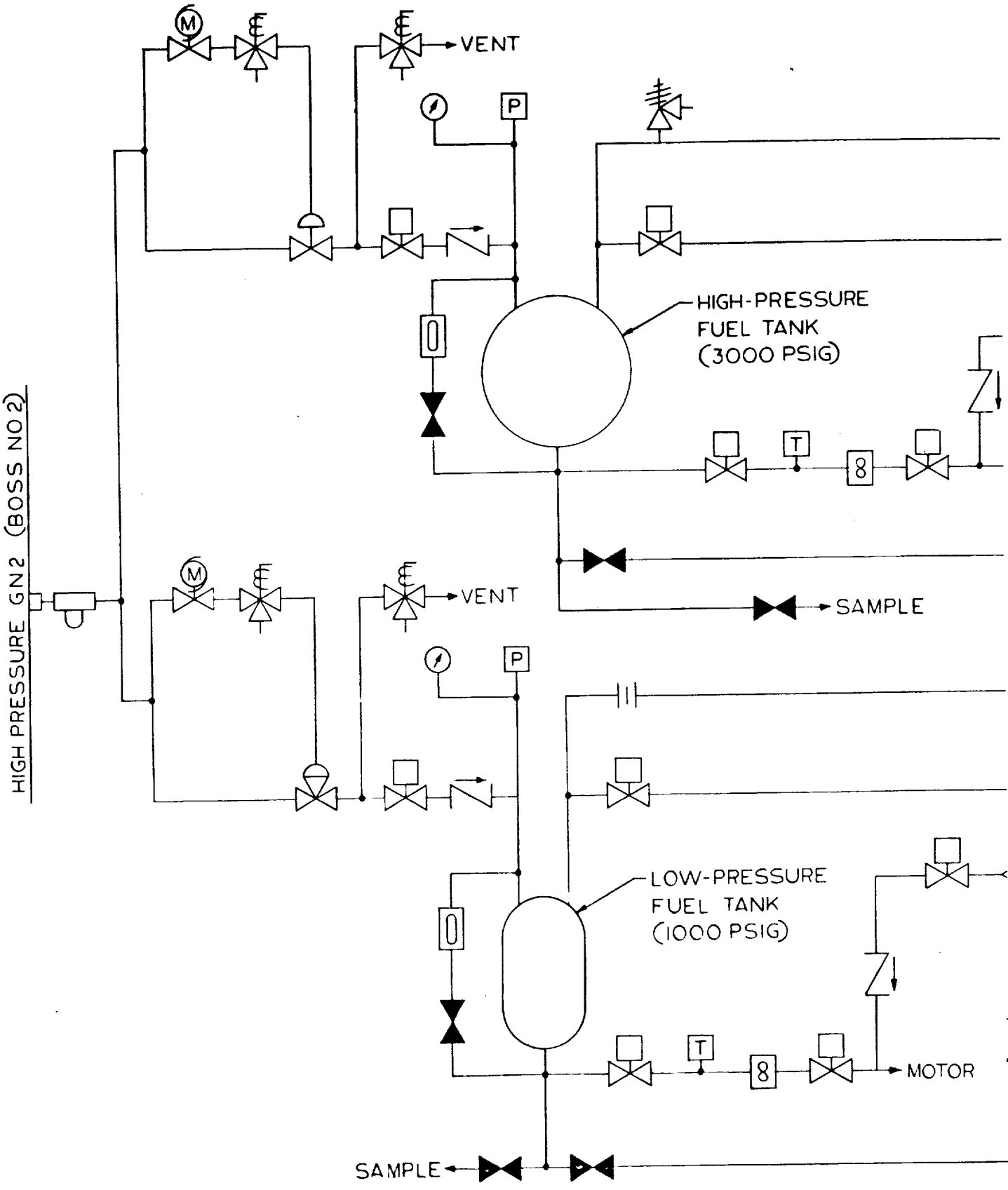




FOLDOUT FRAME 1

R-6288

B1

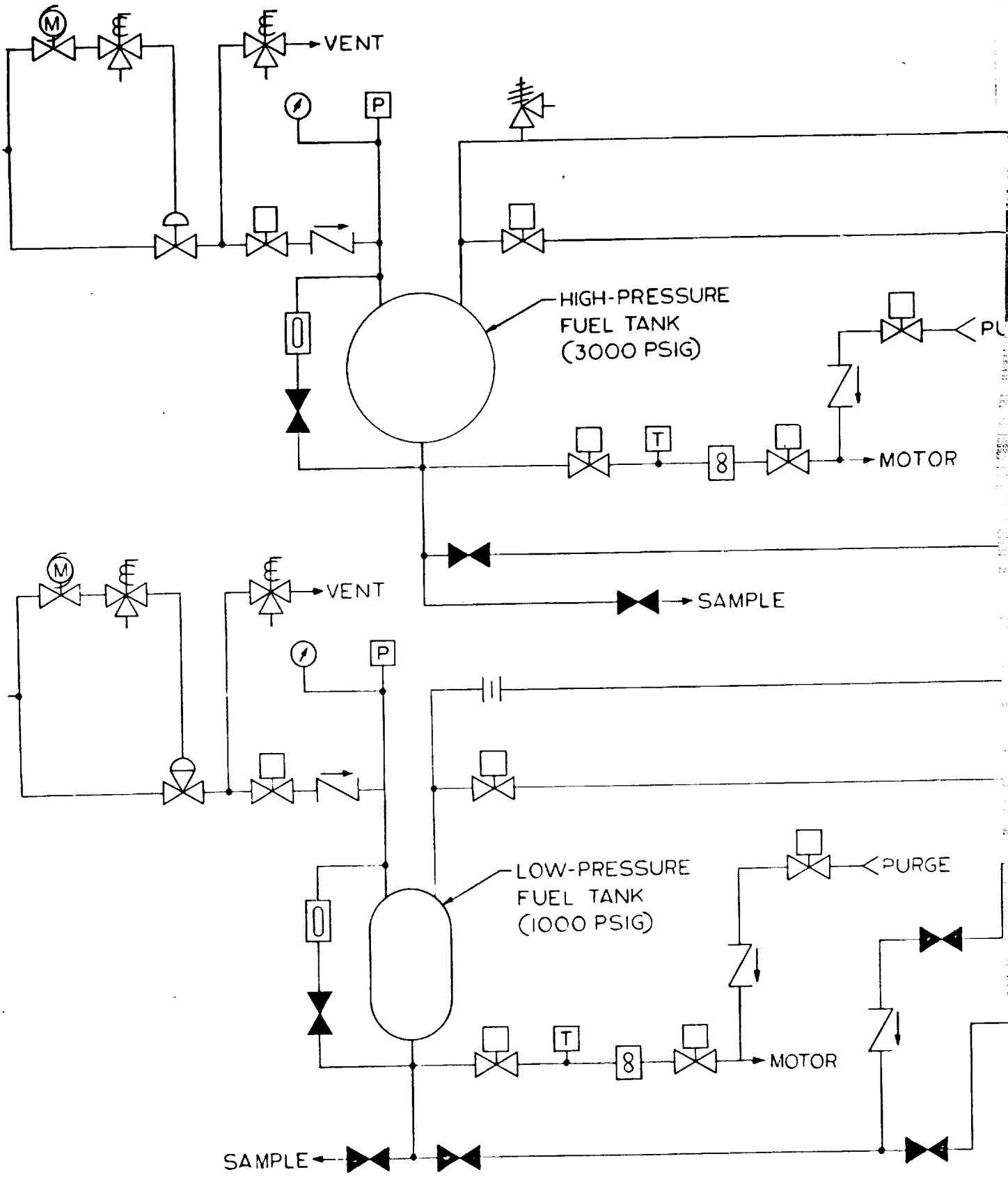


FOLDOUT FRAME 2

R-6288

NOTE: UNLESS OTHERWISE SPECIFIE

B 2

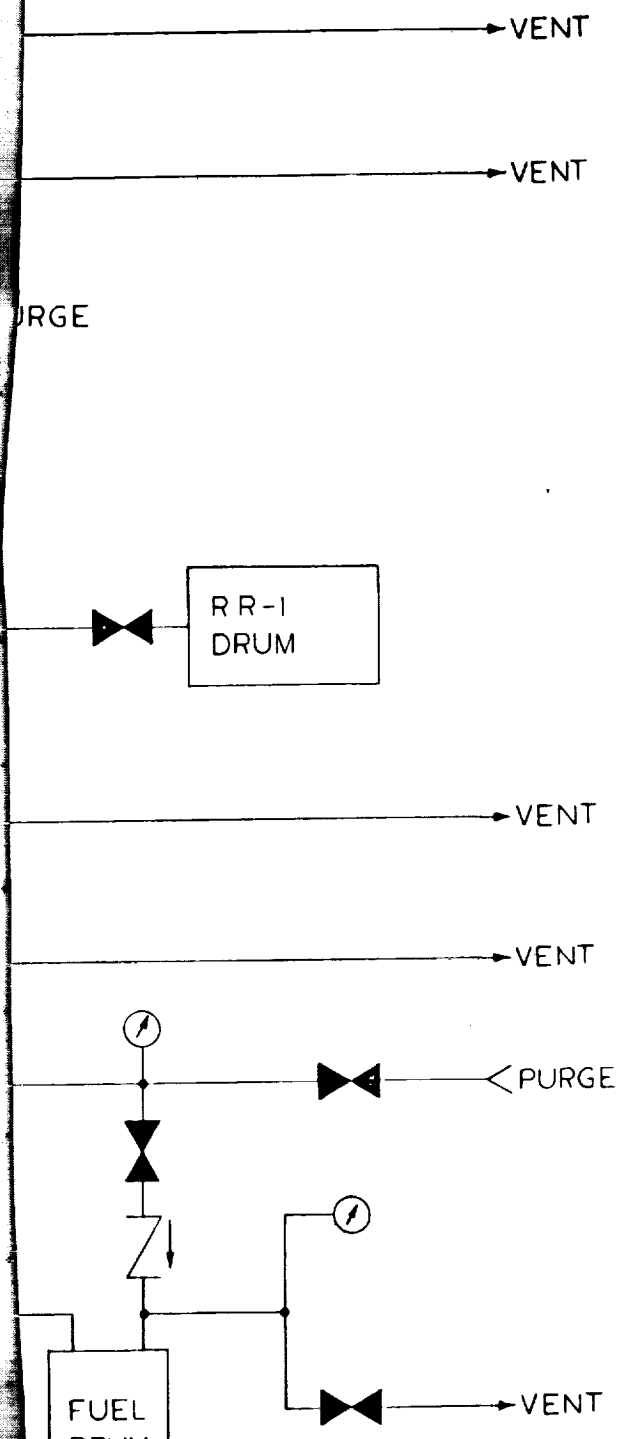


**LEGEND**

- SERVO VALVE
- HAND REGULATOR
- BUTTERFLY VALVE
- BALL VALVE, MANUAL
- NEEDLE VALVE, MANUAL
- GATE VALVE, MANUAL
- GLOBE VALVE, MANUAL
- PRESSURE REGULATING VALVE
- COCK OR PLUG VALVE
- SLEEVE VALVE
- CYLINDER-OPERATED VALVE
- MOTOR OPERATED VALVE
- SOLENOID VALVE
- CHECK VALVE, BALL, SWING OR LIFT
- RELIEF VALVE
- THREE-WAY VALVE (HAND LEVER SHOWN)
- FOUR-WAY VALVE (SOLENOID SHOWN)
- HOSE VALVE
- SCREWED CAP
- LINE STRAINER, 50 MESH AND LARGER
- FILTER, 300 MICRON OR LESS (INLINE, T, OR OFFSET)
- EXPANSION JOINT, SLIDING TYPE
- BELLOWS JOINT, EXPANSION, HINGED OR BELLOWS
- FLEXIBLE HOSE
- BURST DISC
- ORIFICE FLANGE
- PUMP CENTRIFUGAL
- HEAT EXCHANGER
- GAUGE
- BF — BLIND FLANGE
- CROSSING LINES
- CONNECTING LINES
- FLOWMETER, TURBINE
- FLOW STRAIGHTENER
- JACKETED LINE
- INSULATED LINE
- BOSS, A.N.D
- BOSS, SPECIAL PURPOSE
- "FRANTZ" TYPE SCREEN
- F/M — FLOWMETER, INDICATE TYPE
- PUMP, PISTON (INDICATE "VACUUM" IF APPLICABLE)
- PUMP ROTARY (INDICATE "VACUUM" IF APPLICABLE)
- SIGHT GLASS

| | | |
|---|---|---|
| DFMN | GUTHRIE | 9/28/64 |
| CK | E. SUAREZ | 10/5/64 |
| DES | E. SUAREZ | 10/5/64 |
| SUP | [signature] | 10-5-64 |

ROCKETDYNE
A DIVISION OF NORTH AMERICAN AVIATION, INC.
CANOGA PARK, CALIFORNIA

FIELD LABORATORY SCHEMATIC

FLAME STUDY LABORATORY
FUEL SYSTEMS

| CODE IDENT NO. | SIZE | |
|---|---|---|
| FIG. 4 | D | 5409-4 |
| SCALE | | SHEET 2 OF 4 |

FORM 606-A-21 NEW 6-64

5409-4

FOLDOUT FRAME 3

F1

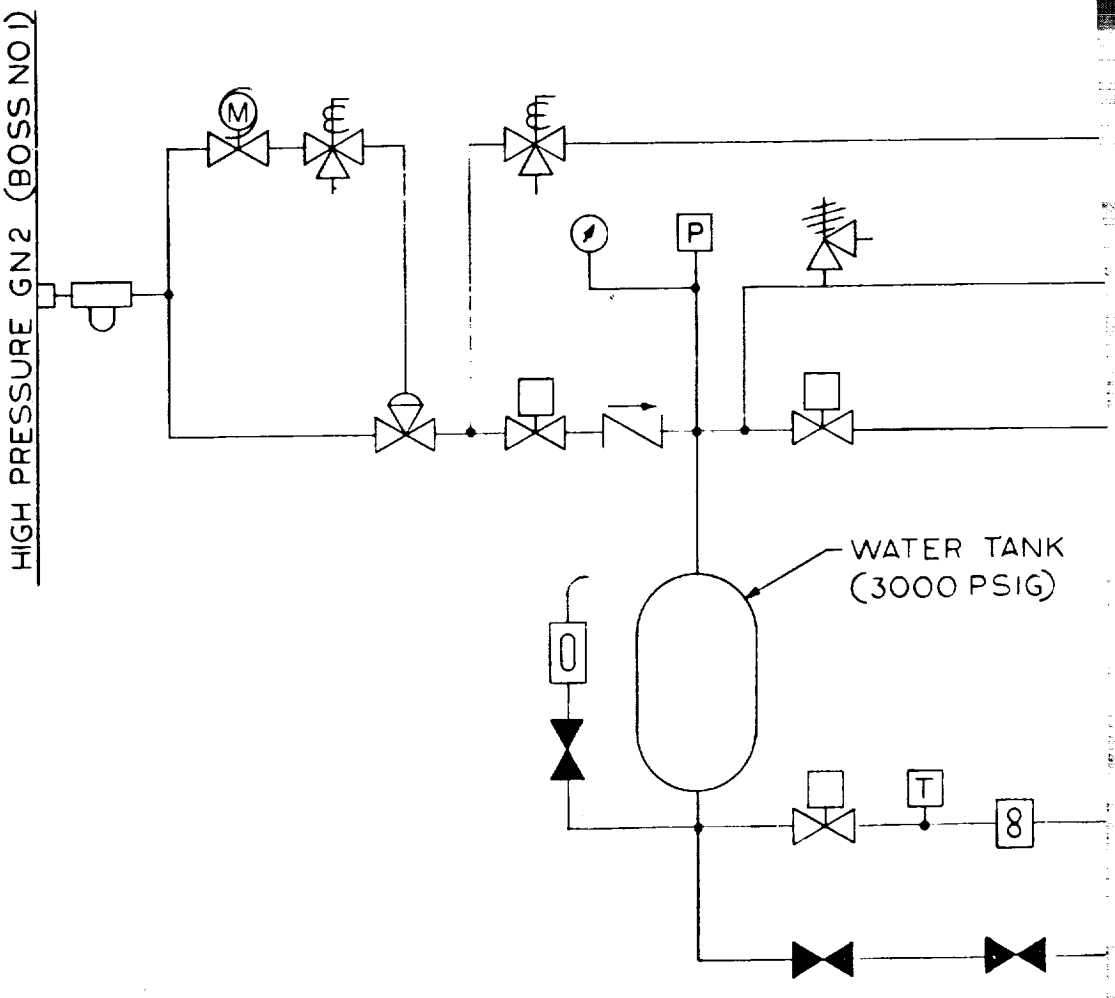

F2

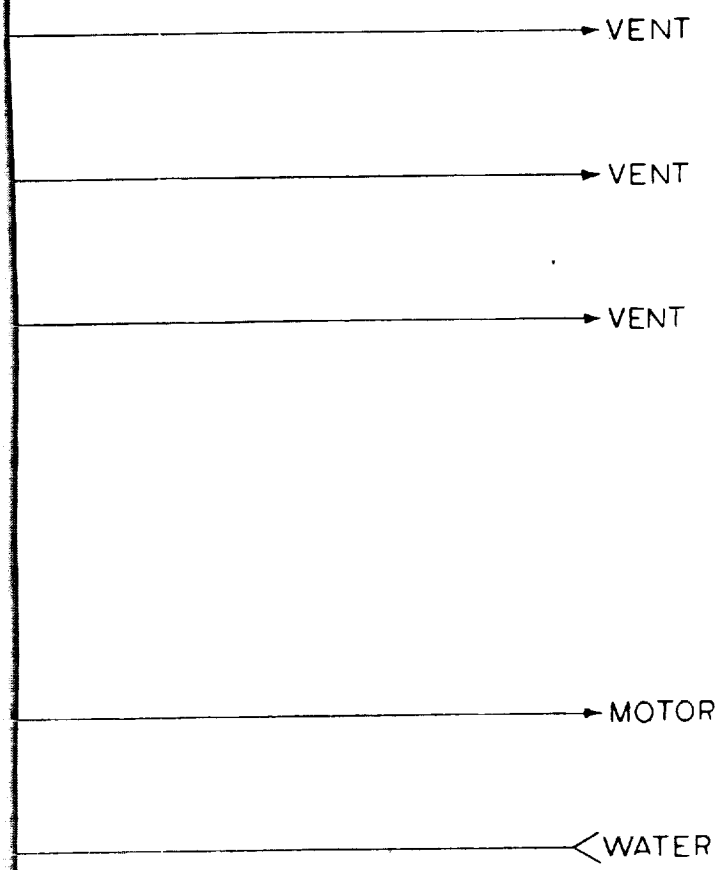


LEGEND

- SERVO VALVE
- HAND REGULATOR
- BUTTERFLY VALVE
- BALL VALVE, MANUAL
- NEEDLE VALVE, MANUAL
- GATE VALVE, MANUAL
- GLOBE VALVE, MANUAL
- PRESSURE REGULATING VALVE
- COCK OR PLUG VALVE
- SLEEVE VALVE
- CYLINDER-OPERATED VALVE
- MOTOR OPERATED VALVE
- SOLENOID VALVE
- CHECK VALVE, BALL, SWING OR
- RELIEF VALVE
- THREE-WAY VALVE (HAND LEV
- FOUR-WAY VALVE (SOLENOID
- HOSE VALVE
- SCREWED CAP
- LINE STRAINER, 50 MESH AND
- FILTER, 300 MICRON OR LESS (INL
- EXPANSION JOINT, SLIDING TYPE
- BELLOWS JOINT, EXPANSION, HINGE
- FLEXIBLE HOSE
- BURST DISC
- ORIFICE FLANGE
- PUMP CENTRIFUGAL
- HEAT EXCHANGER
- GAUGE
- BF BLIND FLANGE
- CROSSING LINES
- CONNECTING LINES
- FLOWMETER, TURBINE
- FLOW STRAIGHTENER
- JACKETED LINE
- INSULATED LINE
- BOSS, A.N.O.
- BOSS, SPECIAL PURPOSE
- "FRANTZ" TYPE SCREEN
- F/M FLOWMETER, INDICATE TYPE
- PUMP, PISTON (INDICATE "VACUUM"
- PUMP ROTARY (INDICATE "VACUUM
- SIGHT GLASS

| | | |
|---|---|---|
| DFMN | GUTHRIE | 9/30/64 |
| CK | E. SUAREZ | 10/5/64 |
| DES | E. SUAREZ | 10/5/64 |
| SUP | [signature] | 10-5-64 |

ROCKETDY
A DIVISION OF NORTH AMERICAN AVIAT
CANOGA PARK, CALIFORNIA

FIELD LABORATORY SCHEMA

FLAME STUDY LABO
MOTOR COOLING SY

| CODE IDENT NO. | SIZE | |
|---|---|---|
| FIG. 5 | D | 5409-5 |

SCALE

FOLDOUT FRAME 2

TE, UNLESS OTHERWISE SPECIFIED

F2

VENT

VENT

VENT

MOTOR

WATER

LEGEND

- SERVO VALVE
- HAND REGULATOR
- BUTTERFLY VALVE
- BALL VALVE, MANUAL
- NEEDLE VALVE, MANUAL
- GATE VALVE, MANUAL
- GLOBE VALVE, MANUAL
- PRESSURE REGULATING VALVE
- COCK OR PLUG VALVE
- SLEEVE VALVE
- CYLINDER-OPERATED VALVE
- MOTOR OPERATED VALVE
- SOLENOID VALVE
- CHECK VALVE, BALL, SWING OR LIFT
- RELIEF VALVE
- THREE-WAY VALVE (HAND LEVER SHOWN)
- FOUR-WAY VALVE (SOLENOID SHOWN)
- HOSE VALVE
- SCREWED CAP
- LINE STRAINER, 50 MESH AND LARGER
- FILTER, 300 MICRON OR LESS (INLINE, T, OR OFFSET)
- EXPANSION JOINT, SLIDING TYPE
- BELLOWS JOINT, EXPANSION, HINGED OR BELLOWS
- FLEXIBLE HOSE
- BURST DISC
- ORIFICE FLANGE
- PUMP CENTRIFUGAL
- HEAT EXCHANGER
- GAUGE
- BF — BLIND FLANGE
- CROSSING LINES
- CONNECTING LINES
- FLOWMETER, TURBINE
- FLOW STRAIGHTENER
- JACKETED LINE
- INSULATED LINE
- BOSS, A.N.D.
- BOSS, SPECIAL PURPOSE
- "FRANTZ" TYPE SCREEN
- F/M — FLOWMETER, INDICATE TYPE
- PUMP, PISTON (INDICATE "VACUUM" IF APPLICABLE)
- PUMP ROTARY (INDICATE "VACUUM" IF APPLICABLE)
- SIGHT GLASS

5409-5

| | | |
|---|---|---|
| DFMN | GUTHRIE | 9/30/64 |
| CK | E. SUAREZ | 10/5/64 |
| DES | E. SUAREZ | 10/5/64 |
| SUP | J. Klein | 10-5-64 |

ROCKETDYNE
A DIVISION OF NORTH AMERICAN AVIATION, INC.
CANOGA PARK, CALIFORNIA

FIELD LABORATORY SCHEMATIC

FLAME STUDY LABORATORY
MOTOR COOLING SYSTEM

| CODE IDENT NO. | SIZE | |
|---|---|---|
| FIG. 5 | D | 5409-5 |

SCALE | SHEET 3 OF 4

FORM 686-A-21 REV 6-64

FOLDOUT FRAME 3

SPECIFIED

B1

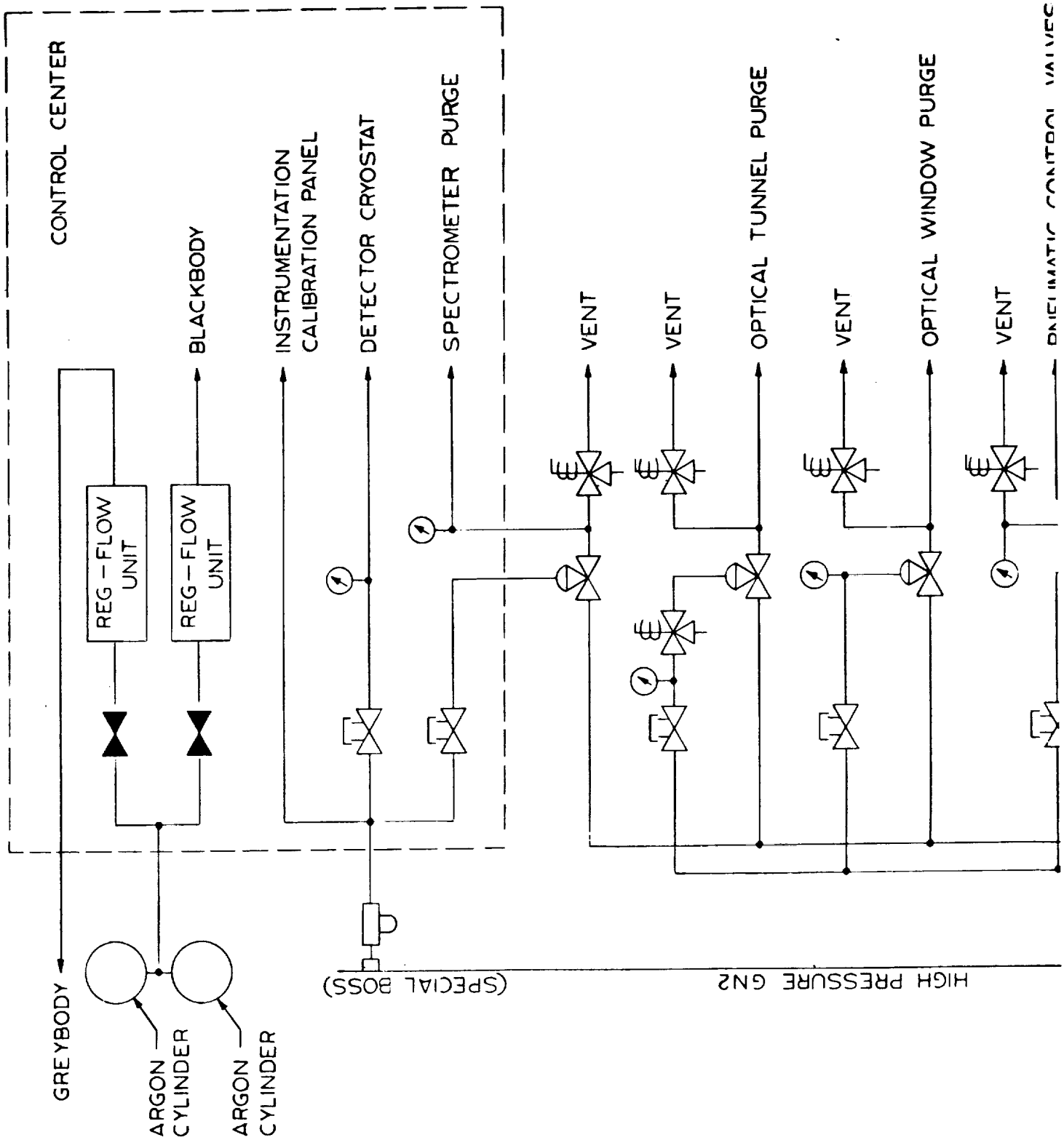




FOLDOUT FRAME 1

B 2

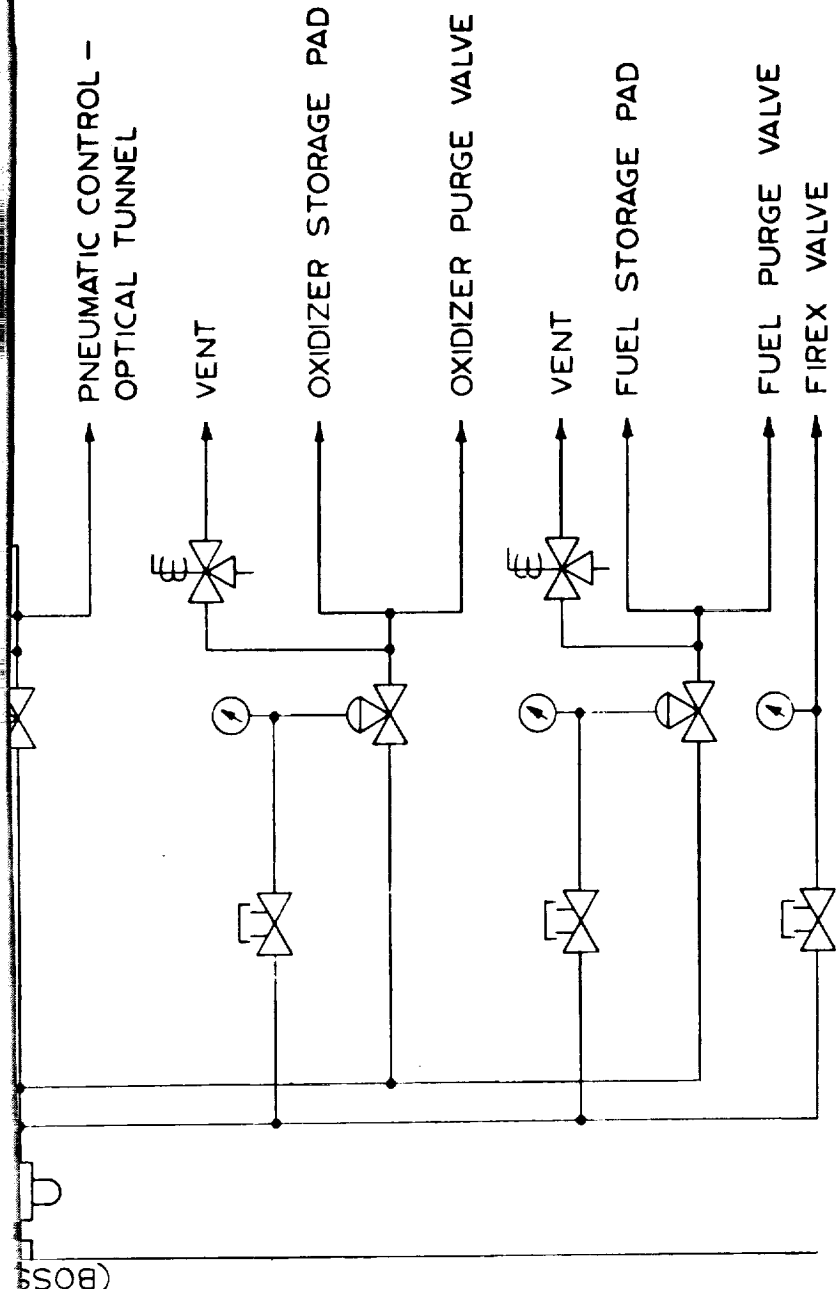


(SSOB)

LEGEND

- SERVO VALVE
- HAND REGULATOR
- BUTTERFLY VALVE
- BALL VALVE, MANUAL
- NEEDLE VALVE, MANUAL
- GATE VALVE, MANUAL
- GLOBE VALVE, MANUAL
- PRESSURE REGULATING VALVE
- COCK OR PLUG VALVE
- SLEEVE VALVE
- CYLINDER-OPERATED VALVE
- MOTOR OPERATED VALVE
- SOLENOID VALVE
- CHECK VALVE, BALL, SWING OR LIFT
- RELIEF VALVE
- THREE-WAY VALVE (HAND LEVER SHOWN)
- FOUR-WAY VALVE (SOLENOID SHOWN)
- HOSE VALVE
- SCREWED CAP
- LINE STRAINER, 50 MESH AND LARGER
- FILTER, 300 MICRON OR LESS (INLINE, T, OR OFFSET)
- EXPANSION JOINT, SLIDING TYPE
- BELLOWS JOINT, EXPANSION, HINGED OR BELLOWS
- FLEXIBLE HOSE
- BURST DISC
- ORIFICE FLANGE
- PUMP CENTRIFUGAL
- HEAT EXCHANGER
- GAUGE
- B.F BLIND FLANGE
- CROSSING LINES
- CONNECTING LINES
- FLOWMETER, TURBINE
- FLOW STRAIGHTENER
- JACKETED LINE
- INSULATED LINE
- BOSS, A.N.D.
- BOSS, SPECIAL PURPOSE
- "FRANTZ" TYPE SCREEN
- F/M FLOWMETER, INDICATE TYPE
- PUMP, PISTON (INDICATE "VACUUM" IF APPLICABLE)
- PUMP ROTARY (INDICATE "VACUUM" IF APPLICABLE)
- SIGHT GLASS

| | | |
|---|---|---|
| DFMN | GUTHRIE | 10/1/64 |
| CK | E. SUAREZ | 10/5/64 |
| DES | E. SUAREZ | 10/5/64 |
| SUP | J.F. Lewis | 10-5-64 |

ROCKETDYNE
A DIVISION OF NORTH AMERICAN AVIATION, INC.
CANOGA PARK, CALIFORNIA

FIELD LABORATORY SCHEMATIC

FLAME STUDY LABORATORY
MISC. PNEUMATIC SYSTEMS

| CODE IDENT NO. | SIZE | |
|---|---|---|
| FIG. 6 | D | 5409-6 |
| SCALE | | SHEET 4 OF 4 |

FOLDOUT FRAME 3

5409-6

The motor test pit of the Plume Studies Laboratory is shown in Figs. 7 and 8. The rocket motor propellant control and purge valves, thrust mount, instrumentation transducer housing, and the absorption source housing are shown best in Fig. 7; whereas, the supersonic diffuser, optical tunnel and tunnel valves are clearly shown in Fig. 8. The interior of the Plume Studies Laboratory recording and control center is shown in Fig. 9.

Rocket Motor Hardware

Rocket motor hardware was designed and fabricated to accomplish the following program requirements:

1. Operate at various chamber pressures, including the pressure of the F-1 engine.
2. Operate at various propellant mixture ratios.
3. Provide variations in the quantity and distribution of the injected fuel near the chamber walls.
4. Provide variations in the residence time of the combustion gases within the combustion chamber.
5. Preclude afterburning reactions of the rocket exhaust gases or provide means of controlling these reactions.

The rocket motor hardware to fulfill the above requirements consists of two thrust chambers, two injectors, and a supersonic diffuser.

The two thrust chambers are identical in design except for their characteristic lengths L* which are 25 and 50 inches, respectively. The two chambers thus provide two residence times of the combustion

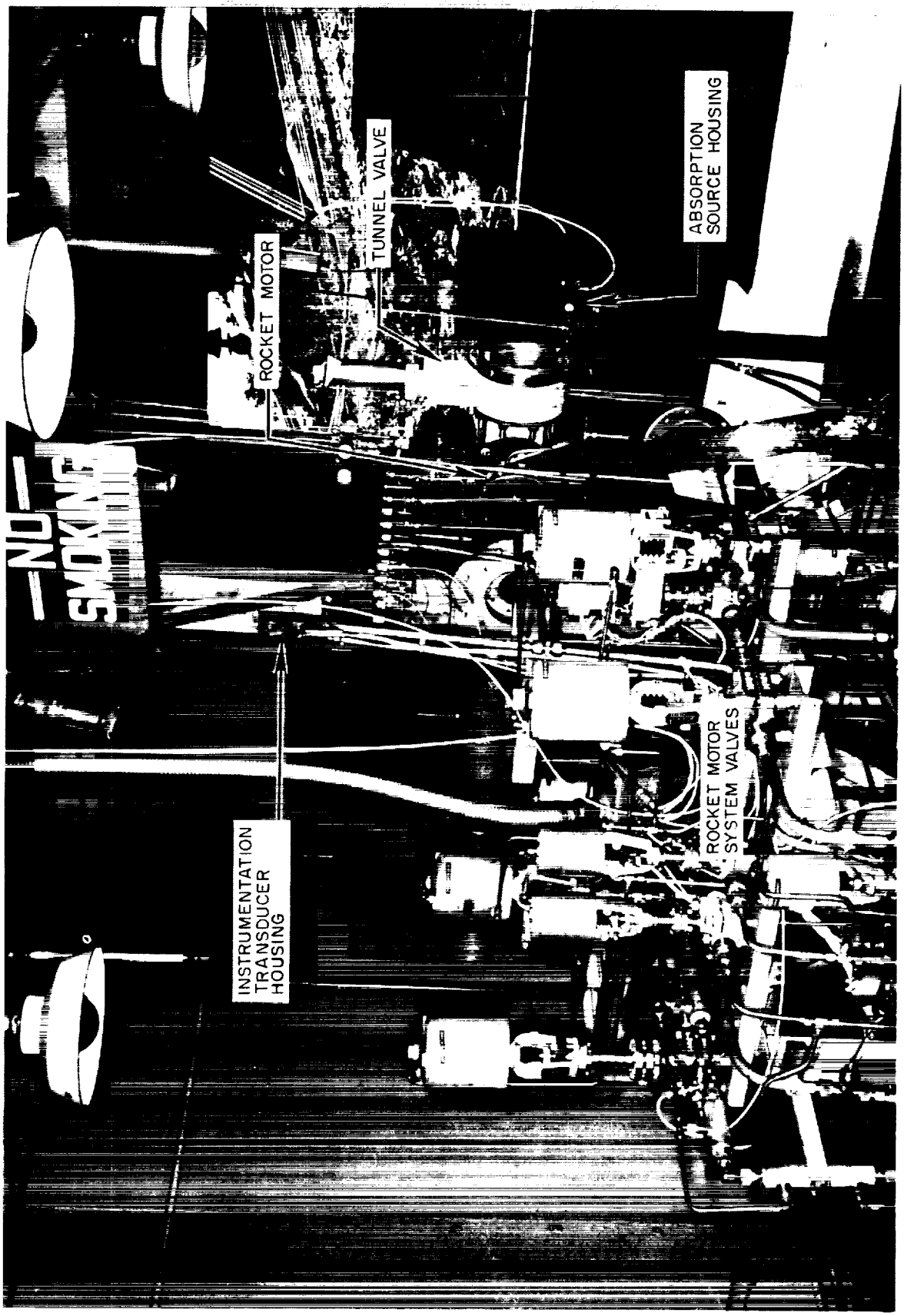


Figure 7. Rocket Motor Test Pit

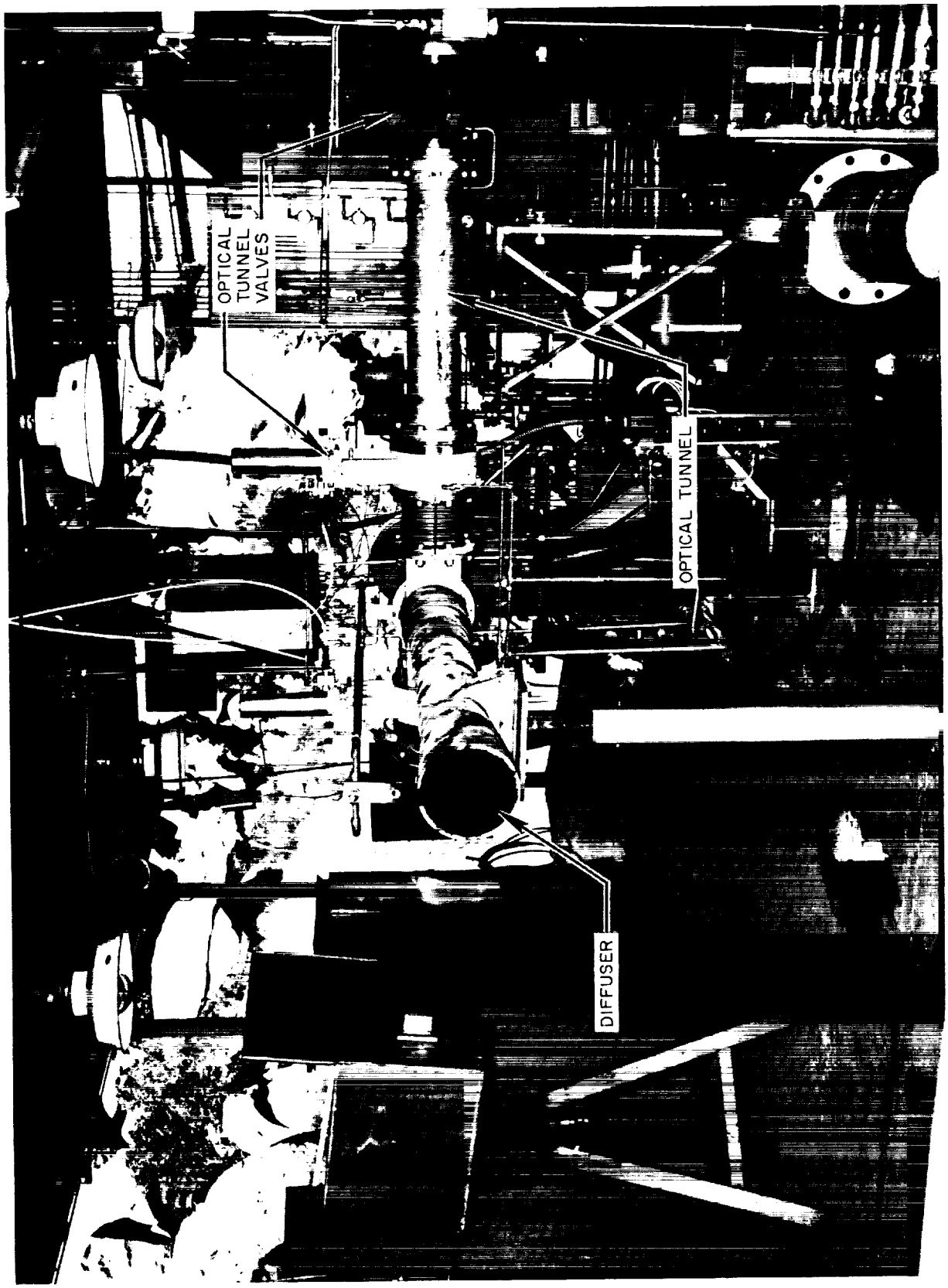


Figure 8. Rocket Motor Test Pit


Figure 9. Plume Studies Laboratory Interior

gases. An assembly drawing of the 25 inch L* motor is shown in Fig. 10. The inner walls were fabricated of copper and externally cooled with water. The chambers were designed to accommodate either the injectors designed for this program for high chamber pressure operation (750 to 1200 psia) or standard ATLAS vernier injectors for operation at lower chamber pressures (250 to 400 psia). The nozzle sections of the combustion chamber are geometrical models of the F-1 nozzle with an attached skirt.

The two injectors were fabricated from heat-treated aluminum and were designed to provide self-impinging patterns with the outer orifices denoted for the injection of fuel. Injector A in Fig. 11 was designed to provide uniform mixture ratio distribution across its face. Injector B was similarly designed; however, the outer fuel orifices provide approximately 15 percent excess fuel. The outer fuel orifices can be partially or totally plugged to provide wide variations in the amount of fuel injected near the chamber walls.

A supersonic diffuser was designed and fabricated to preclude afterburning reactions during normal operation. Controlled afterburning reactions can be achieved by injection of metered quantities of air or other oxidizers into the diffuser inlet section.

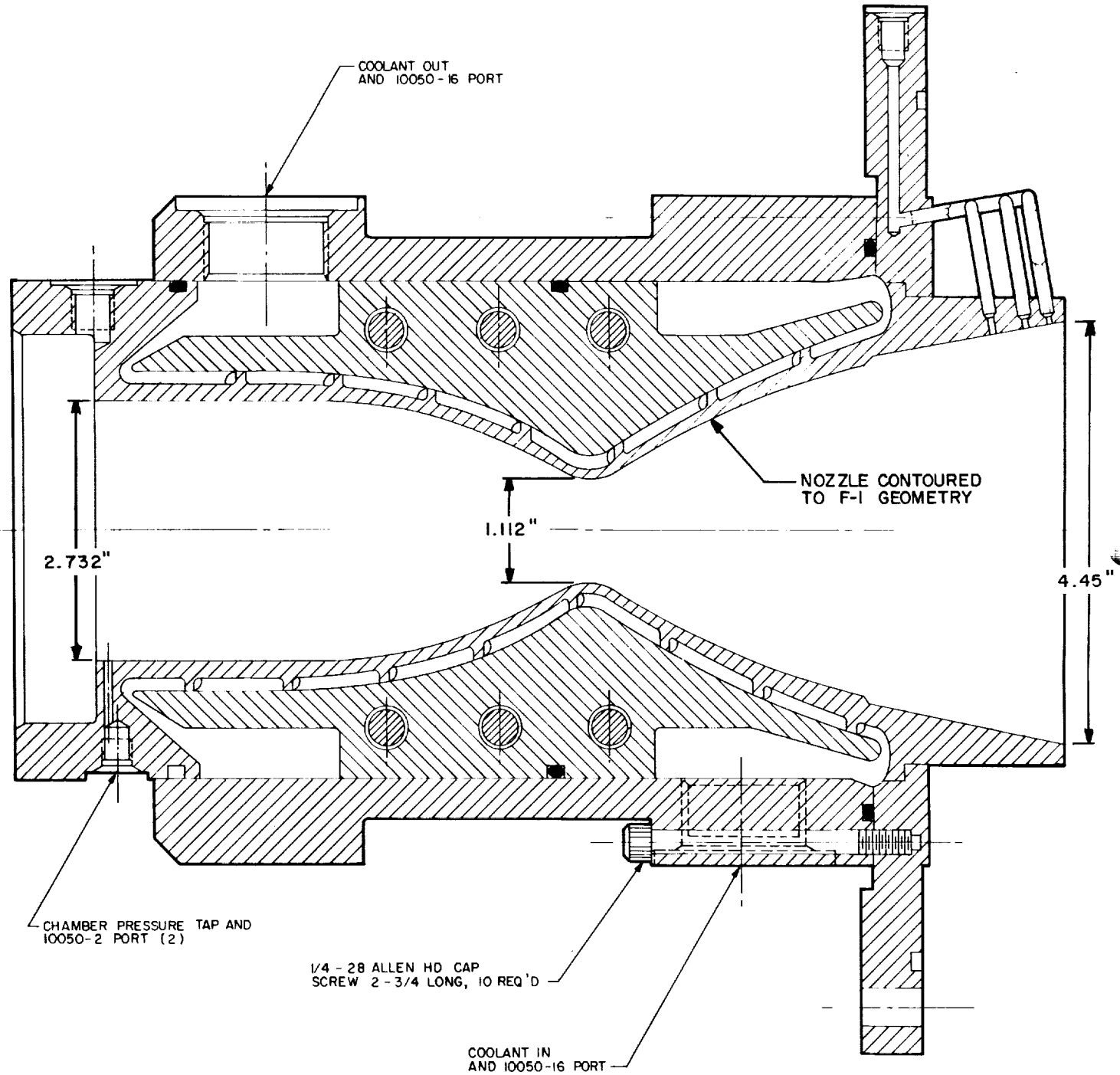


Figure 10. Assembly Drawing of 25 inch L* Motor

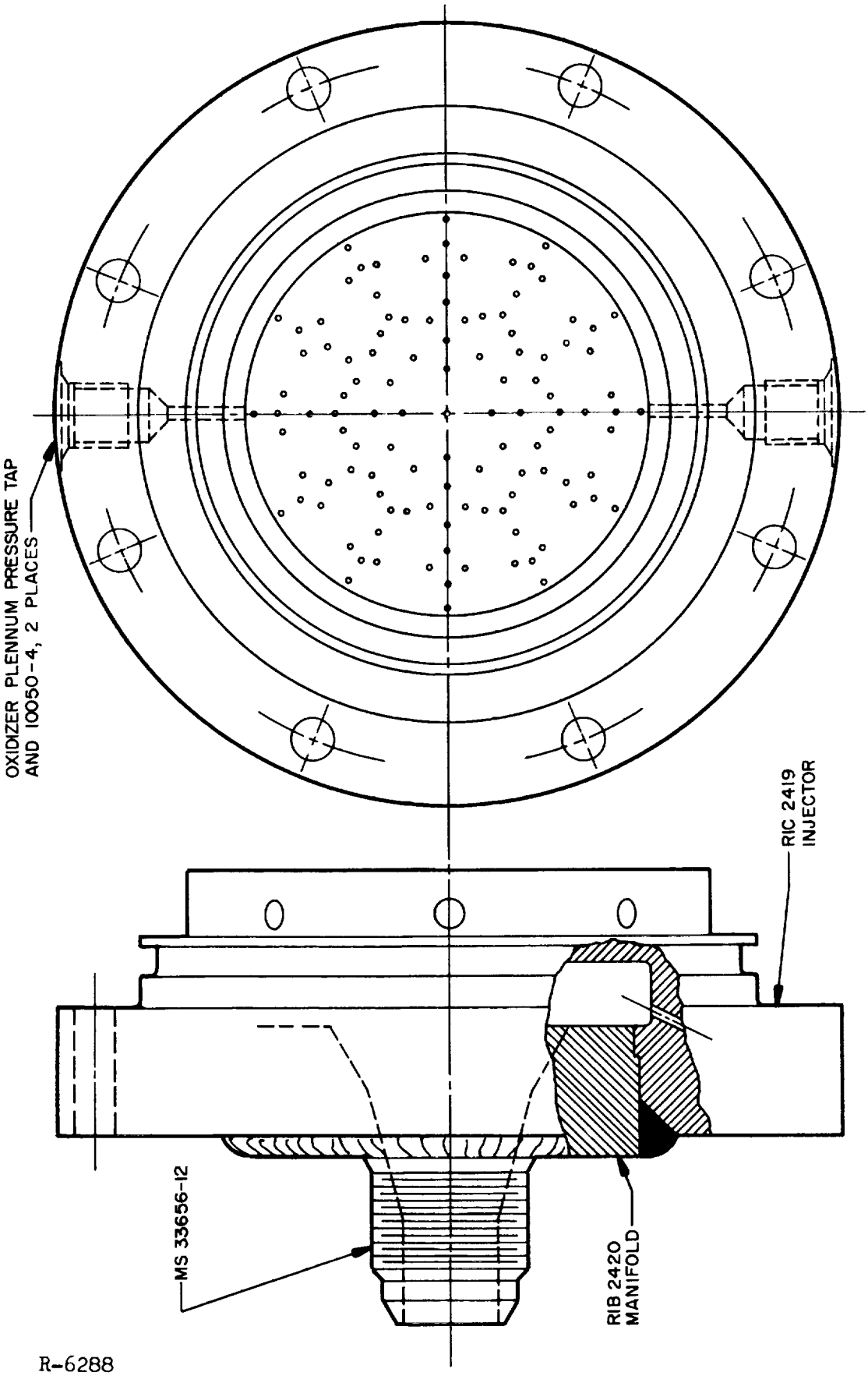


Figure 11. Injector, F-1 Model Motor

Evaluation of the Model Rocket Motor System

The rocket motor system was flow-calibrated prior to the commencement of motor firings to determine that all flow systems, pneumatic systems, and recording-control systems functioned properly. Also, propellant flowrate versus injector pressure drop data for the control of chamber pressure and mixture ratio were obtained.

During coolant flowrate calibration of the 50 inch L* combustion chamber the inner wall ruptured at the throat section. It was ascertained that this failure was the result of overstressing the throat by the high coolant inlet pressure. This condition was corrected; however, subsequent motor test firings were, of necessity, made with the 25 inch L* chamber. A total of ten rocket motor firings were made to thoroughly evaluate the motor, supersonic diffuser, and the total instrumentation system. These were all made using injector A with a uniform mixture ratio distribution to provide relatively uniform temperature profiles during spatial scanning tests with the spectrometer. The results of these tests are shown in Table I.

On several tests there was apparent partial plugging of some of the fuel injector orifices. This was caused by solid particle deposition from the pyrophoric ignitor fluid, a mixture of 15 percent triethylaluminum and 85 percent triethylboron. This plugging was corrected on later tests by changing the motor ignition sequence slightly.

On the final three tests the combination of rocket motor, diffuser and spatial scanning spectrometer were tested. The rocket motor and diffuser operated satisfactorily, and spatially scanned data were collected.

TABLE I

MODEL ROCKET MOTOR PERFORMANCE

| Test No. | Chamber Pressure, psia a | Mixture Ratio | Exhaust Velocity, ft/sec a | Exhaust Velocity Efficiency % | Exit Pressure, psia | Test Purpose |
|---|---|---|---|---|---|---|
| 93 | 946 | 2.16 | 5191 | 89.2% | NM | Motor System, UV Spectrometer, and UV Pyrometer Evaluation |
| 94 | 937 b | 2.13 | 4994 | 85.7% | | |
| 95 | 933 b | 2.39 | 4914 | 85 % | | |
| 96 | 923 | 2.69 | 4926 | 86 % | | |
| 97 | 967 | 2.11 | 4950 | 85.2% | | |
| 98 | 947 b | 2.57 | 4730 | 82.3% | | |
| 99 | 996 | 2.25 | 5100 | 87.5% | | Probe Evaluation |
| 100 | 952 | 2.28 | 5040 | 86.7% | 8.9 c | IR Spectrometer Evaluation |
| 101 | 932 | 2.53 | 4910 | 85.3% | 9.0 c | IR Spectrometer Evaluation |
| 102 | 945 | 2.49 | 4950 | 85.7% | 9.1 c | IR Spectrometer Evaluation |

a Model Motor Nozzle Inlet Conditions

b Partially Plugged Fuel Injector

NM Not Measured

c Calculated From Nozzle Pressure Measured at $\epsilon$ = 14:1

However, subsequent analyses of the scanned data revealed that, although the scanned distance exceeded the diameter of the nozzle exit, the zero radiance point in the exhaust gas plume was not reached during the spatial scans. This was due to free jet expansion of the exhaust gases at the nozzle exit plane into the diffuser cavity. The free jet expansion was appreciably greater than anticipated because the pressure ratio between the nozzle exit pressure and the diffuser cavity pressure exceeded the planned ratio. However, this high ratio permits greater flexibility in the amount of oxidizing gases that can be metered into the diffuser for afterburning studies.

## Recommendations

All components of the instrumentation system as designed and fabricated performed satisfactorily during rocket motor testing. The rocket motor system proved to be capable of achieving the specific program requirements. Recommended variables to be further and more extensively investigated included the following:

1. Vary the quantity and distribution of the injected fuel near the chamber wall.
2. Vary the residence time of the combustion gases within the combustion chamber.
3. Rotate the rocket motor injector about its axial centerline to determine variation in the exhaust plume radiative properties as related to the propellant injection patterns.
4. Comparatively evaluate the differences in the exhaust plume radiative properties between the F-1 geometrical model nozzle and a nozzle of similar design and expansion ratio without the abrupt discontinuity of the F-1 nozzle.

## INFRARED INSTRUMENTATION

Previous investigations of the optical properties of rocket exhaust plumes in the infrared spectral region have been carried out using a single line of sight through the plume. Values of plume spectral radiance and spectral emissivity obtained in this manner can only be called apparent values since the temperature and pressure (or concentration) gradients which existed in the plume were not determined. Values of temperature and spectral absorption coefficients calculated from such radiance and emissivity measurements are also only apparent values. The existence of significant temperature and concentration gradients is postulated for $LO_2$/RP-1 exhausts, where the calculated temperature depends strongly on the wavelength region in which the calculation is made (Ref. 4). Thus, meaningful measurements of the optical properties of rocket exhausts must take into account various gradients that may exist along the line of sight.

If the symmetry of the temperature and pressure gradients is known, it is possible to calculate the distributions in temperature and pressure from a series of line-of-sight measurements of spectral radiance and spectral emissivity. Such is the case for rocket engine exhausts, where, from geometrical considerations, the plume is expected to be radially symmetric about the engine axis in planes parallel to the nozzle exit plane. Therefore, a major aim of this present program was to develop an instrumentation system that would permit absorption-emission measurements to be made on a rocket motor exhaust along parallel chordal optical paths in planes parallel to the nozzle exit plane. The mathematical foundation for calculation of radial distributions from line-of-sight measurements and the system that will permit these measurements is

discussed in following sections.

Mathematical Foundation for Zone Radiometry

Figure 12 shows schematically the experimental arrangement for absorption-emission measurements for a particular line-of-sight. The basic assumptions made in this experiment are: (1) the existence of local thermodynamic equilibrium, and (2) a radially symmetric distribution of temperature and pressure (or species concentration). In this discussion the following symbols are used:

$N_r$ = radial distribution of spectral radiance per unit radial distance (watts $cm^{-2}$ $steradian^{-1}$ $micron^{-1}$ $cm^{-1}$)

$N_x$ = experimentally determined spectral radiance along line of sight at distance x from y axis (watts $cm^{-2}$ $steradian^{-1}$ $micron^{-1}$)

$\tau_x$ = experimentally determined spectral transmittance along line of sight at distance x from y axis (incident intensity divided by transmitted intensity)

$K_r$ = radial distribution of spectral absorption coefficient for a particular species ($cm^{-1}$ $atm^{-1}$)

$P_r$ = radial distribution of partial pressure for a particular species (atm)

For a given x the contribution to $N_x$ from an element of thickness dy located at r is given by

$$N_r dy \exp\left\{-\int_y^{y_o} K_r P_r \, dy\right\} \qquad (1)$$

and therefore

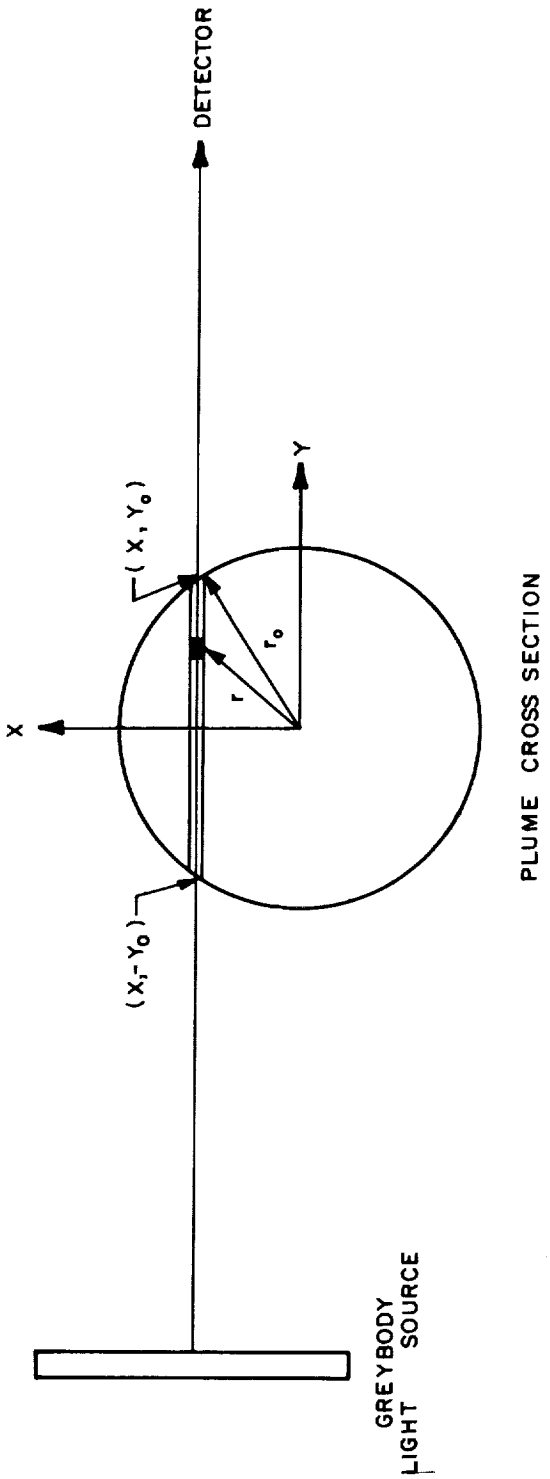


Figure 12. Absorption-Emission Experimental Arrangement for a Single Chordal Path

$$N_x = \int_{-y_o}^{y_o} N_r \exp\left\{-\int_{y}^{y_o} K_r P_r \, dy\right\} dy \tag{2}$$

The plume transmittance for a given x is given by

$$\tau_x = \exp\left\{-\int_{-y_o}^{y_o} K_r P_r \, dy\right\} \tag{3}$$

Experimental measurement of $\tau_x$ for various values of x furnishes a set of simultaneous equations of the form of Eq. 3 which may be solved, in principal, for values of $K_r P_r$. These values of $K_r P_r$ may then be used in the set of simultaneous equations of the form of Eq. 2 to solve for values of $N_r$.

The practical solution of equations of the above type has been made simpler by the mathematician Abel. He found that an equation of the form

$$F(x) = 2\int_{x}^{r_o} G(r) \, (r^2-x^2)^{-\frac{1}{2}} \, r\,dr \tag{4}$$

has as its solution

$$G(r) = -\frac{1}{\pi}\int_{r}^{r_o} \frac{dF(x)}{dx} \, (x^2-r^2)^{-\frac{1}{2}} \, dx. \tag{5}$$

Equations 2 and 3 may be put in the form of Eq. 4.

Equation 5 has been handled by numerical methods by many investigators. The method deemed most suitable for the current problem is that described

by Nestor and Olsen (Ref. 5). In their method, which is an extension of the work of Gooderum and Wood (Ref. 6) the experimental measurements are made at equally spaced intervals of separation a along the x axis, and the exhaust is assumed to contain an equivalent number of zones of width a, each of which is assumed to be constant in temperature and pressure (and radiance and transmittance). This arrangement is depicted in Fig. 13 for a five-zone division of the plume. For a division of N zones, Eq. 5 takes the form

$$G_k(r) = -\frac{2}{\pi a}\sum_{n=k}^{N} B_{kn}F_n(x) \tag{6}$$

The elements of the matrix $B_{kn}$ have been tabulated by Nestor and Olsen.

For solution of Eq. 3 the identifications to be made are

$$F_n(x) = \mathrm{Ln}\left[\tau_n^{-1}(x)\right] \tag{7}$$

and

$$G_k(r) = K_k(r)P_k(r) \tag{8}$$

For solution of Eq. 2 the identifications to be made are

$$F_r(x) = N_n(x)\ 2\left[\tau_n(x)+1\right] \tag{9}$$

and

$$G_k(r) = N_k(r) \tag{10}$$

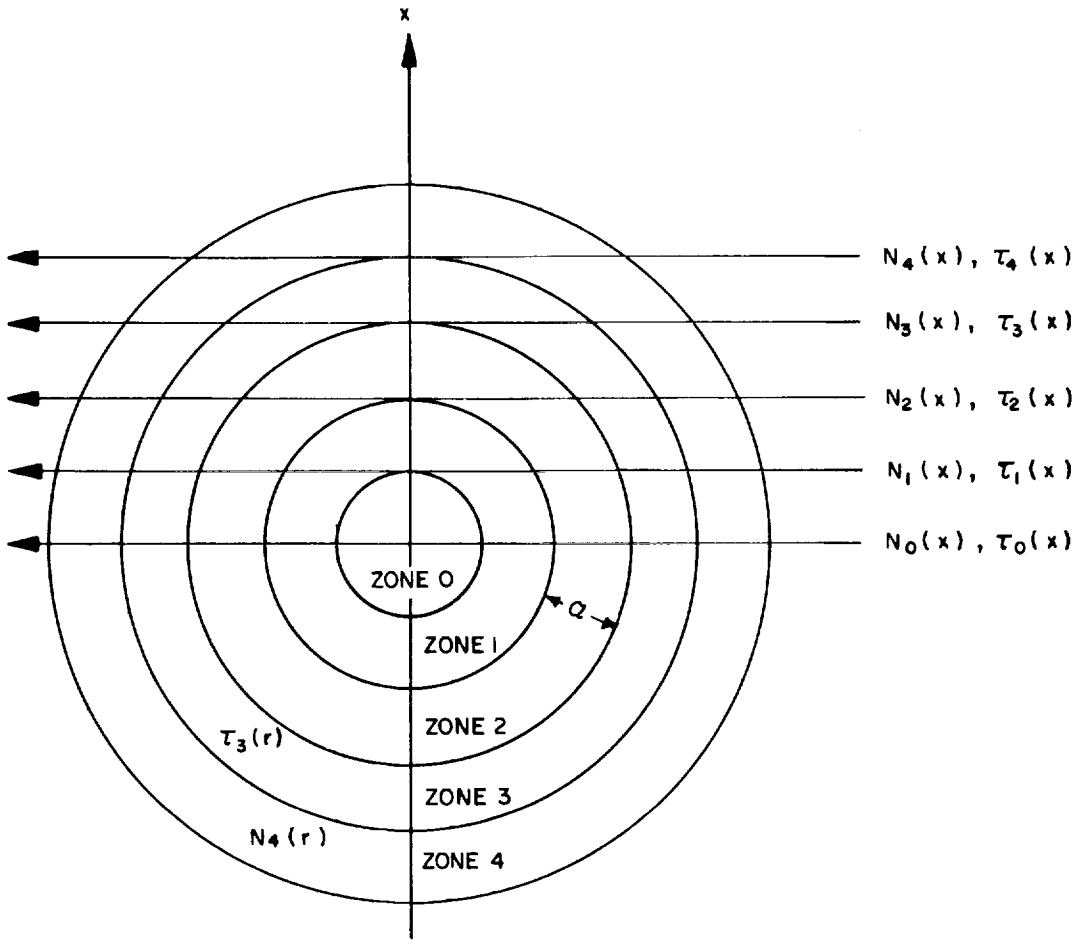


Figure 13. Division of Plume Cross Section into Zones of Constant Temperature and Pressure

The solution of Eq. 2 as given above has been simplified by using an approximation described by Freeman and Katz (Ref. 7) which is sufficiently accurate for plumes whose transmittance along a diameter is 0.70 or greater.

The above section describes how the radial distributions of spectral radiance and linear spectral absorption coefficient (KP) may be obtained from line-of-sight measurement of spectral radiance and spectral transmittance. Calculation of radial distributions of temperature and pressure are described in a later section.

To provide the required line-of-sight radiance and transmittance data the infrared instrumentation system must be able to allow performance of the following experiments:

1. Measure plume spectral radiance by comparing plume intensity with blackbody intensity; radiation is optically chopped between the plume and the detector.
2. Measure plume spectral transmittance by locating a greybody source on the opposite side of the plume from the spectrometer; greybody radiation is optically chopped between the greybody and the plume so that the plume transmittance may be directly determined.
3. Provide for variation of line-of-sight by spatially scanning the images of the plume, greybody, or blackbody that are formed at the entrance slit of the spectroradiometer.
4. Obtain both radiance and absorptance measurements at several different, but accurately reproducible, wavelengths during each individual motor firing.

The actual system is described in the following section.

Infrared Instrumentation System

Figure 14 shows the emission-absorption experimental arrangement. Figures 7 and 8 show that portion of the system which is outside the control center. The greybody consists of an electrically heated carbon rod six inches in length mounted in an airtight, argon-purged housing. The greybody is mounted inside a 400 cps cylindrical "squirrel cage" optical chopper. Calcium fluoride windows 3/8 inch thick and 6-1/2 inches in diameter isolate various portions of the optical path. The three gate valves in the optical path which act as safety shutters are sequenced to open just after motor ignition and to close just prior to motor cutoff. The entire system may be purged with nitrogen to minimize atmospheric absorption.

Figure 15 shows schematically the infrared spectroradiometer, while Figs. 16 and 17 are photographs of the instrument. A Perkin Elmer Model 98G grating monochromator is used with either an uncooled PbS detector or a liquid nitrogen cooled PbSe detector. The internal optical chopper used to chop plume emission is located just inside the monochromator exit slit. This chopper is basically a tuning fork with chopper blades attached to the tines. The tuning fork is electrically driven at the desired chopping frequency (400 cps) when plume spectral radiance is being measured. When plume absorptance is to be measured power is removed from the tuning fork driving mechanism, the tines stop in an open position in approximately one second, and the greybody optical shutter is opened to allow the chopped greybody radiation to pass through the plume.

Spatial scanning of the images of the blackbody, greybody and/or plume

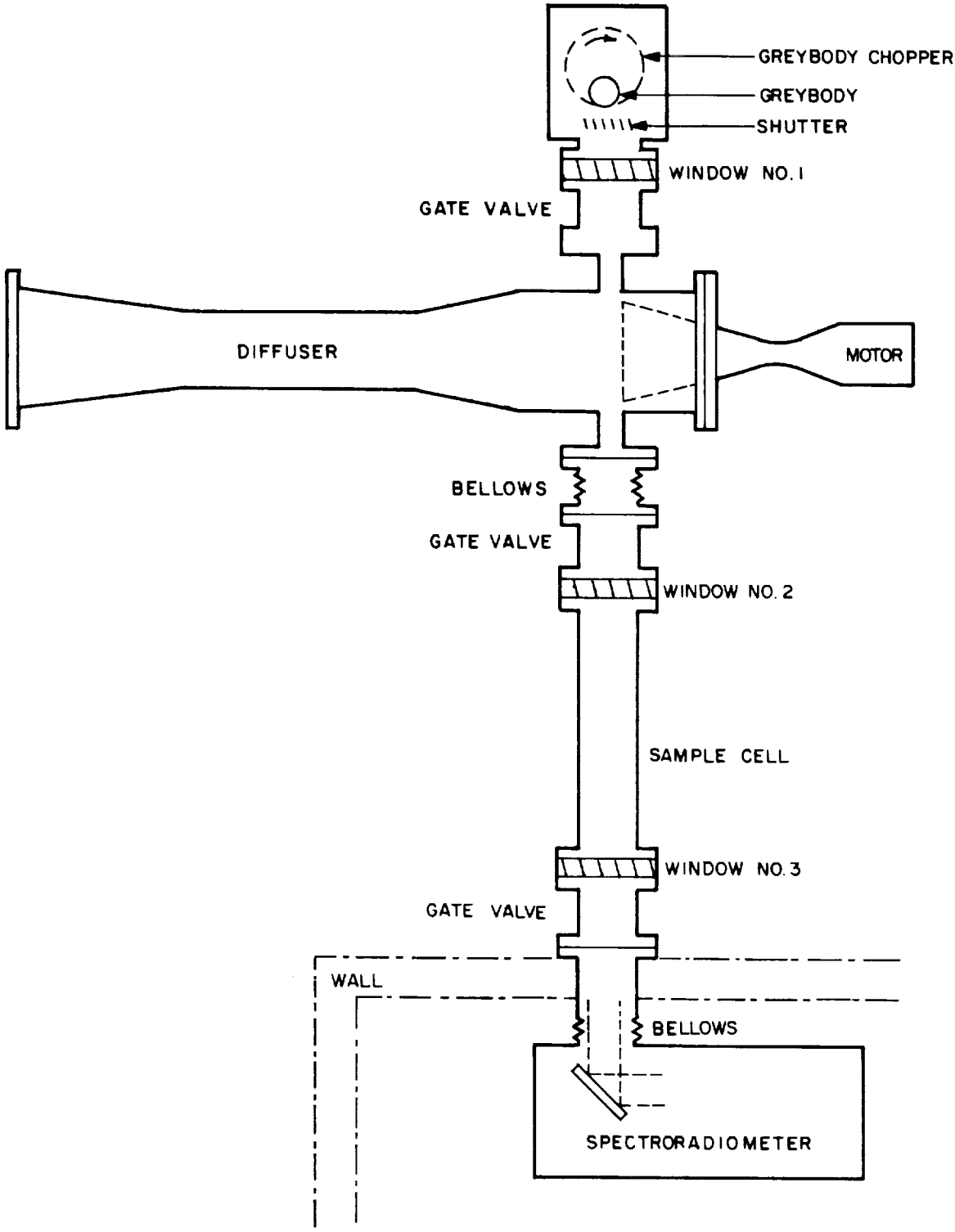


Figure 14. Experimental Arrangement for Absorption-Emission Measurements

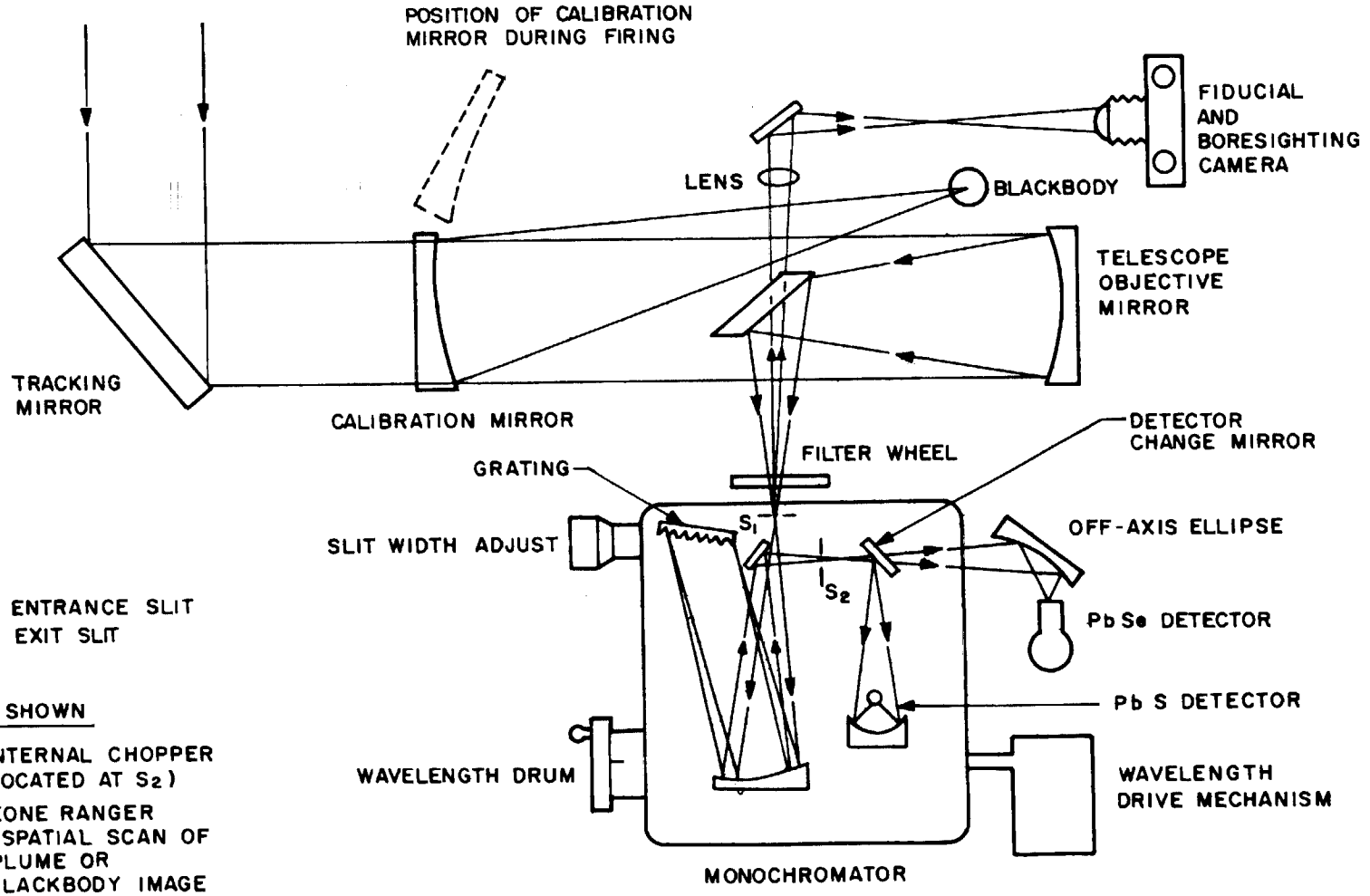


Figure 15. Optical Diagram of Infrared Spectroradiometer

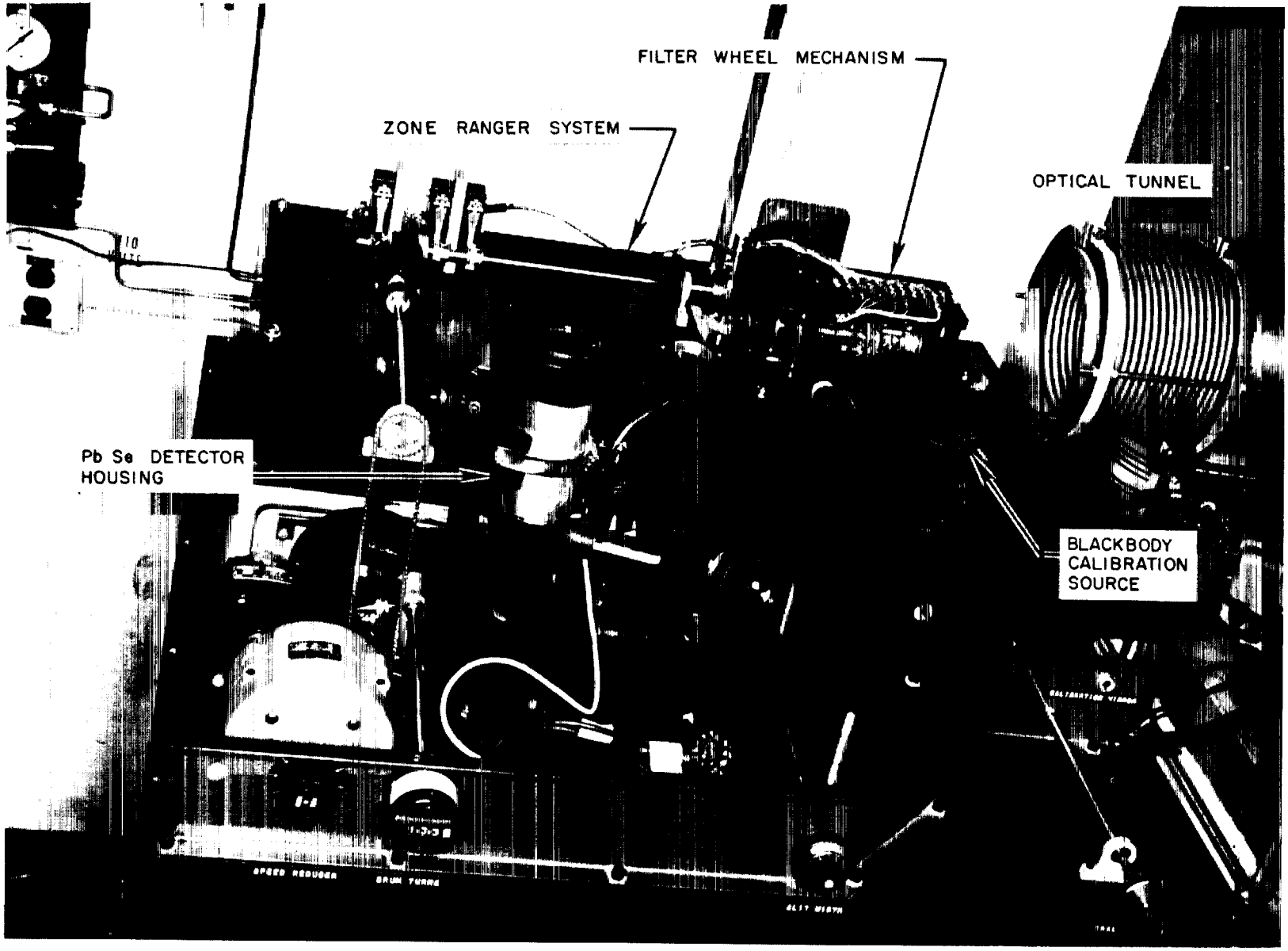


Figure 16. Infrared Spectroradiometer

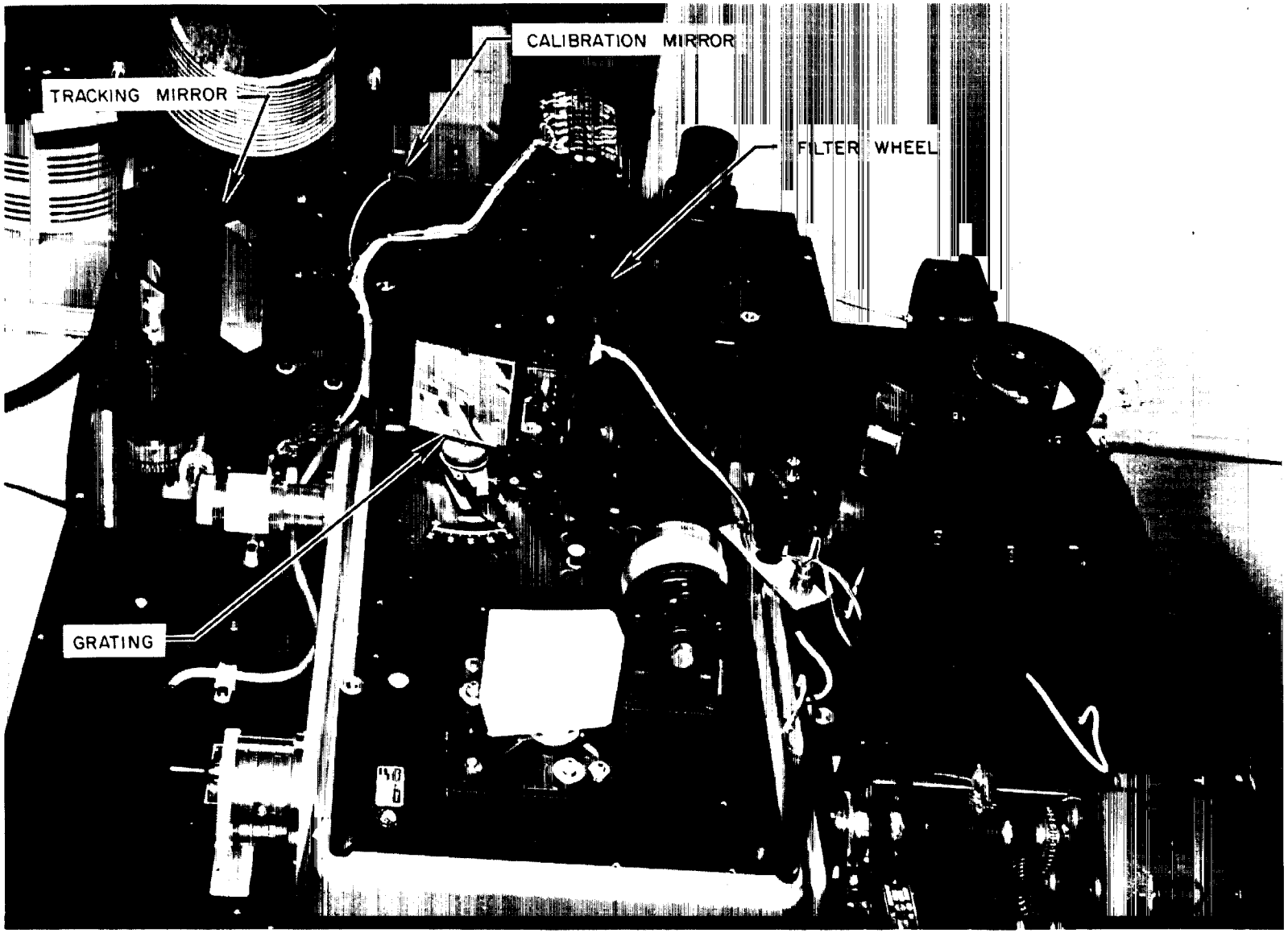


Figure 17. Infrared Spectroradiometer with Zone Ranger System Removed

that are formed at the monochromator entrance slit is accomplished in the following manner. A cam which is rotated at constant angular velocity drives a rod at constant linear velocity up and down in front of, and in a plane parallel to, the entrance slit. This rod, called the zone ranger, contains a small aperture (subtending approximately 1/10 the plume image diameter) which limits the field of view at the plume to 1cm x 0.2cm (the smaller dimension depends on the slit width). Thus, this device is essentially a travelling field stop. The size of this aperture is adjustable. Fig. 18 shows the zone ranger system.

During zone radiometry experiments a filter wheel, in conjunction with a diffraction grating blazed at 30 microns, provides for wavelength selection and accurate reproducibility. A grating with a blaze wavelength of 30 microns was chosen because radiation diffracted by this grating at the blaze angle in high orders falls into spectral regions suitable for the required radiance and emissivity determinations. For instance, at the blaze angle this grating will diffract 4.29$\mu$ energy in 7th order to the detector, thus allowing a determination of the $CO_2$ (gas) radial temperature distribution; similarly, in the 19th order 1.58$\mu$ energy will be diffracted to the detector, thus allowing a determination of carbon particle radial temperature distribution. In this method each desired spectral order is isolated by a narrow band pass, spectral filter, while the 30$\mu$ blaze grating is held fixed at the blaze angle. Four filters are utilized in each motor firing, and the fact that the grating remains fixed insures an extremely accurate wavelength reproducibility for the absorption and emission measurements. The grating is used at the blaze angle to insure that sufficient energy is diffracted into the desired spectral orders.

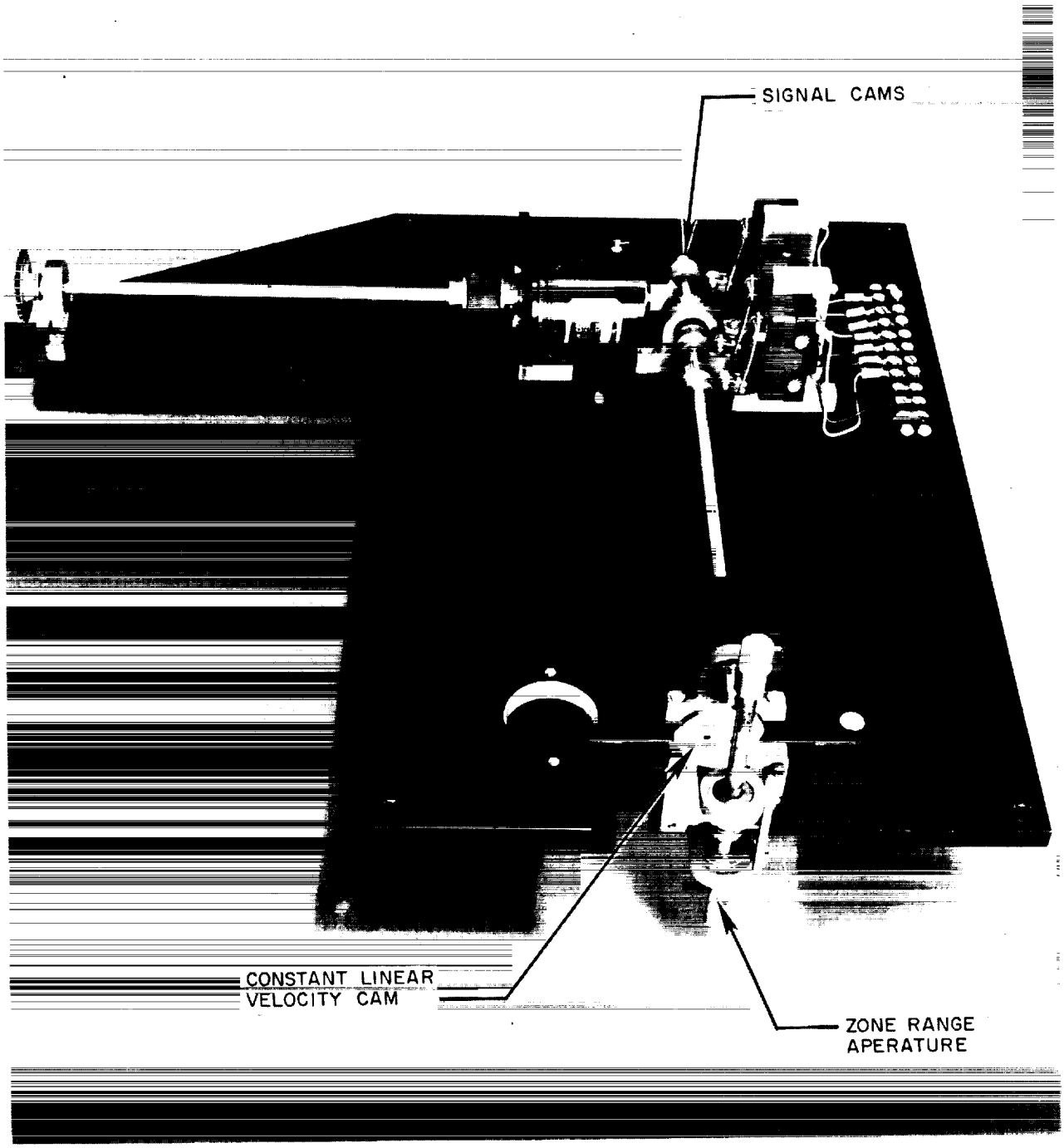


Figure 18. Zone Ranger System

Operation of the zone ranger and filter wheel, as well as the change from tuning fork chopper to greybody chopper, is automatic. A schematic of the control system is shown in Fig. 19. The shaft of the zone ranger cam holds three electrical cams. One electrical cam produces a signal on the recorder event pen to key the zone ranger position. The second electrical cam momentarily disengages the filter wheel positive stop mechanism as the third activates the filter wheel stepping motor. The four-position filter wheel also produces an electrical signal on the recorder during its motion for positive filter identification. The filter wheel is activated after each zone ranger cycle. The filter wheel 30 degree stepping motor drives the filter wheel through a 3:1 gear reduction. Thus the filter wheel makes three revolutions while the stepping motor makes one revolution. After the filter wheel has made one revolution, the wafer switch activates relays which in turn remove power from the tuning fork chopper, switch the 400 cps reference signal from the tuning fork chopper to the greybody chopper, and then open the greybody optical shutter.

Approximately 20 seconds are available for the gathering of data during each motor firing. Spatial scans of the plume in emission and absorption are obtained in the following manner:

1. Prior to motor firing the internal and greybody choppers are activated, the greybody is set at a desired brightness temperature, and the filter wheel is positioned so that filter number one is in the optical train and so that the wafer switch relays have closed the greybody shutter, supply power to the tuning fork chopper, and allow the tuning fork 400 cps reference signal to reach amplifiers.

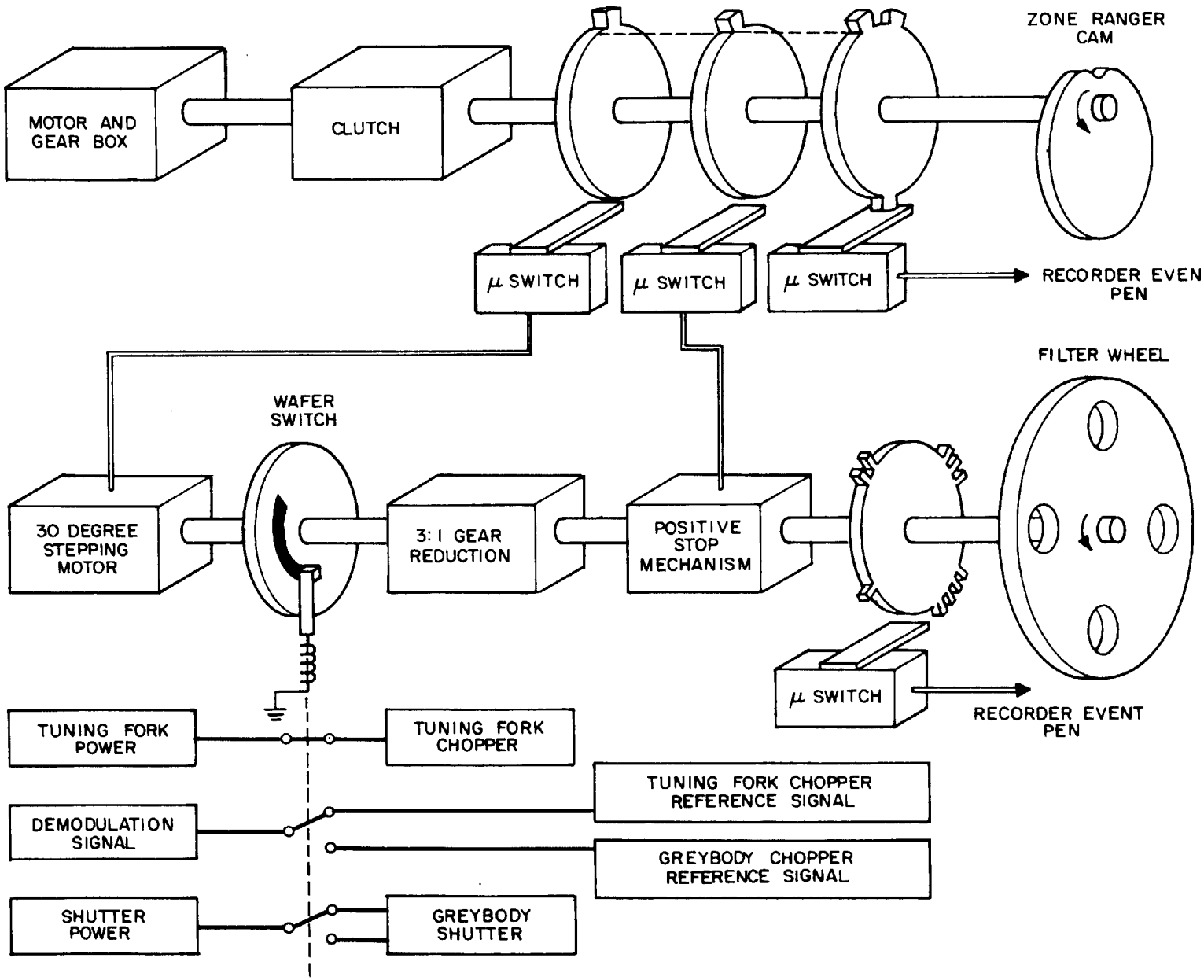


Figure 19. Schematic of Zone Ranger Control

2. After motor ignition the zone ranger mechanism is activated manually (all following operations then occur automatically). The zone ranger scans the plume image radius in one direction in one second. After the zone ranger makes a complete cycle (scans the plume image radius twice) the electrical cams activate the filter wheel stepping mechanism; the filter wheel makes one-quarter of a revolution, allowing energy at a second wavelength to reach the detector. The zone ranger continues to run at $\frac{1}{2}$ cycle per second.
3. After the filter wheel has made a complete revolution (plume radiance will have been measured at 4 wavelengths), the wafer switch activates relays as described above, and the zone ranger now scans at 4 identical wavelengths the chopped greybody radiation that is transmitted by the plume.
4. For intensity calibration purposes, the greybody and blackbody images are similarly scanned before and after each firing.

Conventional spectral scans of plume emission or absorption can also be made. In this case the zone ranger device and the filter wheel are removed from the instrument. For the 1 to 2$\mu$ range a grating blazed at 1.6$\mu$ is used in first order, and higher orders are eliminated by a silicon window. A grating blazed at 4$\mu$ is used in the 2-6$\mu$ spectral region in first order. Below 3.5$\mu$ higher orders are eliminated by a germaniun window and above 3.5$\mu$ by an indium arsenide window.

Data Reduction

Line-of-sight values of plume spectral radiance and plume spectral transmittance (whether from zone ranger spatial scans or from conventional

spectral scans) are calculated from the raw data in the usual manner; comparison of recorder traces of the amount of greybody radiation transmitted by the plume with traces of the greybody radiation itself allows calculation of line-of-sight values of plume transmittance, $\tau_n(x)$. The matrix multiplication indicated in Eq. 6, with the identifications given in Eqs. 7 and 8, yields the radial distribution of the product $K_k(r)P_k(r)$. Comparison of recorder traces of plume emission and blackbody emission at a particular wavelength with identical instrument settings allows calculation of line-of-sight values of plume spectral radiance, $N_n(x)$. The matrix multiplication of Eq. 6, with the identifications given in Eqs. 9 and 10, gives the radial distribution of spectral radiance $N_k(r)$.

The radial distribution of spectral emissivity (assuming local thermodynamic equilibrium for each zone) is given by

$$\epsilon_k(r) = 1 - \exp\left\{- aK_k(r)\ P_k(r)\right\}$$

The spectral radiance of a blackbody, $N_{BB}$, at the temperature of the plume for the $k^{th}$ zone, $T_k(r)$, is given by

$$N_{BB}(\lambda, T_k) = \frac{N_k(r)a}{\epsilon_k(r)}$$

where $\lambda$ is the wavelength at which the original line-of-sight measurements were made. By making use of blackbody tables (Ref. 8) which tabulate blackbody radiance as functions of temperature and wavelength, the radial distribution of plume temperature $T_k(r)$ may easily be inferred.

Two further steps may be taken. In cases where the spectral absorption coefficient $K(cm^{-1}\,atm^{-1})$ is known as a function of temperature and pressure from independent experiments or theoretical calculations, then the radial distribution of partial pressure may be obtained from the expression

$$P_k(r) = \frac{K_k(r)P_k(r)}{K(\lambda,T)}$$

This partial pressure distribution may be compared with that obtained during the exhaust sampling experiments and with theoretical calculations of plume pressure distributions. In cases where no data is available on K for a particular species at the temperatures encountered in the plume, either the theoretical or experimental partial pressure distributions may be used to yield values of K.

Evaluation of Infrared Instrumentation System

As mentioned earlier in the discussion of the F-1 model motor and diffuser performance, the nozzle exit pressure was significantly greater than expected. This greater pressure caused a rapid expansion of the exhaust plume at the nozzle exit, with the result that the plume boundaries exceeded the field of view of the zone ranger. For this reason no transmission or radiance data could be obtained on the outermost zones of the plume, and a meaningful conversion of line-of-sight data into radial distributions could not be made.

In order to demonstrate the successful operation of the zone ranger system and the calculation of radial distributions of temperature and pressures, several sets of data were obtained on $LO_2$/RP-1 firings using

an Atlas vernier engine modified to provide a 25:1 expansion ratio. The motor was fired into a supersonic diffuser in order to assure a full flowing nozzle. On two firings the motor was operated at a mixture ratio of 1.0 so as to produce measurable absorption in infrared spectral regions where carbon particles are the only absorbing species. On two other firings the motor was operated at a mixture ratio of 2.4 in order to simulate optimum operating conditions. It should be mentioned that the F-1 model motor did produce enough carbon to provide measurable absorption when operating at optimum operating condition.

Seven channels of information are recorded during operation of the infrared instrumentation system. The detector output is displayed on four recording channels, each set at a different electronic gain. Four channels are necessary to accomodate the large differences in signal encountered at different wavelength regions due to differences in plume radiance and detector response. The fifth channel is used for filter identification during zone ranger operation. The sixth channel is used for wavelength calibration when the instrument is used in the normal spectral scan mode. The seventh channel is used to record the signal from a photocell - light bulb - coded wheel system that produces continuous pips during zone ranger motion. This system, which replaces the microswitch signal shown in Fig. 19, was necessary to take into account small variations in the recorder chart drive speed. The location of the zone ranger aperture with respect to the motor axis and the edge of the nozzle exit is determined simply by locating two small light sources at these two locations and then allowing the zone ranger to scan the two images formed at the entrance slit. The zone ranger scans one-half the plume image twice at each filter position; the initial scan is from the plume axis towards the plume edge.

Figure 20 shows raw data output obtained during a zone ranger trace of the greybody at 4.29μ just prior to a motor firing. Figure 21 shows the raw data obtained during the zone ranger trace of the greybody attenuated by the plume during a $LO_2$/RP-1 firing at mixture ratio of 1.0. Figures 22-24 show reduced data in the form of radial distributions of spectral radiance, spectral emissivity, and temperature obtained at 4.29μ (mixture ratio 2.4), 4.29μ (mixture ratio 1.0), 1.36μ (mixture ratio 1.0), respectively. Most noticeble in the reduced data are the following items:

1. The difference in $CO_2$ temperature between runs of different mixture ratio (the optical depth of the carbon emitters was too low to permit a carbon temperature determination at mixture ratio 2.4).
2. The temperature distribution and magnitude differences between $CO_2$ and C at the same mixture ratio.

The radial distribution of emissivity at 1.36μ reflects the distribution of carbon particles. The distribution found is consistent with that expected from the injector used in these firings. The injector design provides for a fuel-rich region of poor combustion at the motor axis and at the circumference of the injector. The $CO_2$ and carbon temperatures are highest in a ring, the radius of which is approximately one-half the nozzle exit radius. This is also consistent with the injector pattern, which provides maximum oxygen injection in a ring of approximately one-half the injector radius.

E1

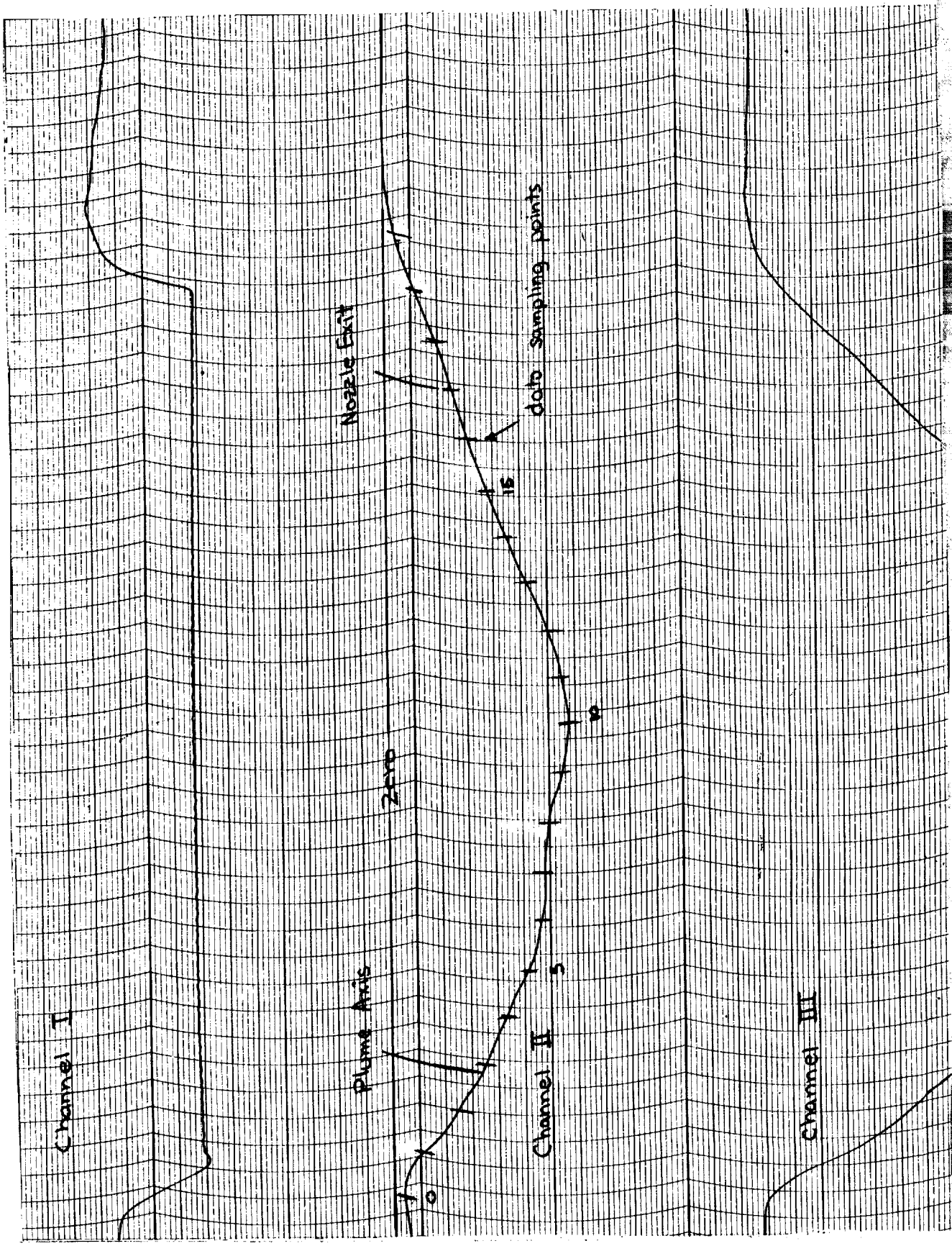
Channel I
Nozzle Exit
data Sampling Points
15
10
Plume Axis
Zero
5
0
Channel II
Channel III

FOLDOUT FRAME 2

E-2

ROCKETDYNE • A DIVISION OF NORTH AMERICAN AVIATION, INC.

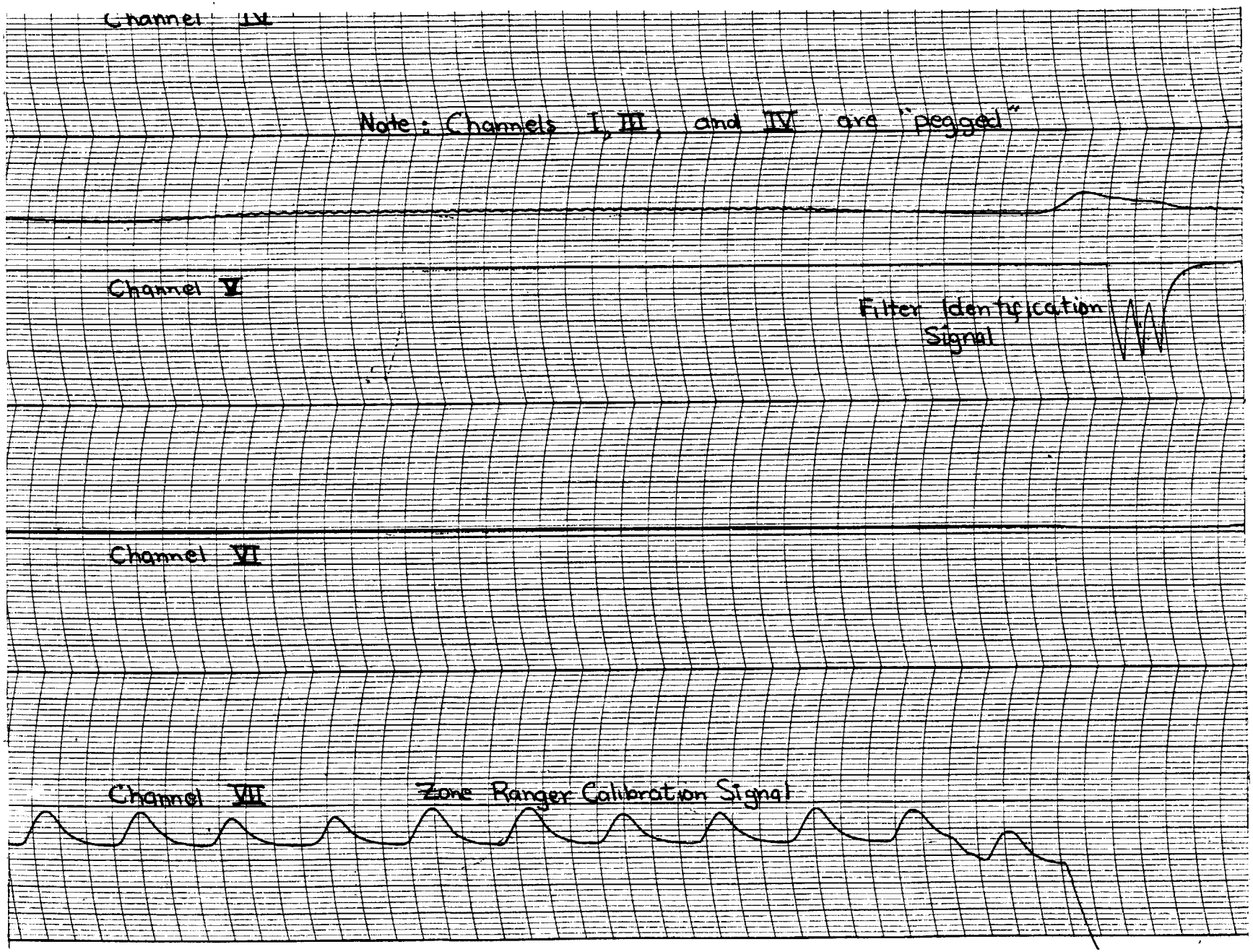


Figure 20. Zone Ranger Trace of Greybody at 4.29 Micron

FOLDOUT FRAME 3

B1

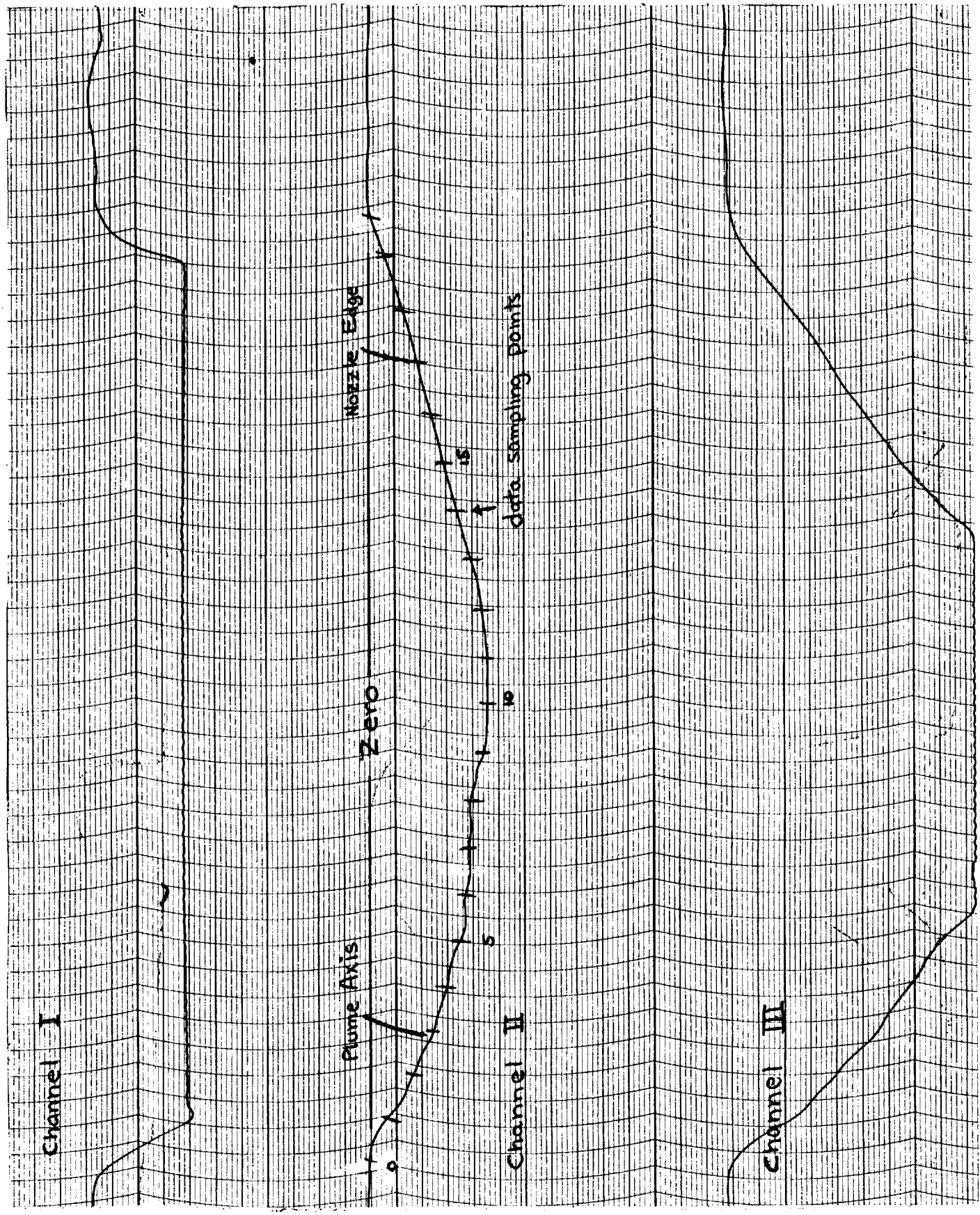




R-6288

FOLDOUT FRAME 1

B1

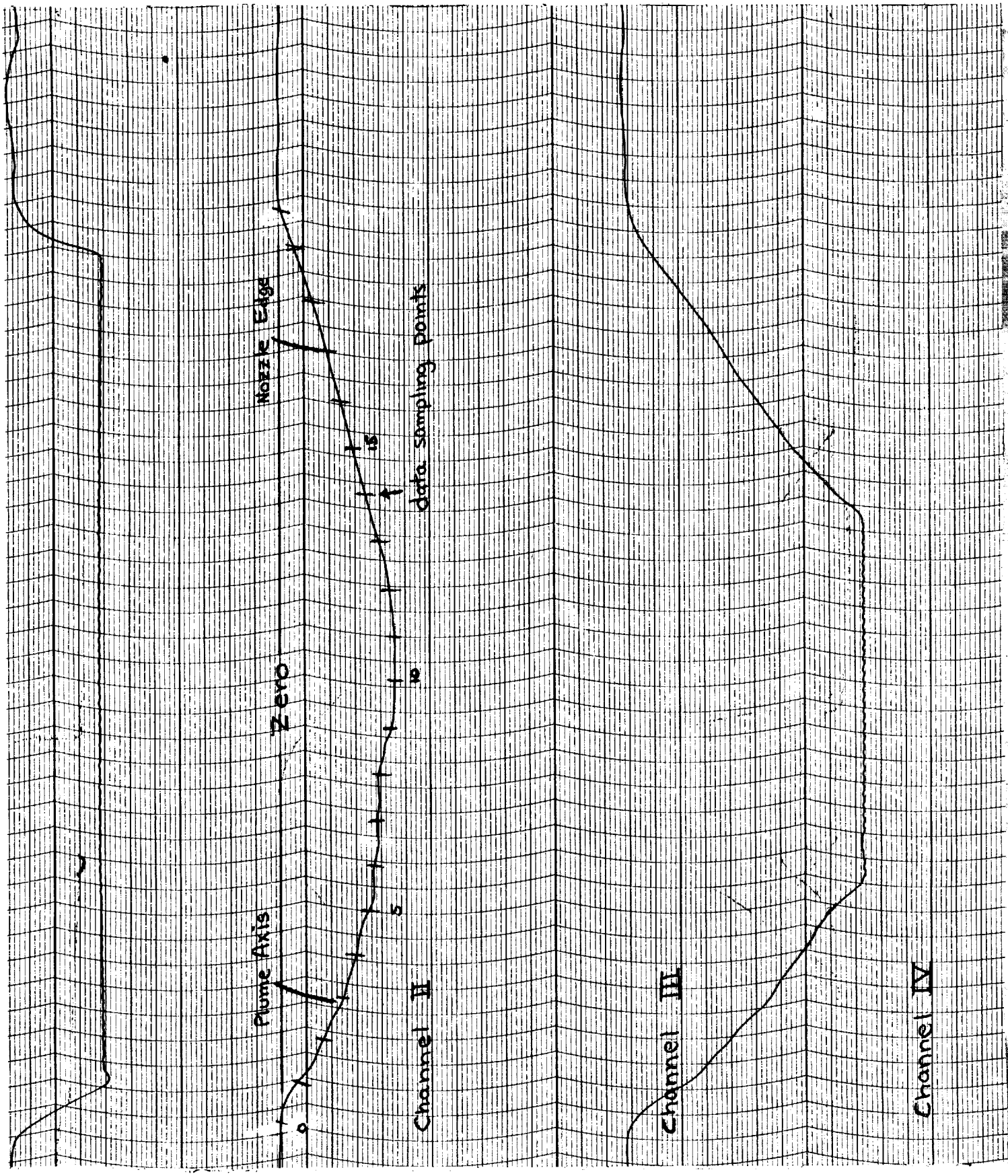


R-6288

FOLDOUT FRAME 2

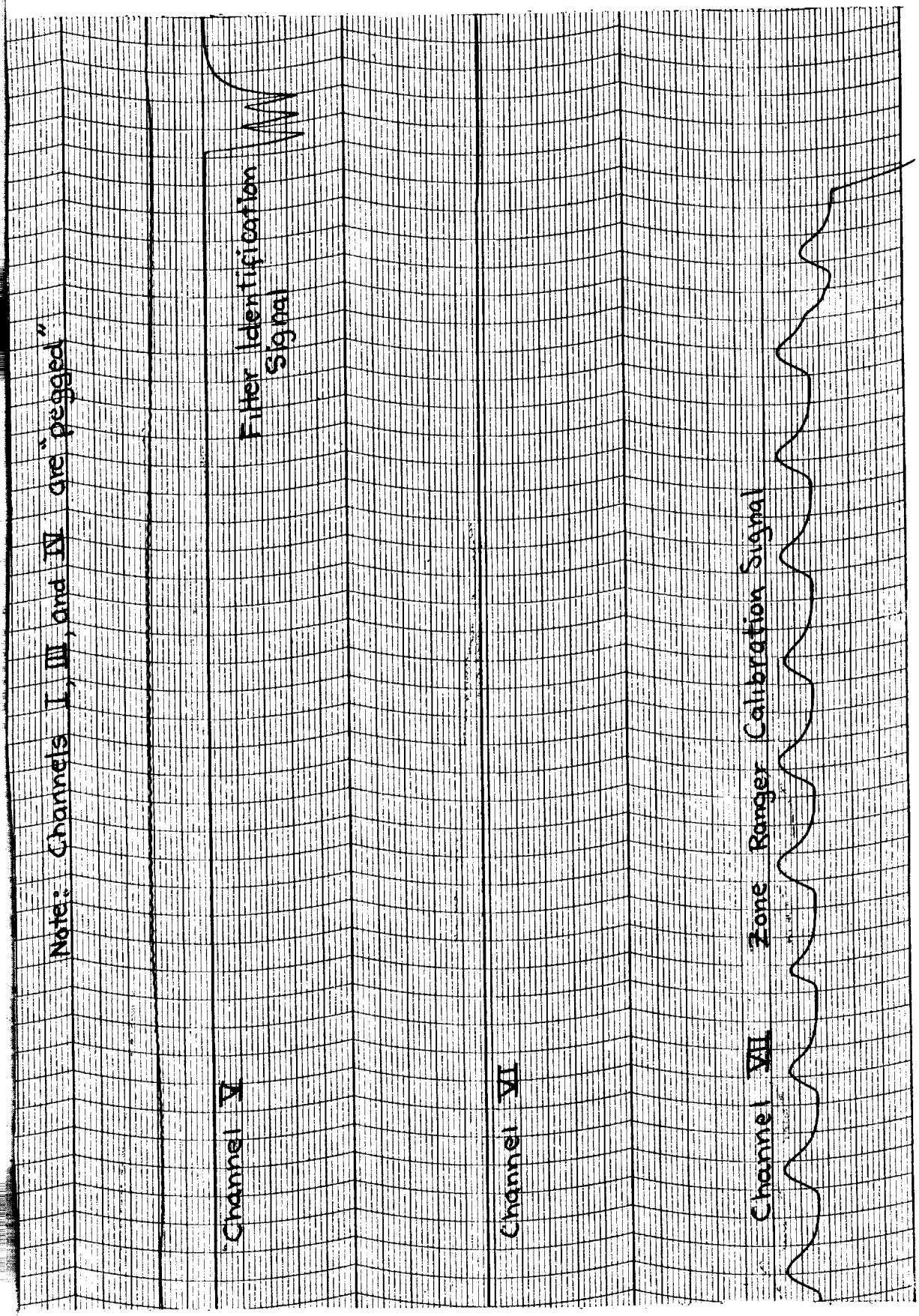


Figure 21. Zone Ranger Trace of Greybody Attenuated by Plume at 4.29 Microns

FOLDOUT FRAME 3

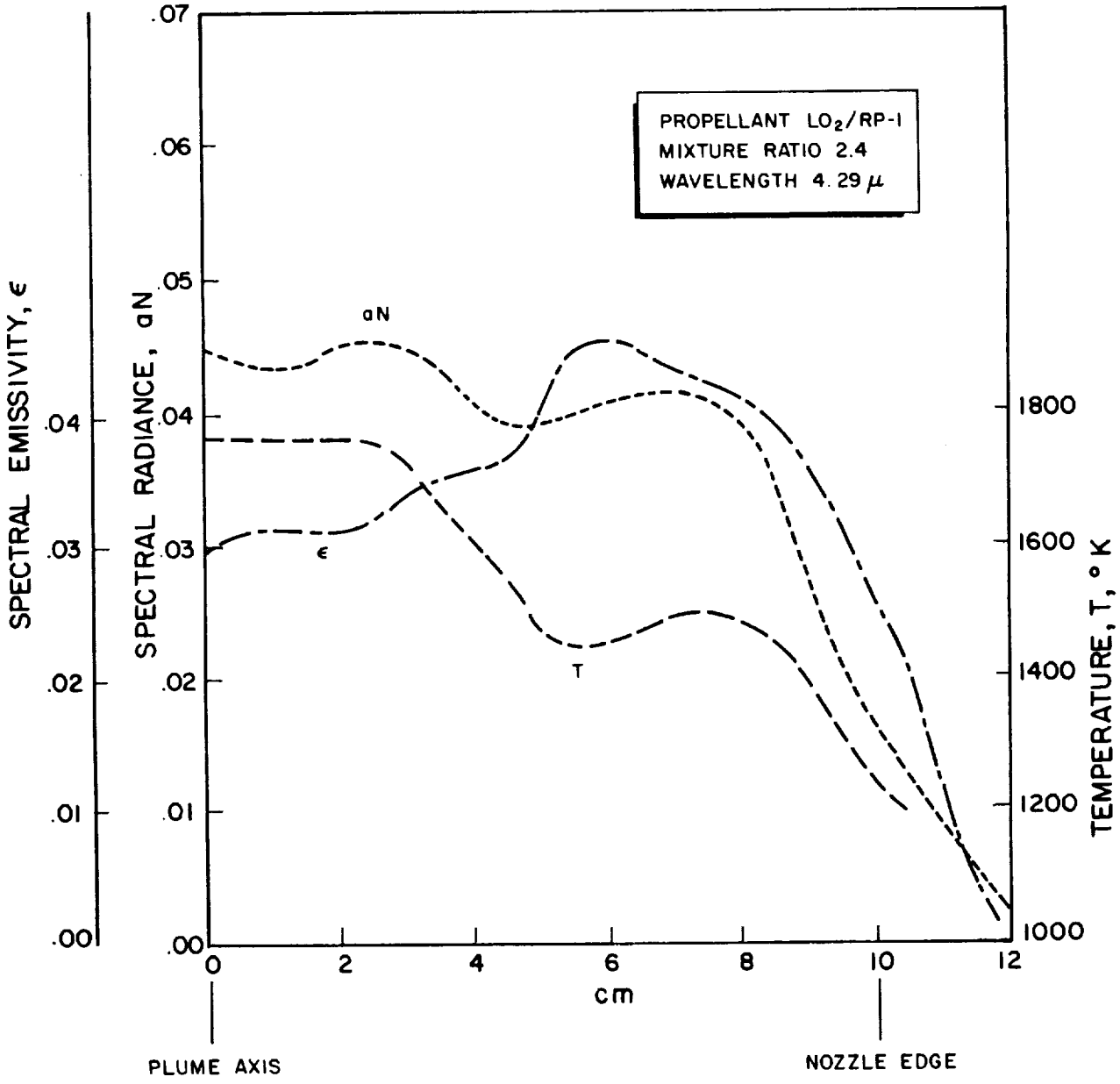


Figure 22. Radial Distribution of Spectral Radiance, Spectral Emissivity, and Temperature at 4.29μ, Mixture Ratio 2.4

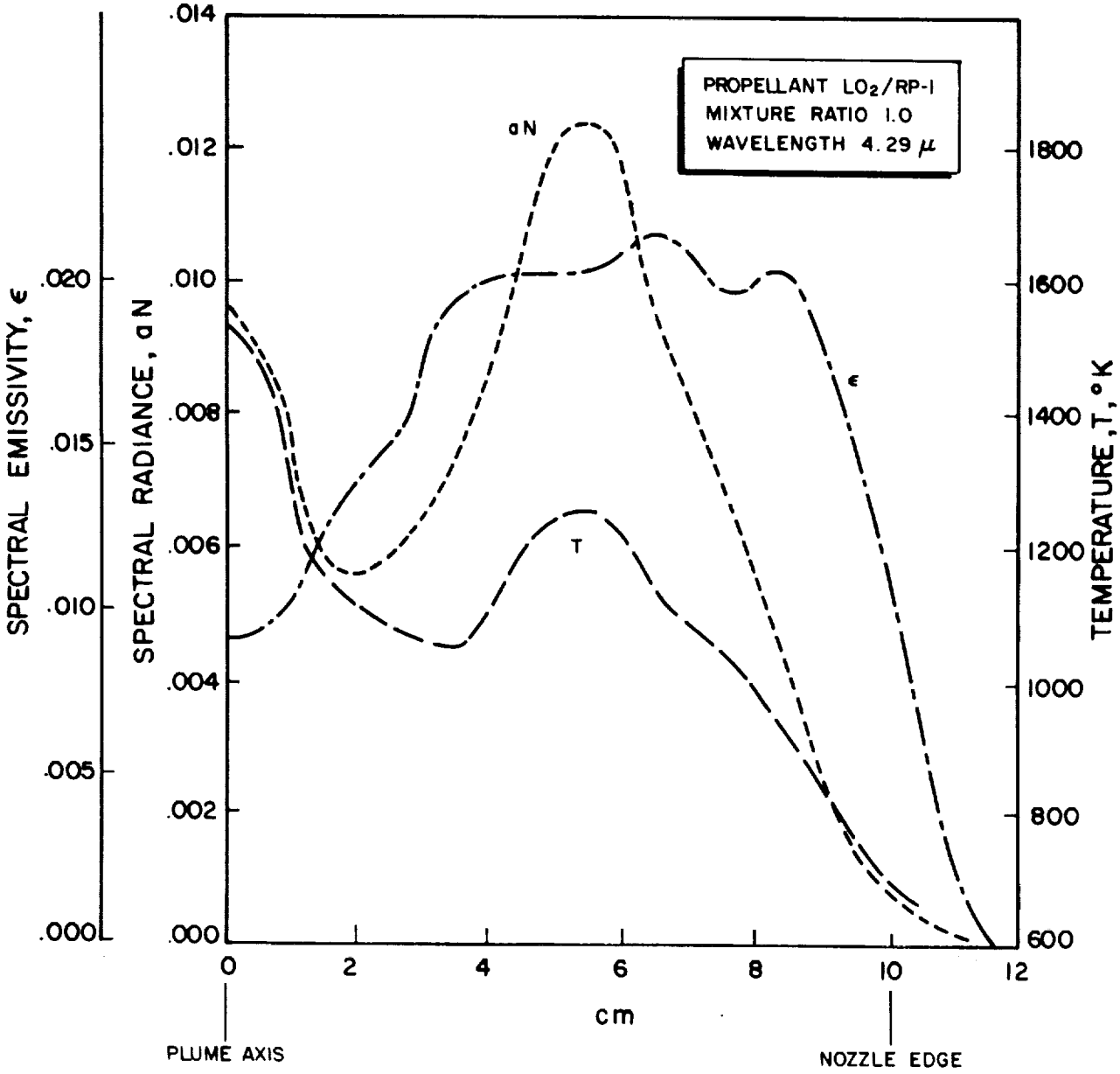


Figure 23. Radial Distribution of Spectral Radiance, Spectral Emissivity, and Temperature at 4.29μ, Mixture Ratio 1.0

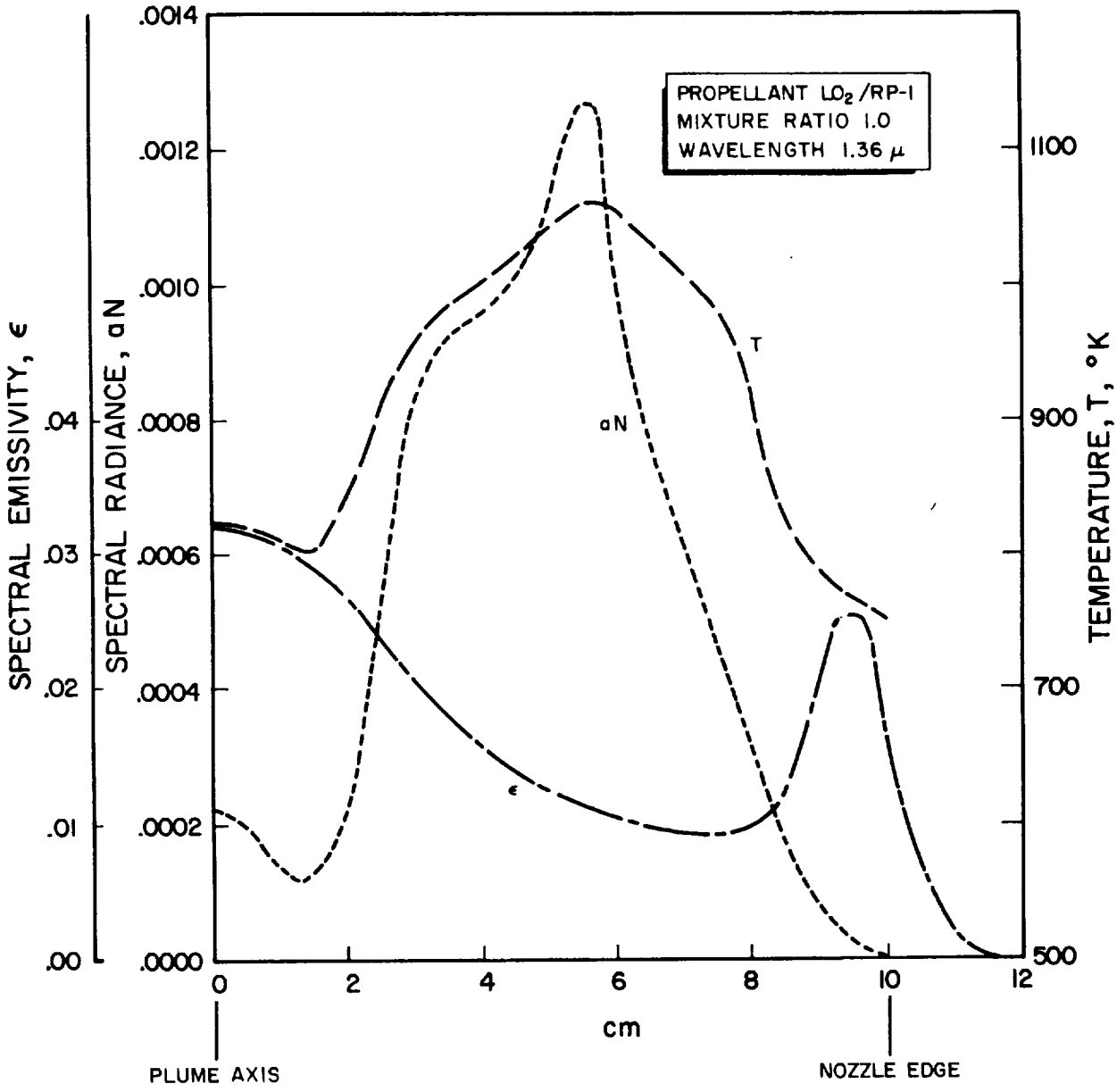


Figure 24. Radial Distribution of Spectral Radiance, Spectral Emissivity, and Temperature at 1.36μ, Mixture Ratio 1.0

Recommendations

No major modifications to the infrared instrumentation system are anticipated. The goal of this portion of the present program - to construct and test an instrument that would spatially scan the exhaust plume in emission and absorption at several accurately reproducible wavelengths during each motor firing - has been achieved.

A few minor modifications, which will serve principally to simplify and increase the accuracy of the data reduction procedure, have been implemented or are under consideration. As mentioned previously, a light-source - coded wheel - photocell unit has been added to the zone ranger system. This unit, which is similar to a typical wavelength marking unit, eliminates errors arising from variation in the recorder chart drive speed or in the zone ranger drive motor speed. The entire data reduction procedure has been carried out by hand for those tests made to date. This is a necessary step in the evaluation of any new experimental system. Portions of the data reduction procedure are amenable to computer calculation and the matrix multiplication has now been programmed for computer calculation. The program allows the plume to be divided into as many as 30 zones. Other portions of the data reduction procedure will also be automated.

The transmission function of the instrument when operating in the spatial scanning mode will be measured. Such a step is necessary to determine whether the zone ranger is affecting the shape of measured line-of-sight curves of radiance and transmittance (an effect identical to that observed when a spectral line is traversed by a slit during conventional spectral scanning). Procedures are available to correct

for the effect of the zone ranger transmission function if necessary. The feasibility of two other modifications, which will simplify the initial handling of the raw data, will be determined. These are (1) the use of a field lens to provide uniform detector illumination during zone radiometry, and (2) conversion of the recorder from a curvilinear to rectilinear mode of operation.

EXHAUST SAMPLING SYSTEM

The sampling problem consists of the development of instrumentation to sample the exhaust of both model and F-1 rocket engines. The purpose of the sampling procedure is to recover particles for size and crystallographic examination and to establish the particle to gas mass ratio.

This was accomplished using a water cooled, cantilever probe which may be inserted into the exhaust jet of a rocket engine. With this probe, sampling of the jet at different locations is possible. The sample is drawn through the probe into an evacuated sampling tank where it is stored for subsequent analysis. The passage through the probe into the tank is as short and direct as possible.

Because of the known tendency of the solid particles in liquid-oxygen/RP rocket engine exhausts to agglomerate, minimal handling of the particles used for size analysis is essential. Therefore, provision is made for catching particles directly on electron microscope viewing grids.

The rocket engine exhaust is sampled during a preselected portion of the test firing and for whatever duration is desired. Prior to the sampling interval a reverse flow of inert gas through the probe serves to prevent entry of exhaust particles and gases into the probe.

The above described system was tested and performed successfully. An exhaust sample was collected from a model F-1 rocket engine of approximately 1000 pounds thrust. The sample was taken during a five-second interval midway through a ten-second duration firing. The probe tip

was located on the engine axis, one-inch downstream of the nozzle exit. The resulting gas-particle sample was analyzed extensively. The results of this sample analysis are presented in this section. In addition, the design considerations of the sampling system are discussed and a detailed description of the system is given.

## Sampling Probe

Probe Environment. Rocket engine exhaust jets are notoriously poor environments for hardware of any sort. The very high velocity, high temperature gases produce extremely high heat fluxes as well as severe mechanical forces on any device inserted into the jet. These factors must be considered carefully in the design of a probe that is to survive such an environment.

As an example, the conditions expected at the nozzle exit of both the model and the actual F-1 engines when operated at a mixture ratio of 2.25 and a chamber pressure of 1000 psi are: a gas static temperature of 1420$^{o}$K, a gas velocity of Mach 3.5 (9,400 ft sec$^{-1}$), a static pressure of 9 psia and a dynamic pressure of 70 psi. These values are based on thermodynamic calculations (Ref. 9 and 10) and on experimental measurements (Ref. 11).

Very little data is available on heat transfer rates under the conditions to be encountered by the probe. Estimates based on long experience with heat transfer measurements in rocket engines ranged from 1000 watts cm$^{-2}$ to "less than 2000 watts cm$^{-2}$" (Ref. 12 and 13). Calculations based on a correlation of Nusselt Number with Reynolds Number given by Dewey

(Ref. 14) yielded a value of 615 watts $cm^{-2}$. The combustion gas transport properties used in this calculation were based on the values given by Svehla (Ref. 15).

Probe Configuration. The configuration chosen for the probe consists of a short entrance section, parallel to the engine axis, supported by a longer section perpendicular to the axis (Fig. 25). The latter section extends through the jet to a support located outside the jet boundary. The probe is fabricated of continuous lengths of tubing with a well rounded bend to facilitate the flow of the sample through it. The entire probe is water cooled with the coolant flowing between the concentric tubes.

This probe configuration has the advantage that the probe tip can be located at any point within the exhaust jet of the model engine simply by repositioning the probe support. The probe is also useable directly on the F-1 engine, provided it does not extend into the exhaust jet beyond the design distance. In the case of the probe fabricated for this program this distance is four inches. A suitable support must also be provided for use on the larger engine.

Probe Stresses. Design requirements stemming from bending stresses caused by the high velocity jet and from the high heat transfer rate are conflicting. From stress considerations alone a thick-walled support of high-strength material is desirable. The conflict arises because the temperature reached by the outer surface of the probe will be proportional to the wall thickness. Thus a compromise must be made on the probe outer wall thickness.

The choice of material to be used for the probe outer wall must also be made with these considerations in mind. The important properties here are thermal conductivity and high-temperature strength. In general, those materials which have high thermal conductivities do not have high strength. For the jet conditions encountered by the probe, copper appeared to be the best choice of material. Its very high thermal conductivity offsets its relatively low strength.

The stresses in the probe derive principally from the aerodynamic forces exerted by the exhaust jet. These forces may be estimated from the dynamic pressure of the jet and the supersonic drag coefficient of the probe. Values of the latter may be found in various works on supersonic aerodynamics. From this information and the exposed length and width of the probe, the bending moment may be calculated. Knowledge of the probe cross-sectional shape makes possible the determination of the moment of inertia. When values of the material constants are included the actual bending stresses in the probe may be calculated.

Preliminary calculations were made for a circular support tube one-inch in diameter with a wall thickness such that a reasonable outer wall temperature is not exceeded at the expected heat transfer rates. The resulting stresses proved too high for the copper material to be used. Therefore, the probe cross-section was designed to reduce these stresses.

The width of the probe support normal to the jet was made $\frac{1}{2}$ inch, while the dimension parallel to the jet was increased from $\frac{1}{2}$ inch at the probe tip to 1-3/8 inches nearer the cantilever root. In this way, the moment of inertia is increased greatly in that area where the bending moment is large. This, coupled with the smaller width presented to the

jet as well as a slightly reduced drag coefficient, reduced the calculated stress levels sufficiently to provide a sizable safety factor.

The probe discussed here was designed to be used with a diffuser of diameter considerably larger than the exhaust jet. Therefore, the probe support had to be located some distance away from the jet boundary. For this reason the copper probe body was joined to a probe extension of heavy wall circular steel tubing with its higher strength. In general use, the probe support would, of course, be located as close to the jet boundary as practicable.

Because of the relatively great length-to-depth ratio of the probe support section the shear stresses are small compared to the bending stresses. There is an additional tensile stress in the probe wall due to the pressure of the cooling water flowing through it. Within the limits imposed by heat transfer considerations, discussed in the next section, the coolant flow paths were designed to minimize this pressure. Consequently, this stress is also small compared to the bending stresses.

Since the probe changes temperature, thermal stresses must also be considered. The probe tip is not restrained; hence, there is no thermal stress due to overall temperature rise. However, there is a temperature gradient in the radial direction in that the outside of the tube wall is considerably hotter than the inside. This gives rise to compressive stresses on the outside and tensile stresses on the inside. Even though these stresses may be large at the surfaces in question they are effective only over very small distances and disappear when averaged over the entire wall thickness.

Probe Heat Transfer. The heat transfer rate to the probe from the rocket engine exhaust jet is nearly independent of the probe wall temperature. This is so because the jet recovery temperature is very much higher than the allowable probe wall temperatures; hence, changes in the latter have relatively little effect on the temperature difference, which is the driving force for heat transfer. If it is assumed that the inside of the probe wall remains at the relatively constant temperature of the coolant, the outer surface temperature is determined by the wall thickness and thermal conductivity. On this basis a 1/8 inch thick copper wall was chosen. At the maximum expected heat transfer rate there should result an outer wall temperature no greater than 400°F. Since somewhat higher wall temperatures are permissible, it is apparent that an increase in wall thickness is possible, should it prove necessary for strength purposes.

The above considerations have assumed that the inside of the probe remained at low temperatures. This, in turn, implies adequate heat transfer rates to the coolant. The expected total heat transfer to the probe is small enough so that relatively low volumetric flow rates will be sufficient to maintain low temperature. However, a certain minimum linear flow velocity is necessary to prevent film boiling with its consequent drastic decrease in heat transfer to the coolant. When this occurs the tube wall rapidly rises to high temperatures and burn-out occurs. Hines (Ref. 16) has given a correlation between the heat transfer rate and the "burn-out velocity". As would be expected, the lower the static pressure of the coolant the higher the required velocity. For example, at the maximum expected heat transfer rate, a velocity of 32 feet per second is required at 50 psi, 18 feet per second at 100 psi, and 7 feet per second at 200 psi. The design pressure chosen for the

probe coolant was 200 psi together with a linear velocity considerably in excess of the minimum.

To simplify the probe design by eliminating the need for a coolant return path, it was decided to allow the coolant flow to exhaust directly into the rocket engine jet through a number of holes located near the probe tip. This water ejection also furnishes added film cooling of the probe exterior surface. The exhaust holes were positioned around the tip to give uniform distribution and were sized to generate a pressure drop of 200 psi at the design flow rate of 20 gallons per minute.

Probe Sample Flow. The purpose of the probe is to sample the rocket engine exhaust jet to determine the relative concentration of exhaust constituents which are important to the optical character of the exhaust. To do this successfully it is necessary to assure that the gas-particle mixture entering the probe is the same as that existing at that point of the jet. In subsonic flow this is achieved by isokinetic sampling; in supersonic flow it can be insured by designing the probe entrance so that the shock wave is attached to the probe inlet. This is necessary because the curvature of a detached bow shock tends to cause separation of particles and gas by diverting a certain fraction of the gas flow from the inlet while a higher portion of the particles continue into the probe entrance because of their greater inertia. The relative concentration of the particles is thus falsely enhanced.

Fortunately, at velocities as high as those to be found at the F-1 nozzle exit it is relatively easy to obtain an attached shock even for moderately blunt bodies (Ref. 17). A probe nose angle 60 degrees from

the axis was chosen.

It is also important that there be no interference with the probe flow due to the probe support. Here again, at the high jet velocities in question, the shock stand-off distance is small (Ref. 18) and a small tip projection from the support is sufficient. The present probe tip projects $\frac{1}{2}$ inch from the leading edge of its support.

Probe Fabrication. Two probes, designed according to the considerations given in the preceding section, were fabricated. The outer copper tube was swaged into the shape shown in Fig. 25 and Fig. 26. The inner copper tube was bent to conform to the curvature of the outer tube at the tip. A probe tip, also of copper, was machined to fit the annular space between the ends of the tubes and was welded in place. The coolant outlet holes were then drilled around the periphery of the probe tip. A tube spacer for support of the inner tube was introduced at the junction of the copper tube with the steel tube. Fig. 27 is an X-ray photograph of the two tubes. Probe number 1 was used in the tests discussed in the following section.

The cantilever, probe-support block (Fig. 26) is located well outside the rocket engine exhaust jet boundary. This support member also serves to introduce the coolant flow to the base of the probe. The inner tube, carrying the sample gases and particles, passes directly through the support block and into the sampling tank.

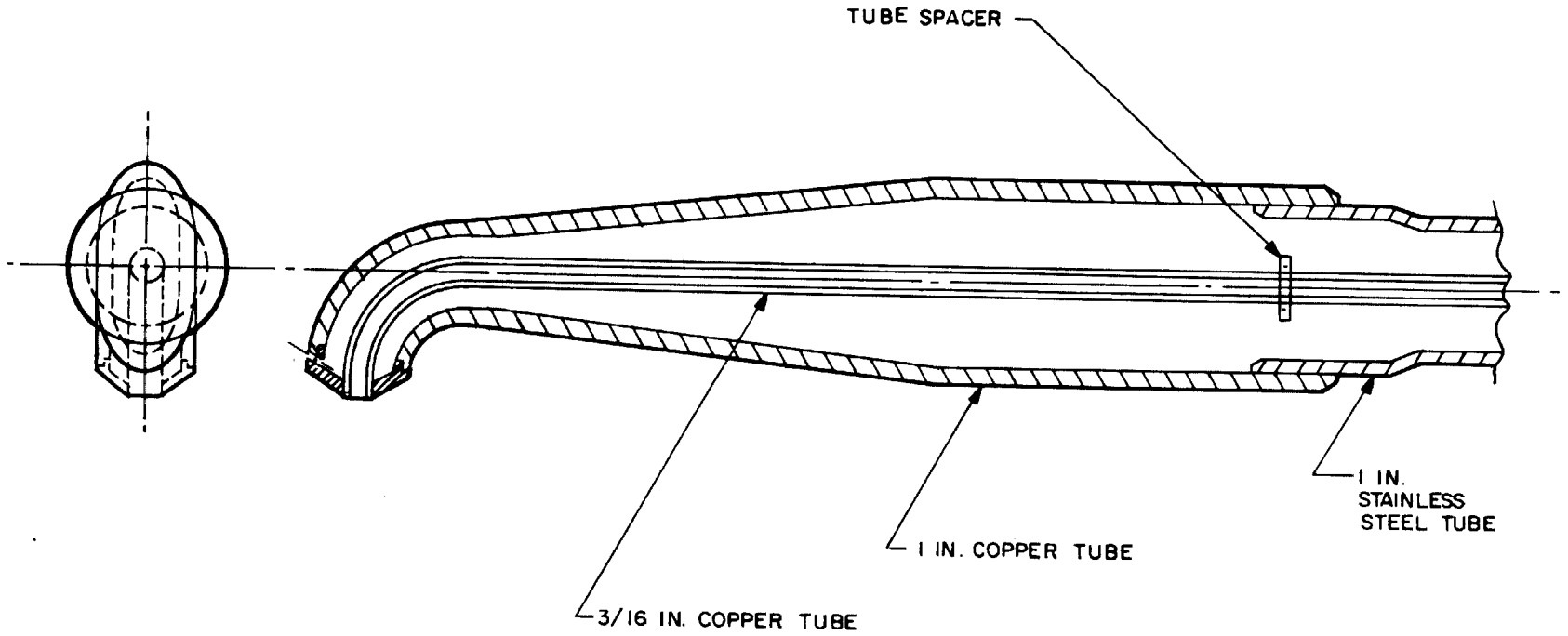


Fig. 25. Sampling Probe Cross-section

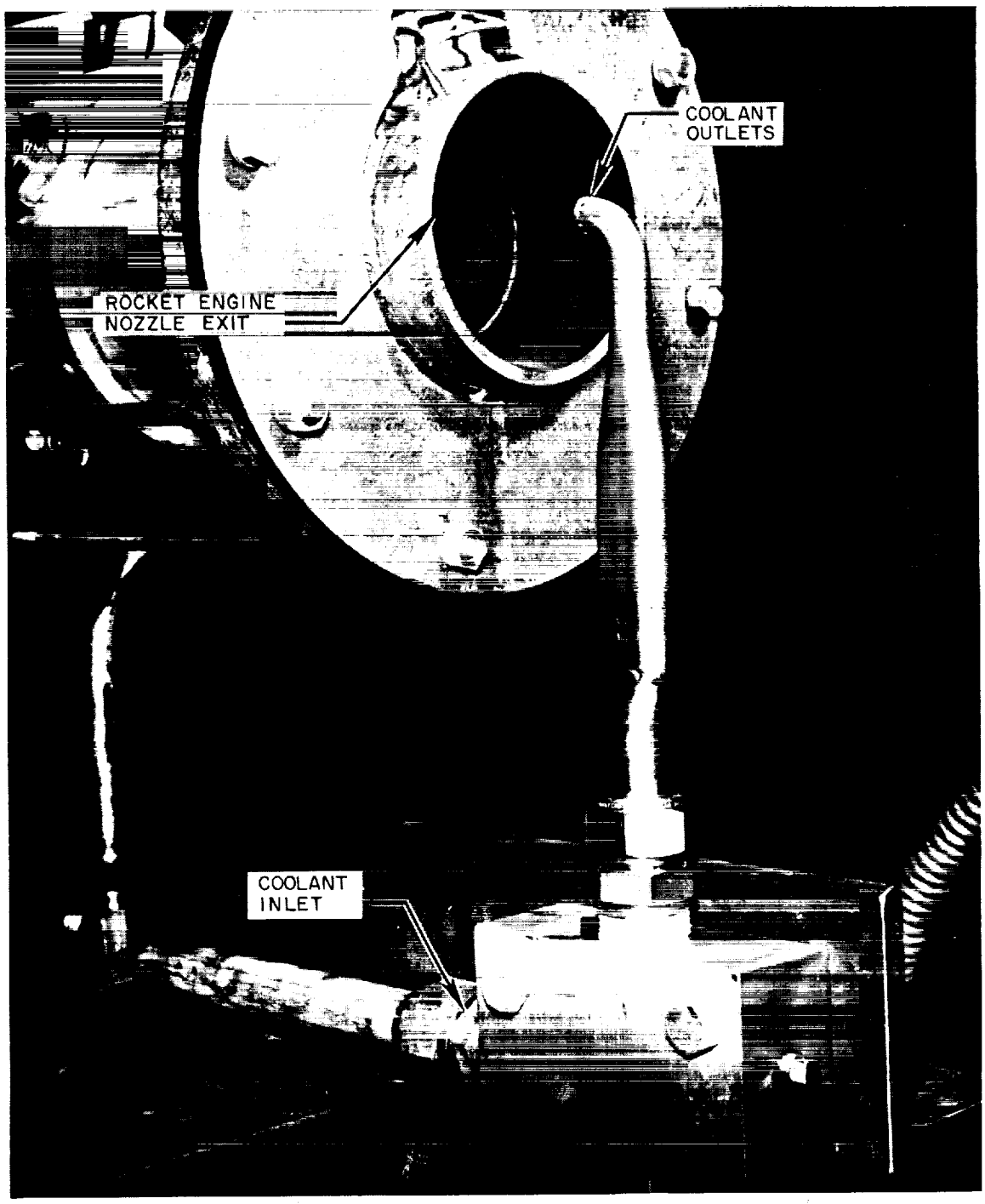


Figure 26. Sampling Probe Mounted at Rocket Engine Exit

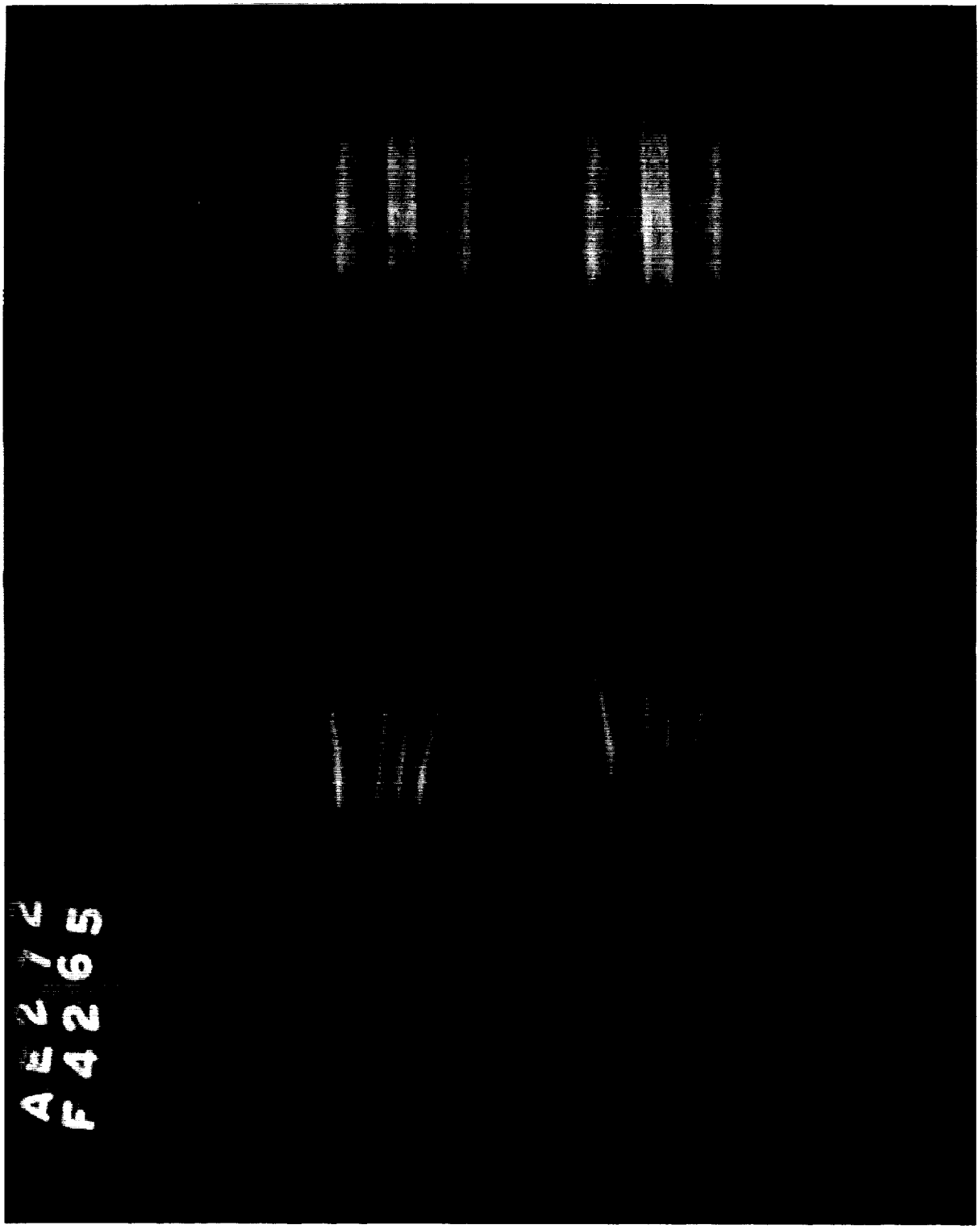


Figure 27. X-Ray of Sampling Probe

Probe Test Results. The probe, as well as the rest of the sampling system, was tested during a single F-1 model rocket engine firing. The engine was fired at a chamber pressure of 1000 psi at a mixture ratio of 2.25.

The probe successfully withstood the rigors of the exhaust jet with no ill effects. A sample was successfully taken. Fig. 28 and 29 are successive frames of high speed motion pictures taken during the test. The important features of the flow around the probes are apparent. In particular, the change in the stagnation region of the probe tip with and without the purge gas flowing can be seen. The photograph of the latter condition indicates that the shock is indeed attached to the probe tip during the time of sampling.

A considerable amount of solid material was deposited on the outside of the probe (Fig. 30). This very probably is a deposition of products of the ignitor reaction. The ignitor is a mixture of triethylboron and triethylaluminum.

Soot deposits were found throughout the length of the probe inner tube indicating that there is a tendency to separate out the particles in the sample as it passes through the probe to the sampling tank.

## Sampling System

Figure 31 is a schematic of the entire sampling system. The sample passes through the probe directly into a sampling container through 2 valves. These are $\frac{1}{4}$ inch diameter ball valves which provide straight through flow for the sample when they are open. A similar arrangement

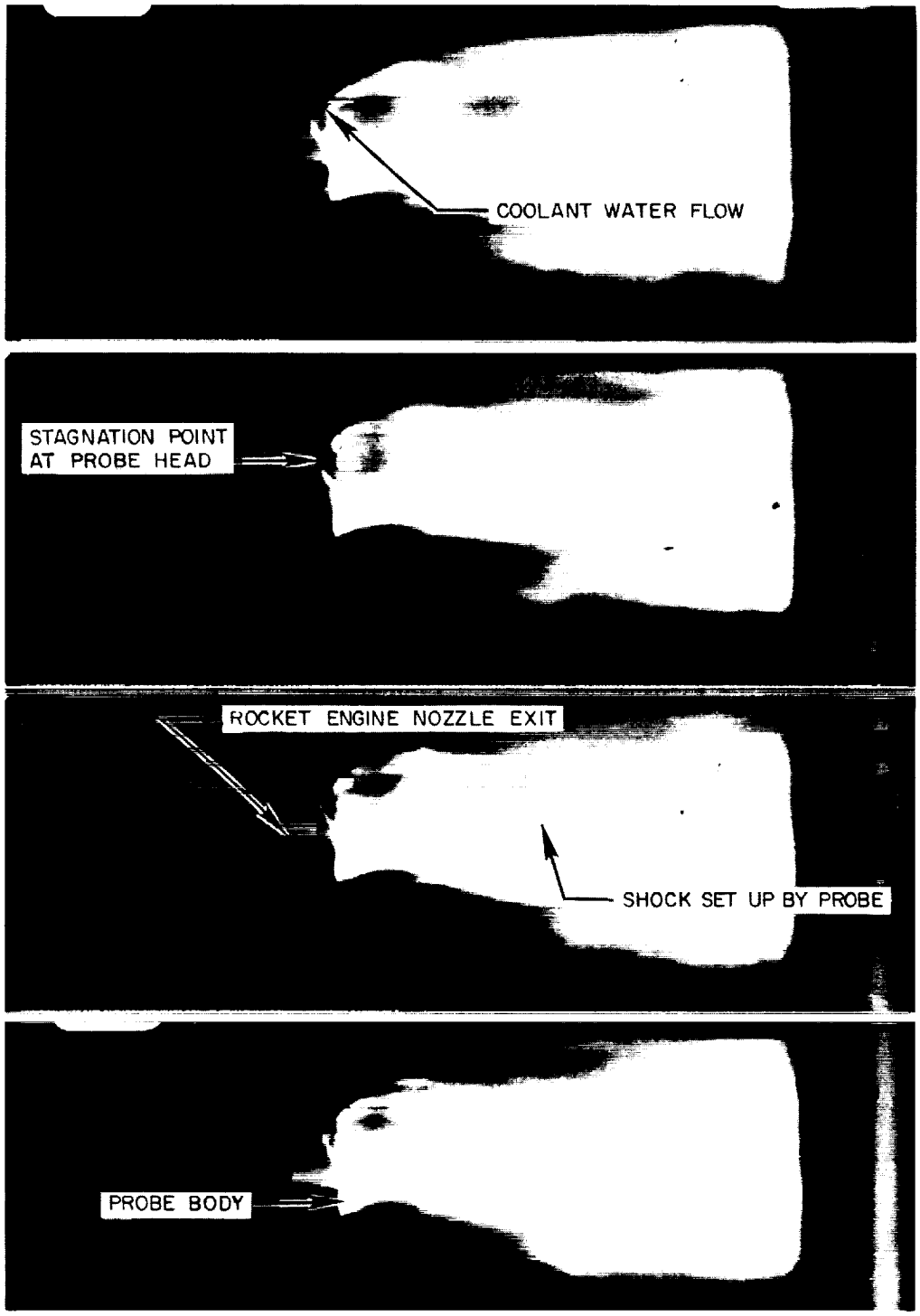


Figure 28. Probe in Exhaust Jet, Purge on
(Pictures taken at 1 Millisecond Intervals)

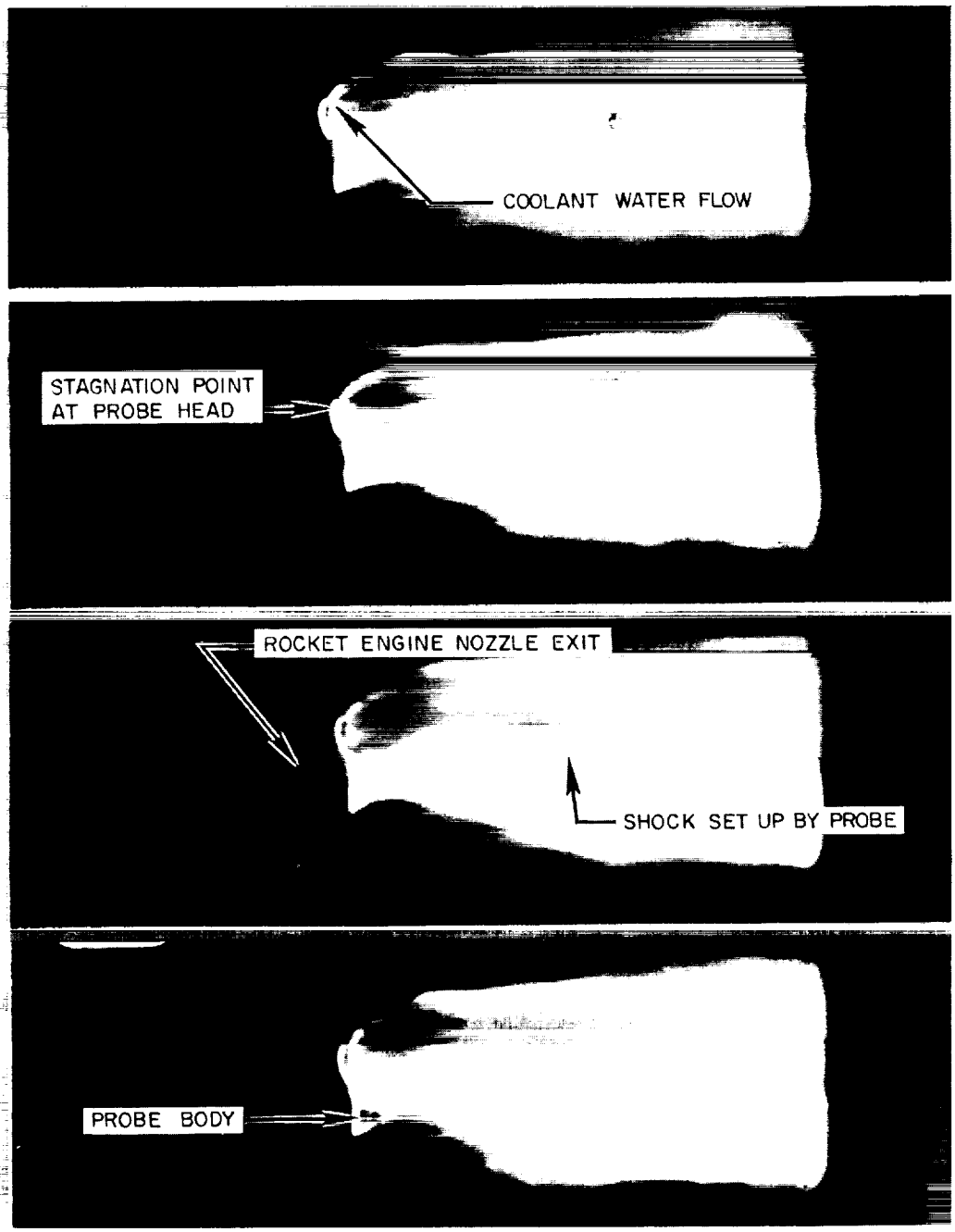


Figure 29. Probe in Exhaust Jet, Purge Off,
(Pictures Taken at 1 Millesecond Intervals)
R-6288

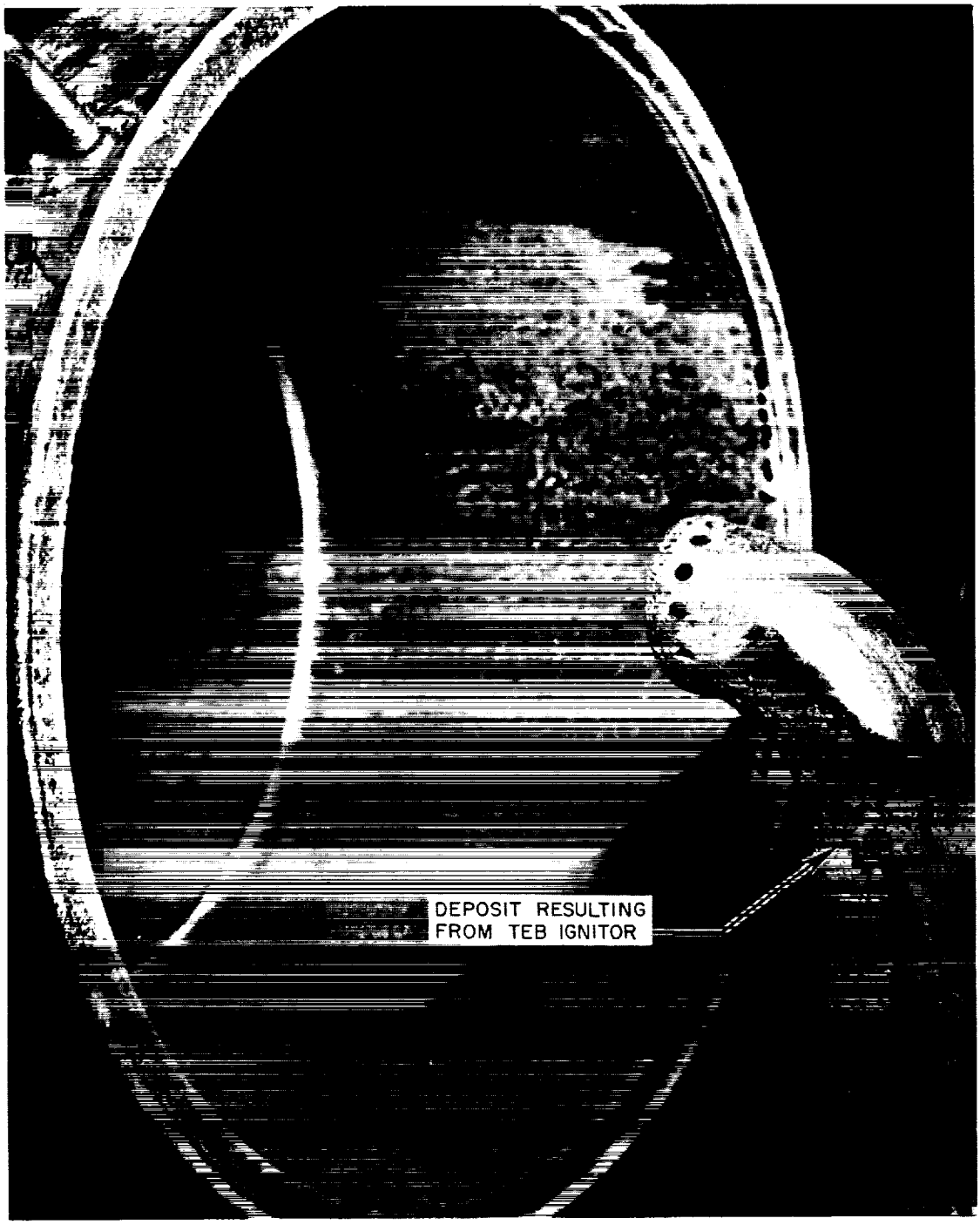


Figure 30. Probe Tip After Engine Firing

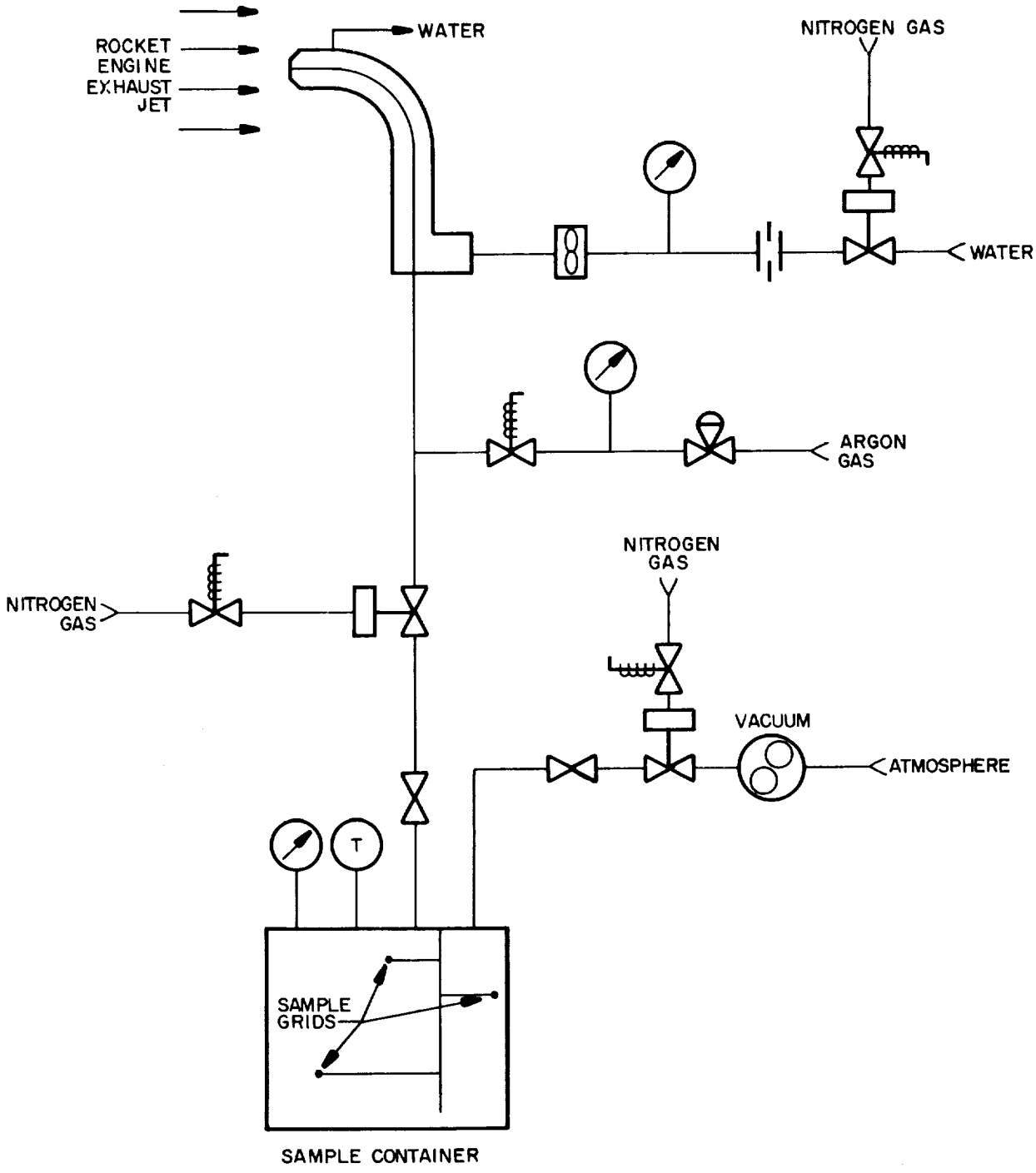


Figure 31. Schematic of Sampling System

is used on the tank outlet. The hand valves are inserted in the system so that the sampling tank can be isolated and then removed from the remainder of the sampling system for transportation to the laboratory for analysis.

Temperature and pressure gages are provided for the tank to furnish information about the quantity of the collective sample. These are shown in Fig. 32. Figure 33 presents an overall view of the sampling system including the probe and its support.

Operation of the inert gas purge and water coolant systems is straightforward and their place in the sequence of operation is given next.

Operating Sequence. Both hand-operated valves and the outlet gas-operated valve are open at the start of a test sequence. The inlet gas-operated valve is closed, and the vacuum pump is on. Before the test the outlet gas-operated valve is closed, and the argon purge is turned on. Next the cooling water is turned on just before the rocket engine is ignited. At the start of the sampling period the purge is turned off and the inlet gas-operated valve opened simultaneously. At the end of the sampling period, these two operations are reversed. The rocket engine is then shut down, the coolant flow turned off and the argon flow stopped. The two hand-operated valves are then closed, and the sampling tank is ready to be removed from the system.

The following sketch shows graphically the sequence of the automatically controlled events in the above sequence. The presence of the bar indicates open or "on" condition.

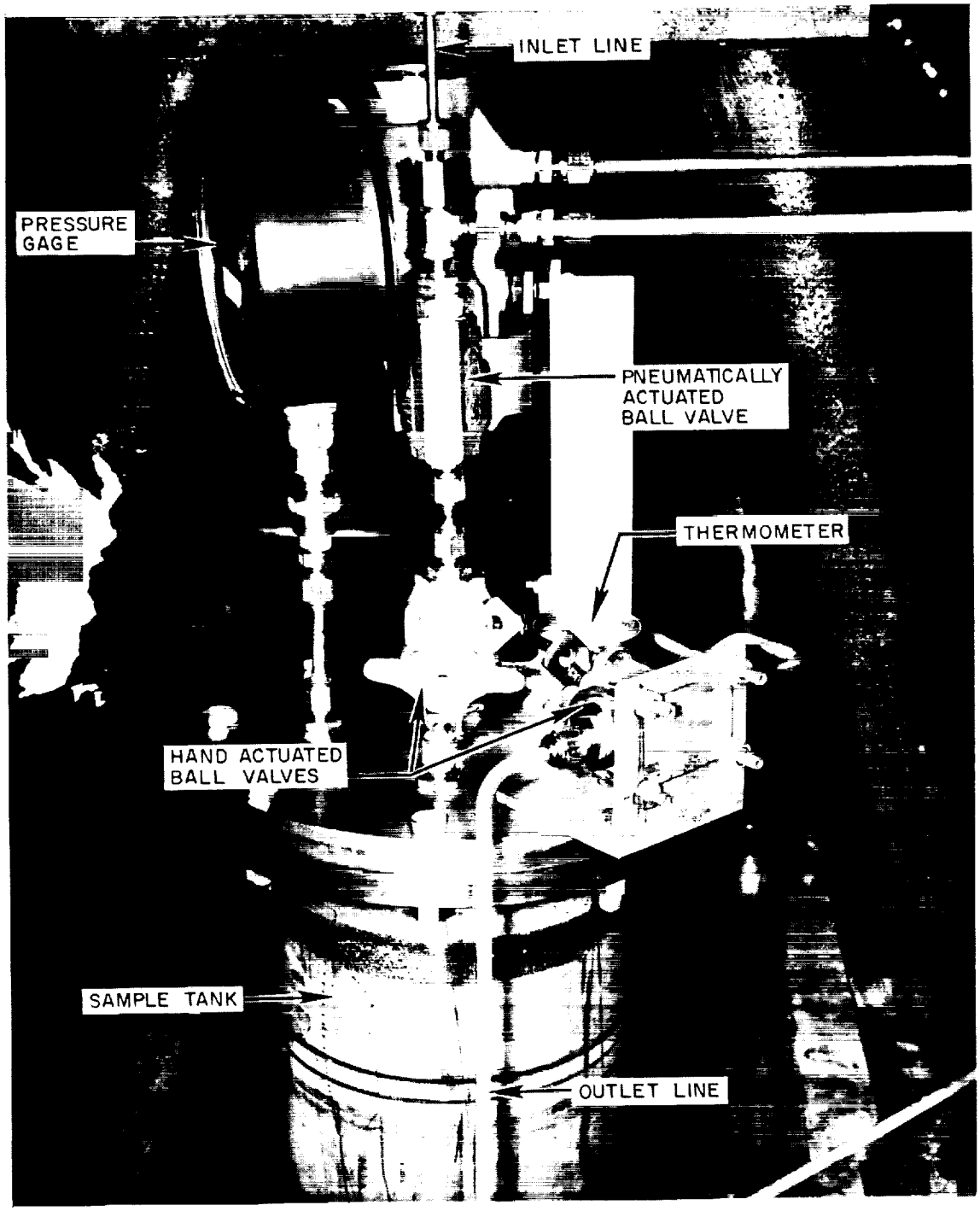


Figure 32. Sampling Tank with Valves and Gages

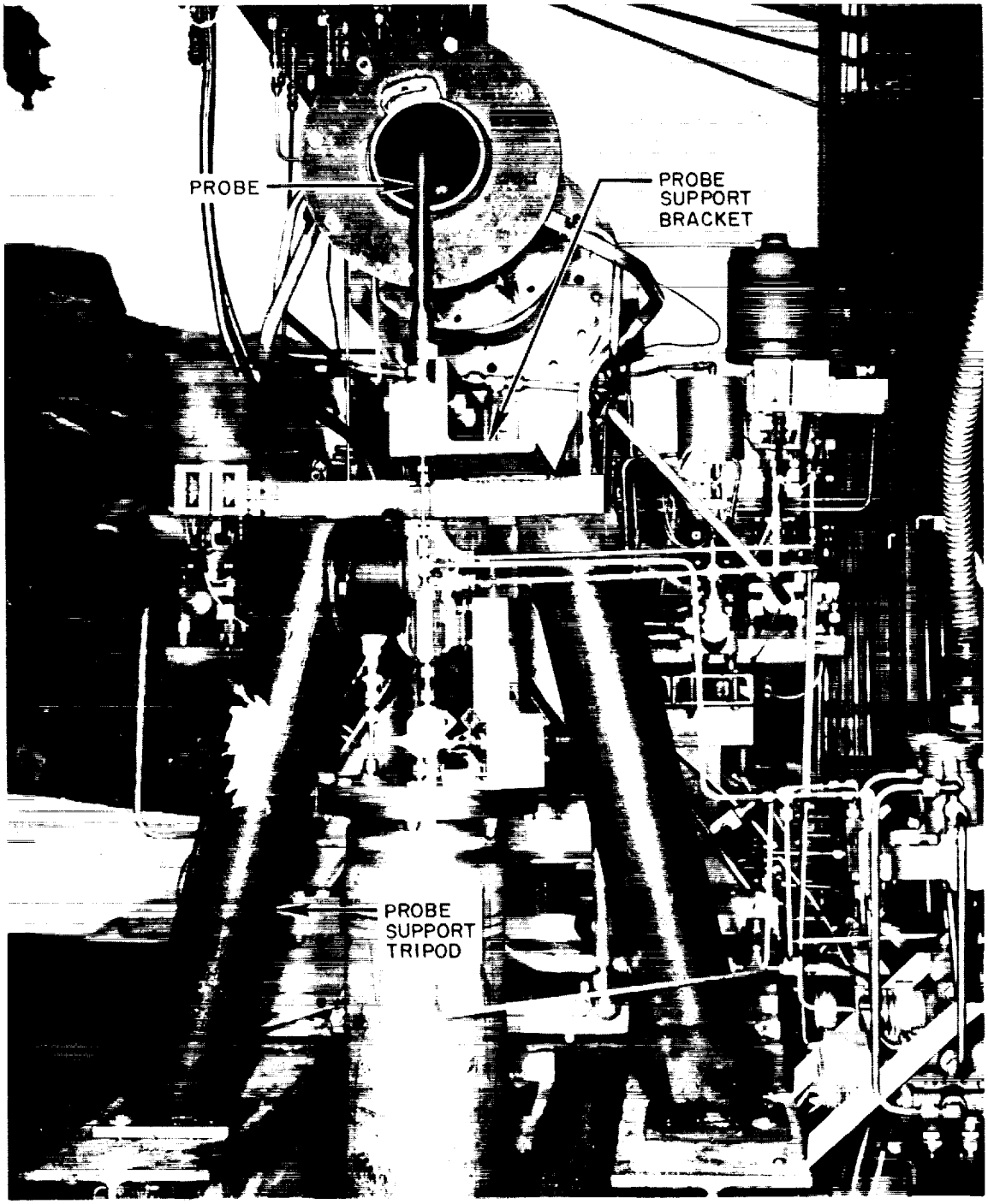


Figure 33. Complete Sampling System

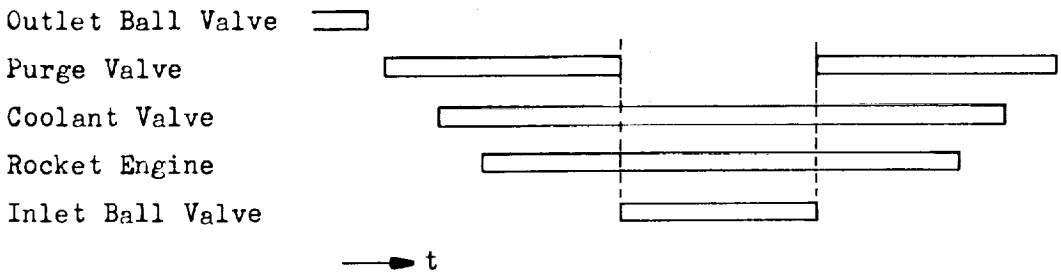


Sampling Tank. The sampling tank furnishes a space for the collection of the sample drawn from the rocket engine exhaust. The tank used in this experiment has a volume of 12 liters. Since the purpose of the experiment is to analyze the sample, particularly with reference to the particulate matter, the tank was designed to facilitate this, the tank is a circular cylinder closed by flat plates at each end. This provides easy access to the interior for removal of solid material. In addition, the inside surface of the tank was given an extremely smooth finish by means of honing, lapping and finally, optically polishing. The purpose, again, was to facilitate removal of solid particles in the sample.

One facet of information desired about the particulate matter in the sample is the size distribution of the particles. Since the soot particles are known to agglomerate readily, provision was made to avoid all handling of the particles prior to examination for size. This was done by providing a number of electron-microscope viewing grids throughout the tank interior. A total of 4 grids, with different orientation to the tank axis, were located at the top, middle and bottom of the tank. Locations at the center and near the outer edge were also represented. The purpose of this distribution of locations was to determine whether different size particles settled preferentially in certain areas of the sampling tank.

The electron microscope grids consisted of 200 mesh stainless steel screens, 1/8 inch in diameter, on which a 20 Å carbon film had been deposited. These grids could be removed directly from their holders (Fig. 34) and inserted in an electron microscope without disturbing the particles in any way.

Sampling System Test Results. A sample containing gas and solid particles was successfully collected from the exhaust of the model F-1 motor. The soot was easily removed from the polished surface of the tank. The soot collecting electron microscope grids also worked satisfactorily. However, the sampling tank proved to have a slow leak which apparently admitted air to the sample container prior to analysis. This raised the possibility of ambiguous results in the quantitative analysis of the sample gas constituents.

## Sample Analysis

Gas Analysis. The collected sample, as it entered the sampling tank, was undoubtedly composed of gases and solid particles. However, after cooling to room temperature in the sampling tank liquids were expected to be found due to condensation. Therefore analysis for all three phases was provided for.

The analysis of the gases (Ref. 16) included a mass spectrometer analysis of a small subsample. From this the various species present as well as their mol percentages were determined. The total quantity of gases present was calculated by means of the perfect gas law using the measured temperature and pressure along with the known volume of the

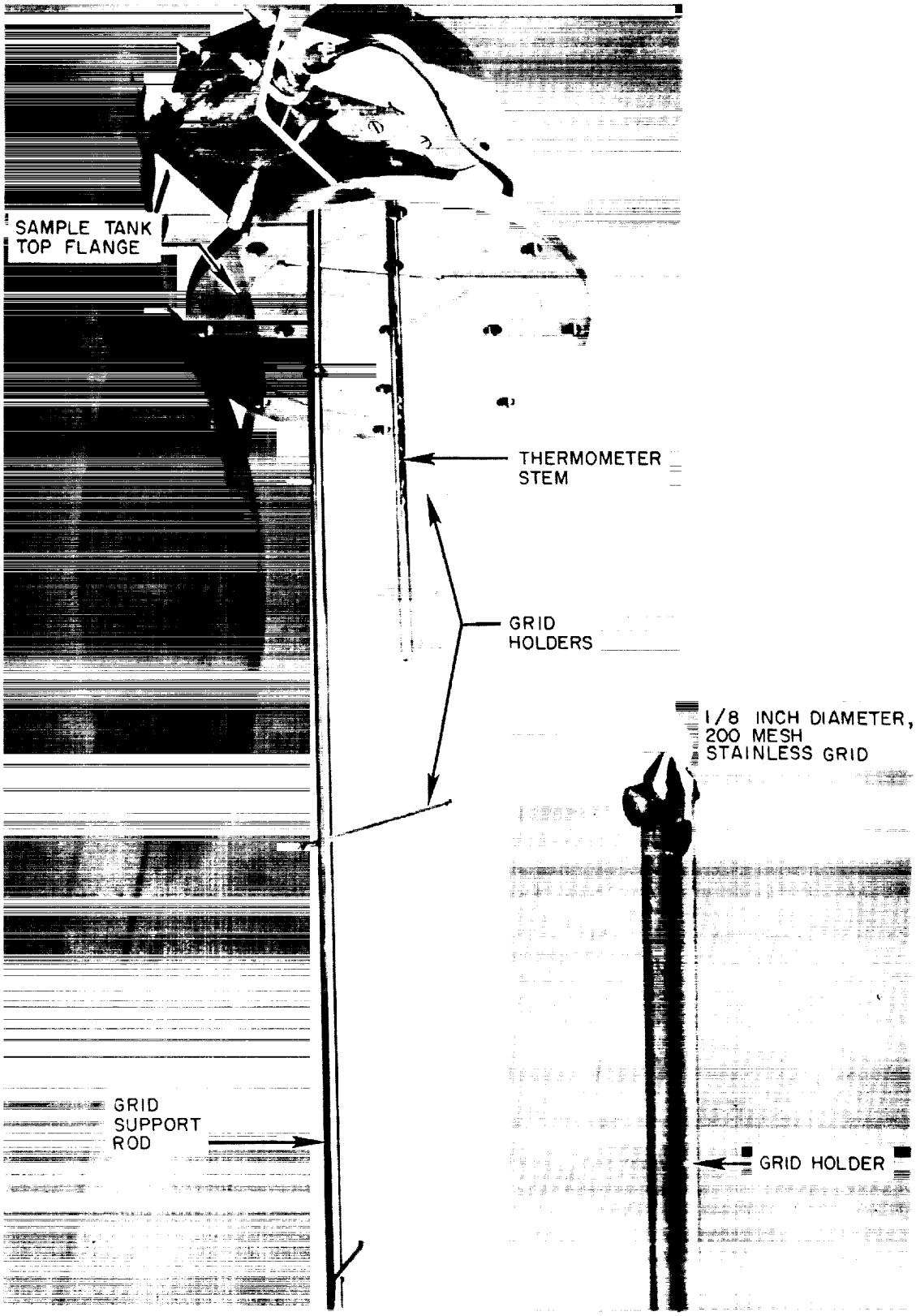


Figure 34. Sampling Tank Grid Support Arrangement

sampling tank. In addition to the species expected several hydrocarbons were found.

Liquids Analysis. After the gases had been pumped out of the sampling tank, the liquids were pumped out and collected in a cold trap. They were then analyzed by Karl Fisher titration (for water) and by mass spectrometer. It was determined that at least 98% of the liquid was water.

Solids Analysis. After having pumped out the gases and liquids, air was admitted to the sampling tank and it was opened. Figures 35 and 36 show the appearance of the particulate deposits at various locations within the tank. The amount of soot deposited on the top plate of the tank was far less than that deposited on the bottom. It should be mentioned here that the gases were pumped out through a filter because it was anticipated that some particles would still be suspended in the gas even though it was several days after the collection of the sample. However, no deposits were found on the filter.

The solids were removed from the tank and from the interior of the probe. The probe had to be brushed out, and the tank was washed out with a solvent. Analysis of the two samples revealed 95.8% carbon with 1% hydrogen for the tank sample and 73.2% carbon and 3.4% hydrogen in the probe sample.

An X-ray diffraction analysis was performed on the same samples (Ref. 20) resulting in the finding that the tank sample consisted of a very "low-structure" thermal carbon with no measurable amount of any other crystalline

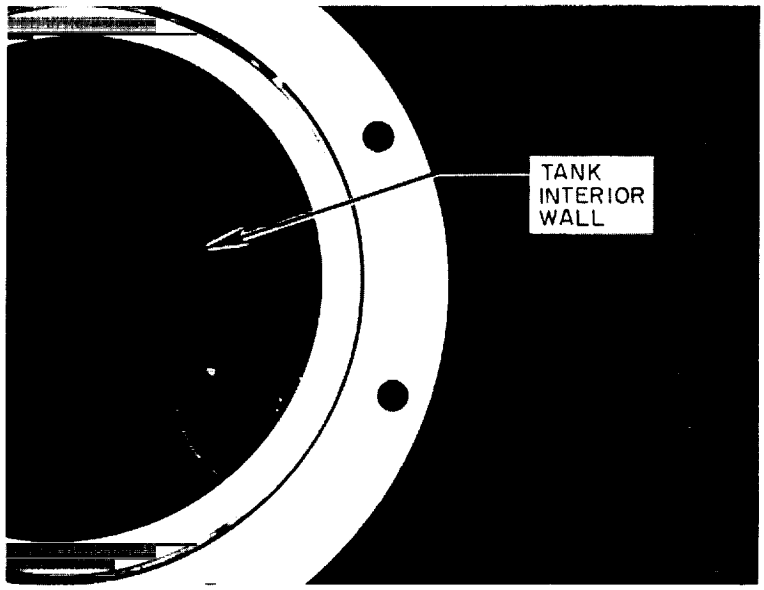


Tank Interior

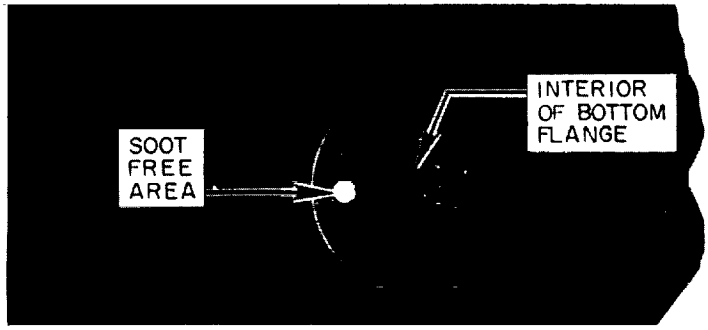


Tank Interior

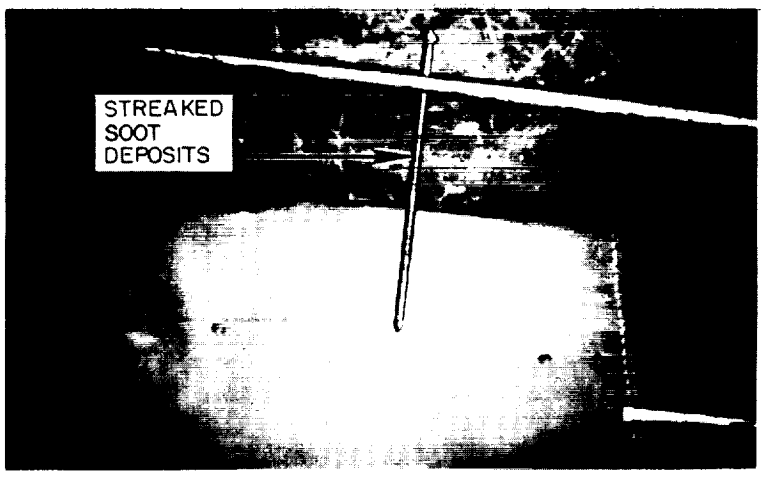


Grid Support Rod

Figure 35. Sampling Tank with Soot Deposits, B

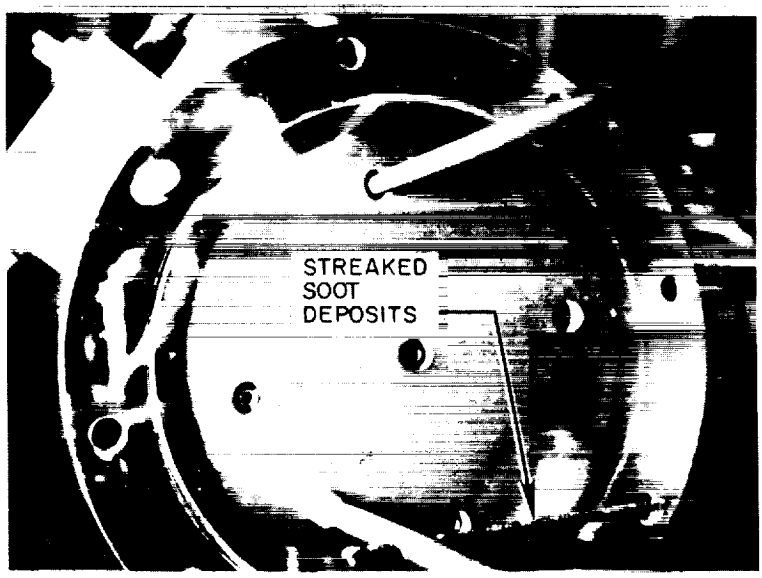


Interior of Top Flange

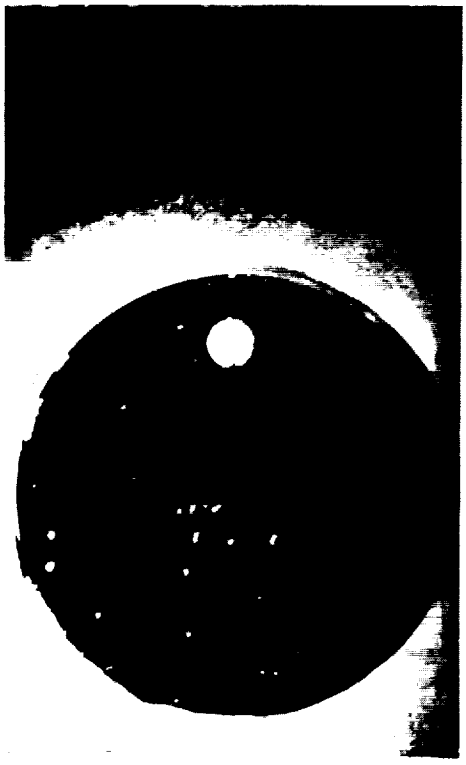

Interior of Bottom Flange,
Top Lighted

Interior of Bottom Flange,
Edge Lighted

Figure 36. Sampling Tank with Soot Deposits, B

material. The sample from the probe was similar, except that it contained less than 10% of contamination made up of other crystalline material. This appears to be a cubic material with a lattice parameter a = 4.25 Å. This material has not been identified.

Several electron micrographs were made of representative areas on each of the electron microscope grids (Ref. 20). Figure 37 is typical of these. The analysis of these micrographs indicates a high state of agglomeration of the soot particles. Individual particle size distribution appeared to be the same on all grids. Counts of particle size (where possible) show a range of diameters between 100 Å and 500 Å with a maximum apparently at 300 Å.

Summary of Analysis Results. The following table is a summary of the mol percentages of the various species found in the sample. The amount of carbon used is based only on that portion found in the sampling tank. Presented along with these experimental results are theoretically expected values for frozen and shifting equilibrium (Ref. 9).

The particle-to-gas mass ratio lies between 2.46% and 3.17%. These values are arrived at using the solid deposits in the tank only and the total solid deposits respectively.

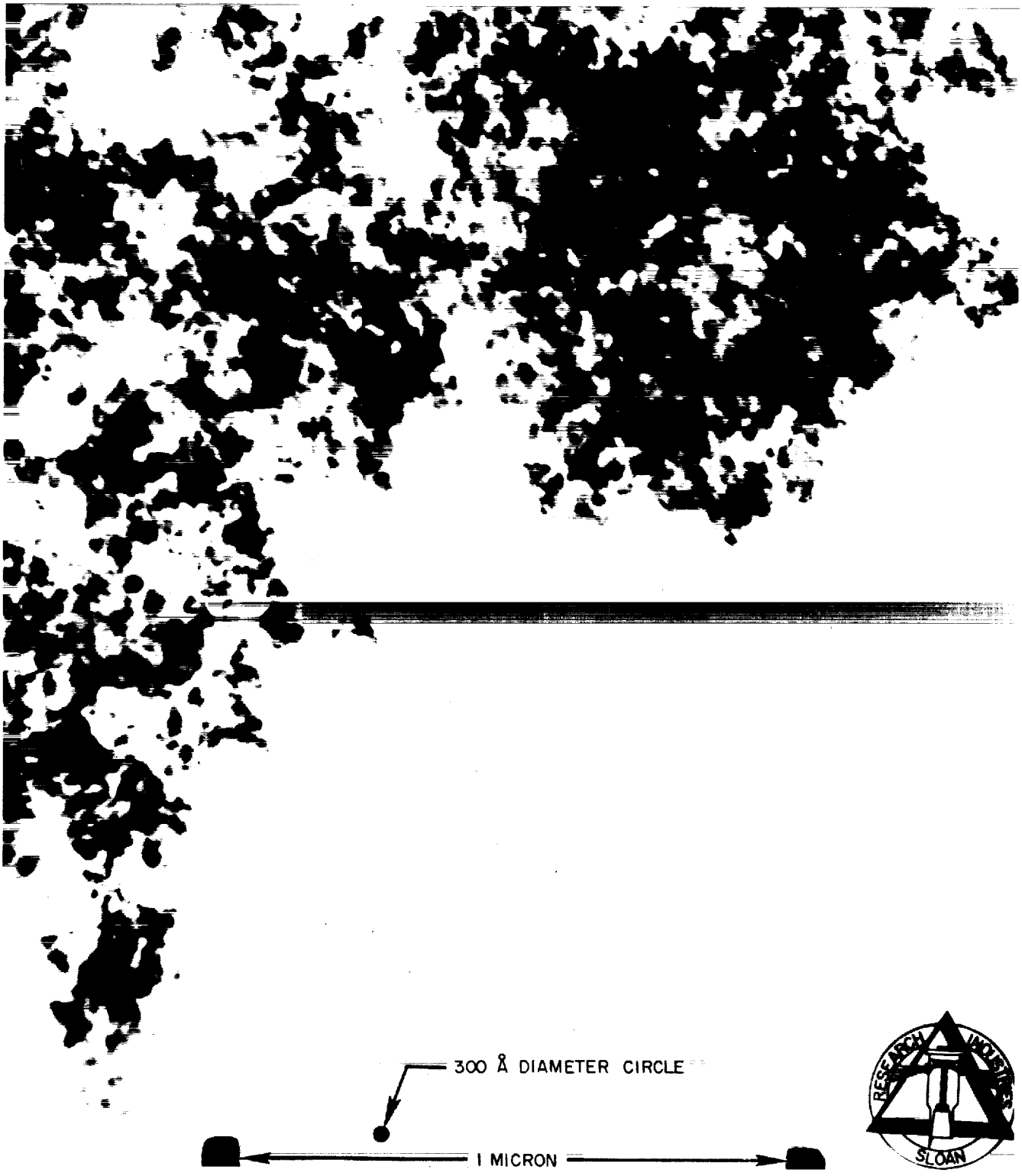


Figure 37. Electron Micrograph of Collected Soot Particles

TABLE II

MOL PERCENTAGE OF VARIOUS SPECIES

| Specie | Frozen Equilibrium | Experimental | Shifting Equilibrium |
|---|---|---|---|
| CO | 38.41 | 32.73 | 34.94 |
| $CO_2$ | 10.36 | 4.14 | 15.65 |
| H | 2.90 | – | .01 |
| $H_2$ | 14.07 | 33.85 | 18.40 |
| $H_2O$ | 30.67 | 21.01 | 31.00 |
| O | 0.40 | – | – |
| $O_2$ | 0.34 | – | – |
| OH | 2.87 | – | – |
| $CH_4$ | | 2.27 | |
| $C_2H_2$ | | 2.11 | |
| HCN | | 0.17 | |
| $C_2H_4$ | | 0.31 | |
| C | | 3.25 | |
| Misc. Organic | | <0.17 | |

## Recommendations

There was deposited on the walls of the probe almost 30% as much solid material as in the sampling tank. It would be highly desirable to eliminate, or at least greatly reduce, this deposit. It is recommended that the use of inert gas flow through a porous wall sampling tube be investigated with respect to this problem. Such gas flow would also tend to speed the quenching of any chemical reactions occurring as the sample proceeds through the probe.

# ULTRAVIOLET INSTRUMENTATION

## Ultraviolet Photographic Pyrometer

It is required to monitor the emission spectra of the OH molecule, a well-defined vibration-rotation band system of the $^2\Sigma^+ = {}^2\Pi$ electronic transition in the 2500 - 3500 Å region (Ref. 21).

This instrumentation must be capable of producing a photographic image of the afterburning region as indicated by the ultraviolet emission from the OH molecule; thus it must have an optical system with adequate transmission in the 2500 - 3500 Å spectral region.

Calibrated intensity standards are photographed simultaneously with the plume, so that a quantitative reduction of the radiometric data can be performed, resulting in a spatial mapping of the apparent brightness temperature of the plume. With such a graphic representation of the plume, sharp isoradiant contours defining the afterburning region can

readily be distinguished. This technique is referred to as photographic pyrometry.

Principles of Photographic Pyrometry. The principles of radiometric measurement employed in the photographic pyrometer are discussed briefly below.

For a given source, characterized by a spectral radiance (radiant flux emitted per unit wavelength interval per unit area of the emitter into a unit solid angle) the recorded signal (film density) is produced by the irradiance on the film. The irradiance is proportional to the quantity

$$\int_{y_1}^{y_2} \tau(\lambda)\ N(\lambda)d\lambda$$

where $\tau(\lambda)$ is the spectral transmission of the optical system traversed by rays from the source of spectral radiance $N(\lambda)$. This optical system includes any filter which is present in the path. The interval $\lambda_2-\lambda_1$ is a spectral interval which completely includes the spectral region for which $\tau(\lambda) > 0$.

The data provides a measure of either

$$\int_{y_1}^{y_2} \tau_1(\lambda)\ N_p(\lambda)d\lambda \text{ or} \tag{11}$$

$$\int_{y_1}^{y_2} \tau_2(\lambda)\ N_s(\lambda)d\lambda \tag{12}$$

where $N_p$ and $N_s$ are the radiances of the exhaust plume and standard sources, respectively, and $\tau_1(\lambda)$ is the spectral transmission of the camera lens plus an attached filter used to define the region of OH emission, while $\tau_2(\lambda)$ is the spectral transmission of the lens, OH filter, plus the mirror-attenuator system for imaging the tungsten filament.

The most direct way to evaluate either of the above integrals is to select a spectral region sufficiently narrow that all quantities in the integral can be considered constant over this interval. This is essentially the procedure followed in spectral radiometry using a monochromator, where the spectral slit width, $\Delta\lambda$, is the interval $\lambda_2-\lambda_1$, and is, for most cases, satisfactorily narrow. However, in the present case of photographic pyrometry of the OH emission bands, this cannot be done, since the present state-of-the-art of ultraviolet narrow band filters has not permitted construction of the required narrow band pass.

Since $N_s(\lambda)$ is a slowly varying function of wavelength, as is the spectral transmission through the mirror system, the expression (12) can be written as

$$\tau_M N_s(\lambda) \int_{\lambda_1}^{\lambda_2} \tau_f(\lambda)\,d\lambda \qquad (13)$$

where $N_s(\lambda)$ is the standard source radiance and $\tau_M$ is the transmission of the mirror system (including step attenuator) in the interval $\lambda_2-\lambda_1$, and is for all practical purposes, constant.

The integration in expression 13 can be performed graphically, so that the entire expression (13) can be evaluated in units of flux per unit area per unit solid angle. This is done for each of the zones of the step-attenuator, the difference in each being, in principle, only the difference in $\tau_M$ resulting from the differences in transmission of the various zones. From these five values and the corresponding film image densities, a graph is plotted of the film responsivity for each exposed frame. An example of such a graph is seen in Fig. 56. The manner in which this graph is constructed is discussed in a later section describing the telespectrograph.

For any point in the plume image, the measured density is used to enter the film responsivity curve and, from this, to obtain a value of the quantity expressed by expression (11).

In this manner, all spatially resolvable regions in the plume can be expressed in absolute units of radiant power effective in irradiating a unit area of the film within the weighted spectral interval represented by the filter transmission curve, $\tau_f(\lambda)$. An example of such a curve is given in Figure 38.

Optical System. The chief requirements of this instrumentation include the following:

1. The camera must be equipped with an automatic rewind capability to permit a sequence of exposures during any given test firing.
2. The photographic lens must transmit ultraviolet radiation (in the 2500 to 3500 Å wavelength region).
3. The film format and lens must provide a sufficient field to

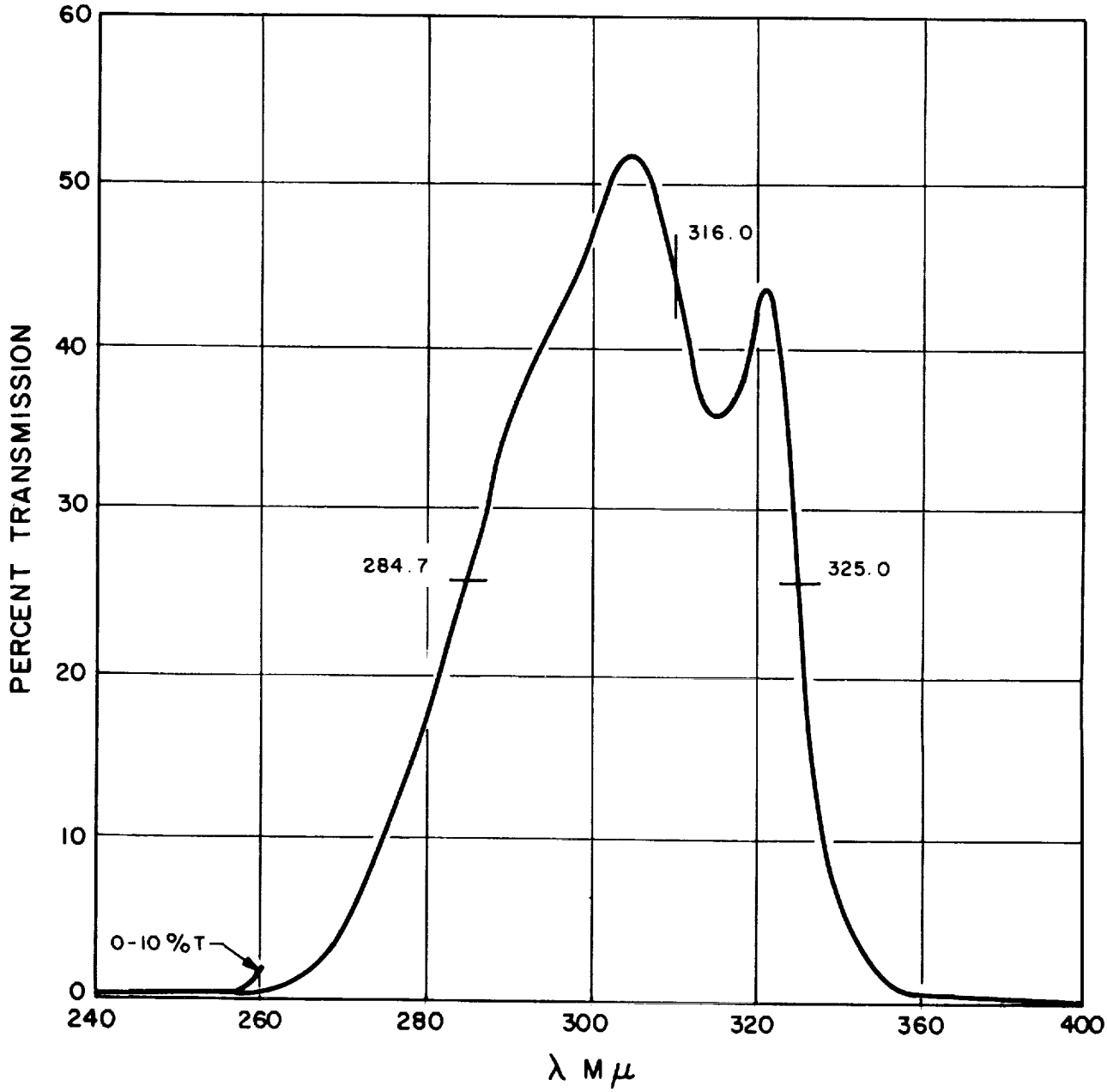


Figure 38. Ultraviolet Filter Spectral Transmission

cover most of the exhaust plume (approximately 8 feet in length).

4. A standard intensity source must be used with appropriate optics to provide an intensity calibration scale. This intensity scale must be photographed with the plume at each exposure, so that the images of both the exhaust and the intensity scale on the film will be subject, as nearly as possible, to the same development.

To accomodate the automatic rewind capability, a Nikon Model F 35mm single-lens reflex camera was selected for the photographic pyrometer. This camera has the capability of exposure rates as high as four per second.

The test pit where the model motor is operated is bounded on one side by a steep earthen incline. The photographic pyrometer is located about 18 feet up this incline from the test pit. This location is approximately 21 feet from the plume axis measured along a normal to the plume axis; thus, an 8 foot plume length subtends an angle of $22^{o}$ for this pyrometer location.

The calibration source is a tungsten ribbon filament lamp equipped with a quartz window. This is G.E. lamp #30A/T24/17. This same type of lamp has been successfully used as an ultraviolet radiation intensity standard in previous programs concerned with ultraviolet radiometry of rocket exhausts (Ref. 22).

This lamp is supplied with a spectral radiance calibration from 2500 Å to 7500 Å (17 calibration wavelength points) by the Eppley Laboratories

of Newport, R. I.

For purposes of compactness, portability, and ease of operation there is only one such calibration lamp in the instrument; therefore, in order to achieve a range of intensities or film densities (intensity scale), the filament of the lamp is imaged onto a step filter. The step filter provides an amplitude division in five different portions of the filament image, which is then transformed into a virtual image in the plane of the exhaust. Thus, the five resulting portions of the calibration filament are photographed simultaneously with the exhaust plume, with the camera focused on the plane of the exhaust. The optical system which acomplishes this is schematically diagrammed in an isometric view in Figure 39. The selection of a 4 inch focal length lens for a 35mm format provides a convenient field of view for this geometry. The field-of-view angles are such that the horizontal (sagittal) view angle is $21.6^{\circ}$, so that slightly less than 8 feet of the plume can be photographed from this position. A suitable clearance exists between the test-pit roof and retaining wall to permit viewing of the length and width of the exhaust. A roof-support stanchion can be removed if further lateral clearance is required.

Calculation of the required speed of the photographic lens was based on the observed brightness of liquid oxygen/RP-1 exhaust afterburning in the 2800 - 3300 Å (OH emission) region (Ref. 22). This calculation indicated that a speed of f/16 would be sufficient for a nominal lens-filter transmission of 20% and a 0.01 second exposure time. To allow for a decrease in ultraviolet intensity relative to the large engine data in Ref. 22, the lens specifications called for a relative aperture of f/8.

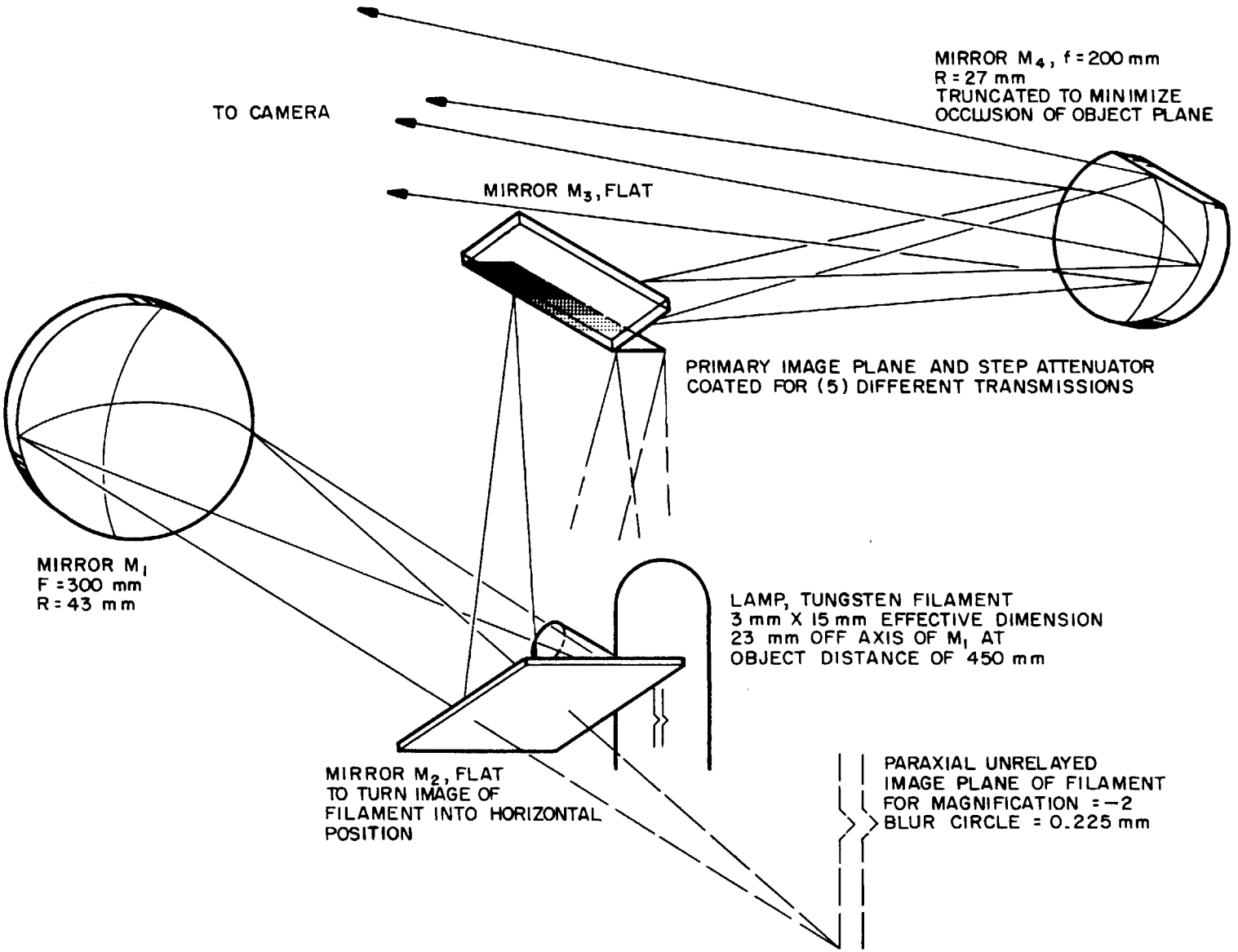


Figure 39. Schematic of Ultraviolet Photographic Pyrometer

These same specifications required a resolution on the film of at least 30 line pairs per mm, this corresponds to a spatial resolution of approximately 2mm at the exhaust. Furthermore, the field illumination was required to vary by no more than 10%; this is the maximum variation in illumination across the film format determined in previous tests of the Nikon F camera equipped with a Nikkor (visible transmitting) lens. Since a primary image plane is required, all imaging optics other than the photographic objective are to be reflective to permit visual alignment and focus in the primary image plane without chromatic aberrations.

The plume will be imaged horizontally on the film, i.e. the length of the plume will occupy the 1-½" dimension of the film format. The tangential (vertical) field-of-view of the camera is $14.5^{\circ}$, or $7.25^{\circ}$ half-angle, so at 21 feet half the object field is 21 tan $7.25^{\circ}$ = 800mm = 32 inches, which is ample for the width of the exhaust plume.

Since it is desirable to image the tungsten filament horizontally on the film, to take advantage of the longer dimension of the format, a relay mirror must be used to rotate the image of the filament from a vertical to a horizontal position. This rotation is accomplished by mirror $M_2$ shown in Figure 39. Thus $M_1$, in combination with $M_2$, forms a horizontal primary image of the tungsten filament in a plane above the axis of $M_1$. Note that the relay function of $M_2$ serve to make the optical system more compact as well as achieving image rotation. The primary image thus formed by $M_1$ and relayed by $M_2$ is then spatially divided into zones of differing intensity and then serves as the object for the mirror $M_4$. $M_4$ then nearly collimates the light which diverges from the primary image and sends it to the camera. Thus $M_4$ forms at the plane of the exhaust plume a virtual, erect image of the step-attenuated primary image.

The completed instrument is shown in Figures 40, 41, and 42. In Figures 40 and 41, the 35mm camera shown is the Nikon F with the ultraviolet-transmitting lens attached. Figure 41 shows clearly the step filter, reflected in the flat mirror $M_3$. Figure 42 shows the instrument with the cover in place. The meter in the cradle attached to the side of the cover is the ammeter for the tungsten filament lamp. This meter is equipped with an anti-parallax scale and must be used in the horizontal position shown.

For the calibration lamp filament and the plume to be simultaneously in focus, the filament must appear to the camera as if it were in the plane of the exhaust, i.e. approximately 20 feet from the camera; thus, light from the filament must be nearly collimated before being directed to the camera. This collimation requires a mirror with the object (primary image of filament) near the focus, yet sufficiently off-center to allow the collimated light to reach the camera without occlusion. A convenient focal length for this "collimating" mirror ($M_4$) is 200mm. For focal lengths shorter than this, the aberrations become large.

With the camera lens focal length 100mm, a magnification of $\frac{1}{2}$ is achieved by mirror $M_4$ and the camera lens. The smallest filament image size on the film will be for the greatest viewing distance (approximately 21feet). A lower limit on this film image size (width) of the calibration filament is arbitrarily chosen to be 3mm, to be centered in the lower half (12mm) of the image field. This 3mm width of the calibration image on the film requires, therefore, a 6mm wide calibration source as the object for the "collimating" mirror, $M_4$. The object for $M_4$ is the step-attenuated primary image of the filament formed by $M_1$ and relayed and rotated by $M_2$. Thus for the 3mm wide lamp filament, mirror $M_2$ must work at a

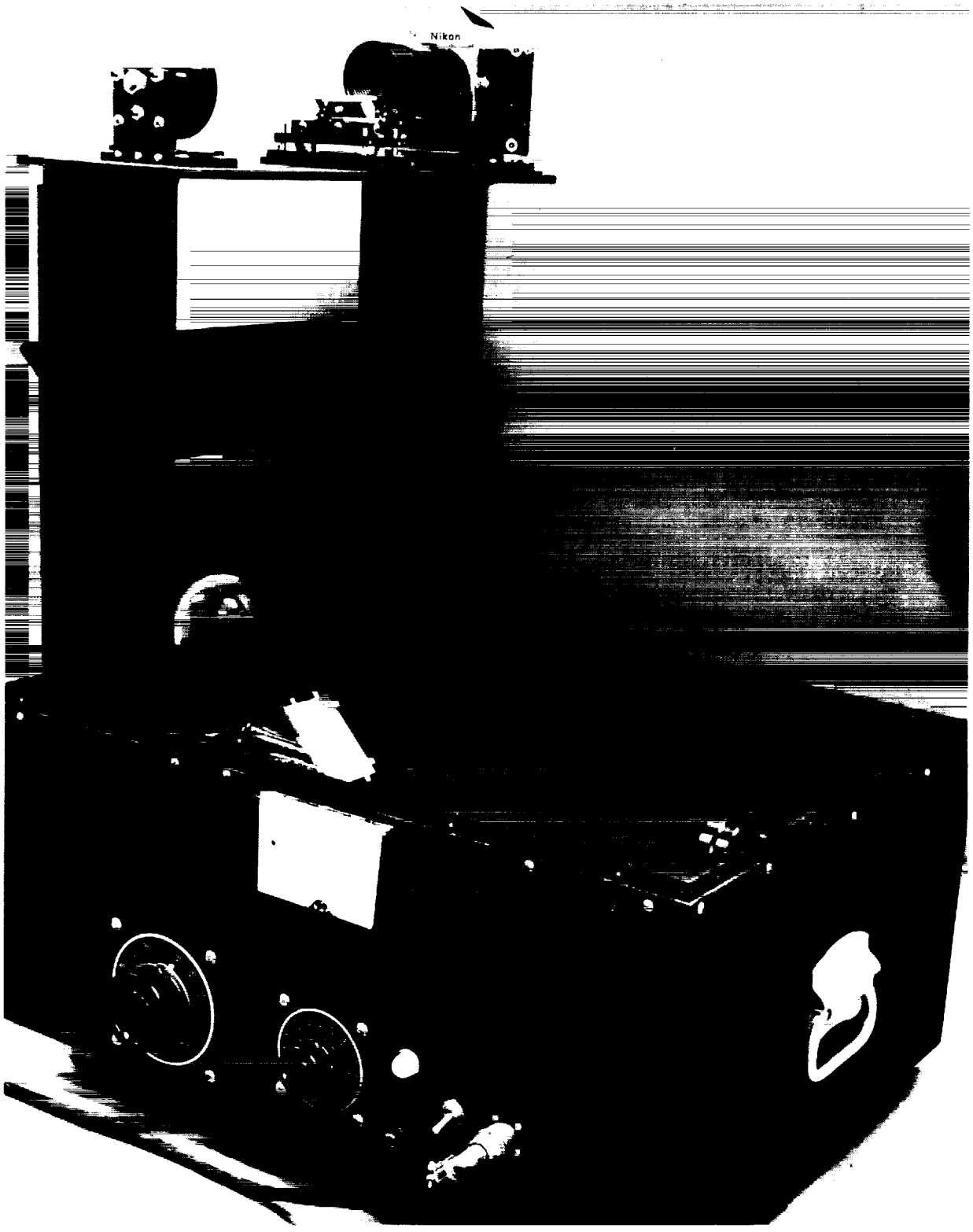


Figure 40. Ultraviolet Photographic Pyrometer, Cover Off

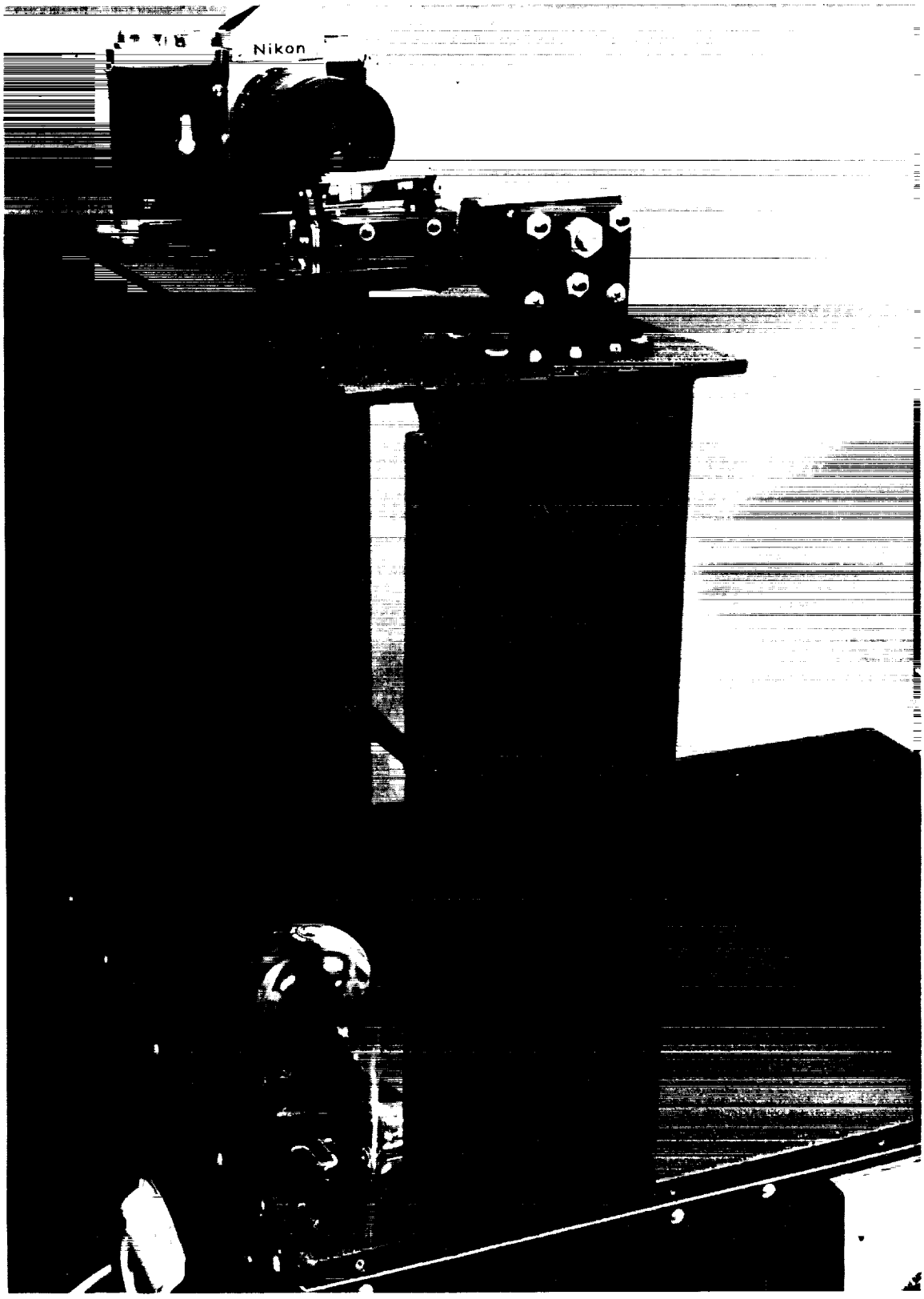


Figure 41. Ultraviolet Photographic Pyrometer, Cover Off

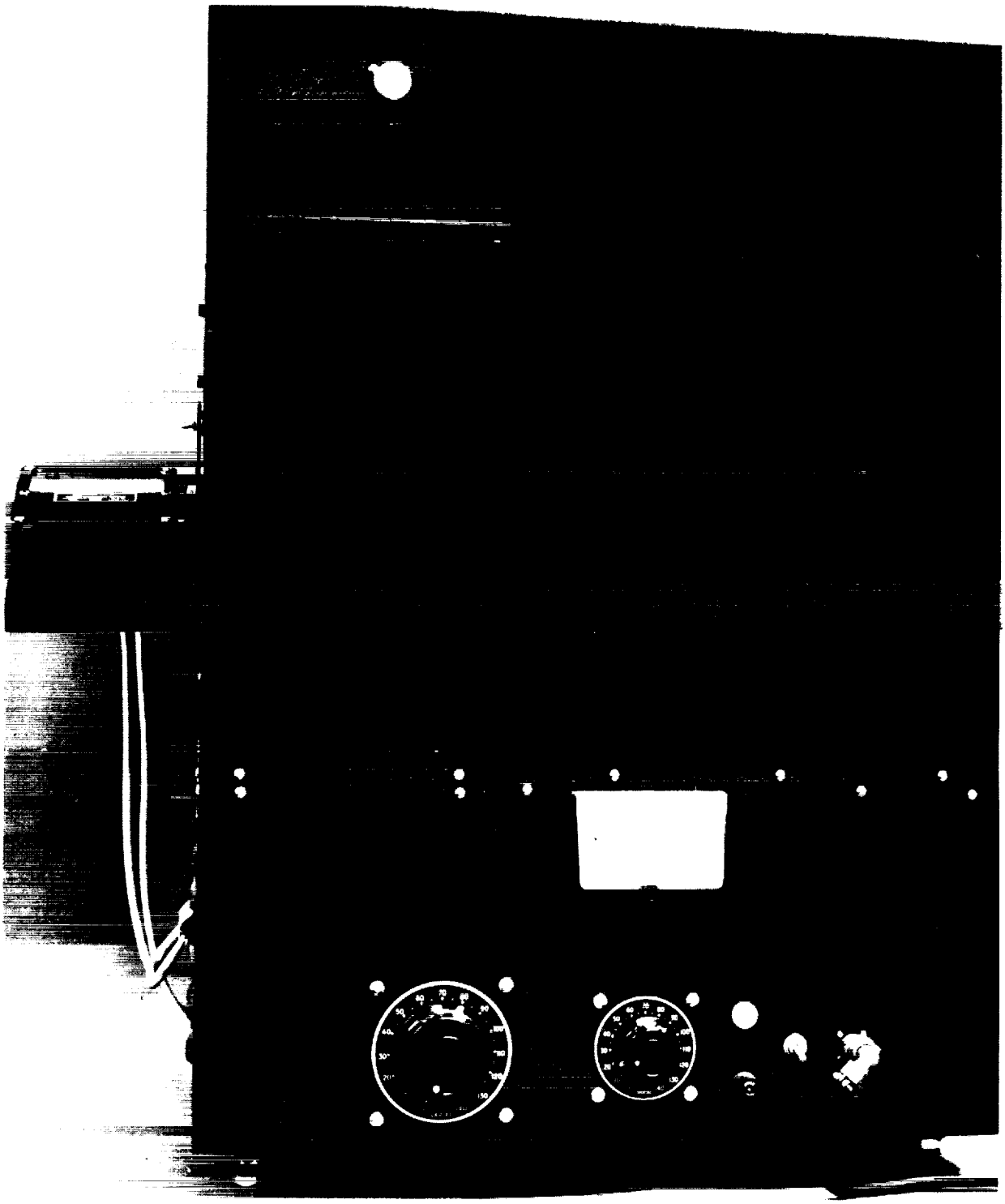

Figure 42. Ultraviolet Photographic Pyrometer, Cover On

magnification of -2 to provide a real primary image 6mm wide.

The overall system including mirrors and camera lens thus provides unit magnification of the tungsten filament, so that the filament image on the film is approximately 3mm x 15mm (horizontally displayed), for approximately a 20 foot separation between camera and exhaust plume.

Step Attenuator for the Photographic Pyrometer. Several metals and alloys were investigated as possible transmission coatings for the quartz base plate of the step attenuator. The principal criteria used in evaluating these materials were that they exhibited fairly constant transmission in the spectral region of interest (2500 Å to 3500 Å) and could be readily coated in thin films. In addition, durability, availability, and complexity of coating procedures were also considered. During the course of this preliminary work, it was found that the variation of transmission with wavelength in the ultraviolet region is not well known for many metals and data for most alloys is non-existent.

Aluminum was considered as a first choice because of its wide use as a mirror coating, and the prodigious amount of published data on transmission vs wavelength at different coating thicknesses. Figure 43 shows transmission data in the spectral region of interest, for three different thicknesses of aluminum. These data were taken from Ref. 23.

The nickle-chromium alloy, inconel, was a second choice. This material has approximately twenty times the hardness of gold or aluminum, is much more durable, and is also easier to clean. However, its transmission properties were unknown in the ultraviolet region of the spectrum and

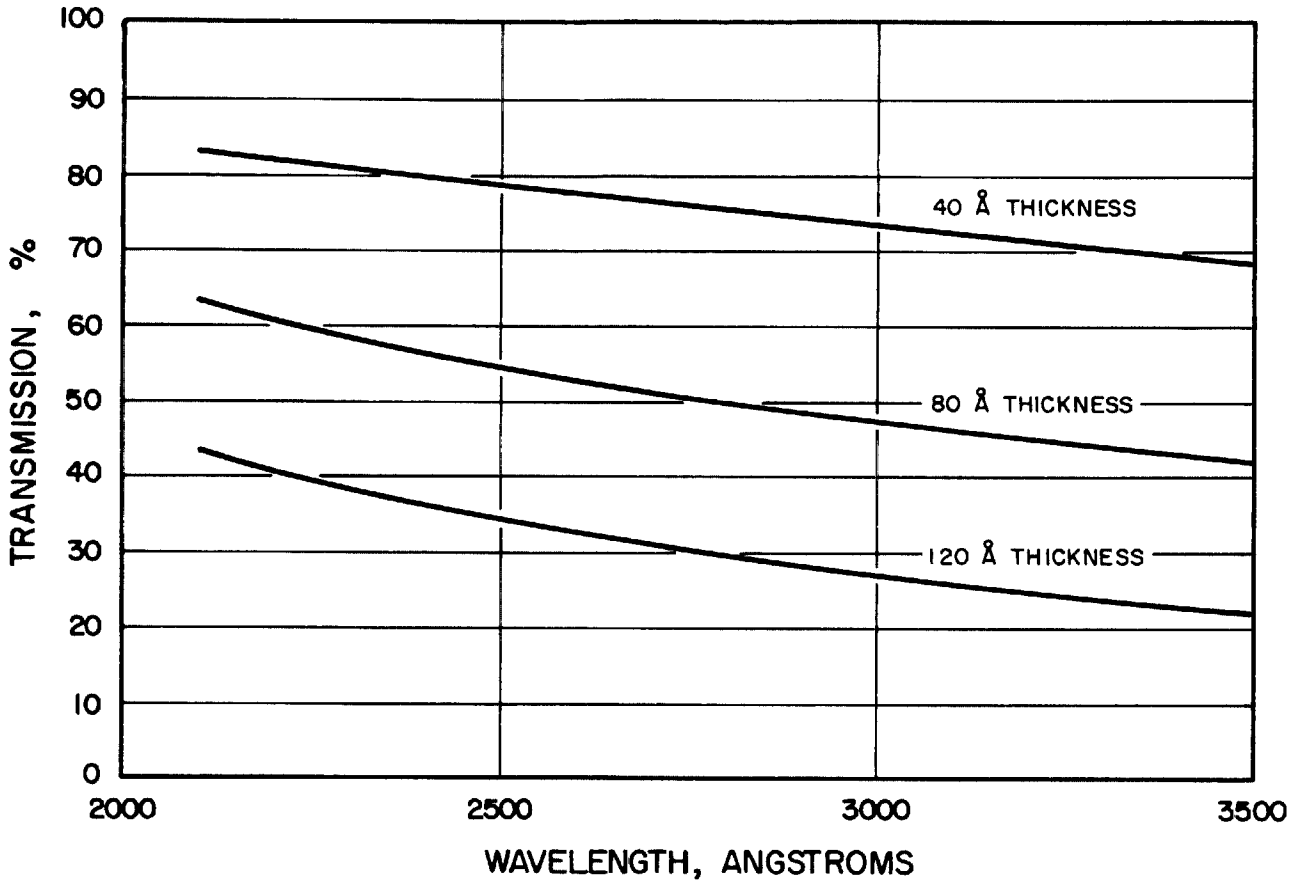


Figure 43. Spectral Transmission for Three Thicknesses of Aluminum

were known only qualitatively above 4000 Å. The results of some transmission measurements on inconel made in our laboratory (with a McPherson Vacuum Ultraviolet Spectrometer) are shown in Fig. 44. It can be seen that transmission varies slightly with wavelength, so that inconel, as well as aluminum, fulfills most of the principal requirements of the present application.

In order to obtain a wide range of transmission data from the plume, three step filters were purchased. The first, coated with aluminum, and the second, coated with inconel, have five zones each; 100%, 80%, 60%, 40%, and 20% transmission at 3000 Å. The last filter, also coated with aluminum, has zones of 80%, 70%, 60%, 50%, and 40% transmission at 3000 Å.

Evaluation of Ultraviolet Photographic Pyrometer. Typical UV pyrograms of the exhausts of small rocket motors burning LOX/RP-1 are shown in Figures 45 to 49. The type of engine and the operating parameters are indicated in the figures. The exhaust plume can be seen in the upper portion of the photographs, with the nozzle exit region on the left. As mentioned previously, the dark band across the plume is a roof support. The image of the calibration lamp filament filtered by the inconel step attenuator is located in the lower portion of some of the figures. It should be noted that the middle zone of the step attenuator has an uneven appearance due to flaws in the inconel coating. The zone appearing on the left in the photographs corresponds to the uncoated portion of the step attenuator. The lamp filament temperature was about 2630°K. At 3000 Å, the radiance of tungsten at this temperature is equivalent to that of a blackbody at 2520°K.

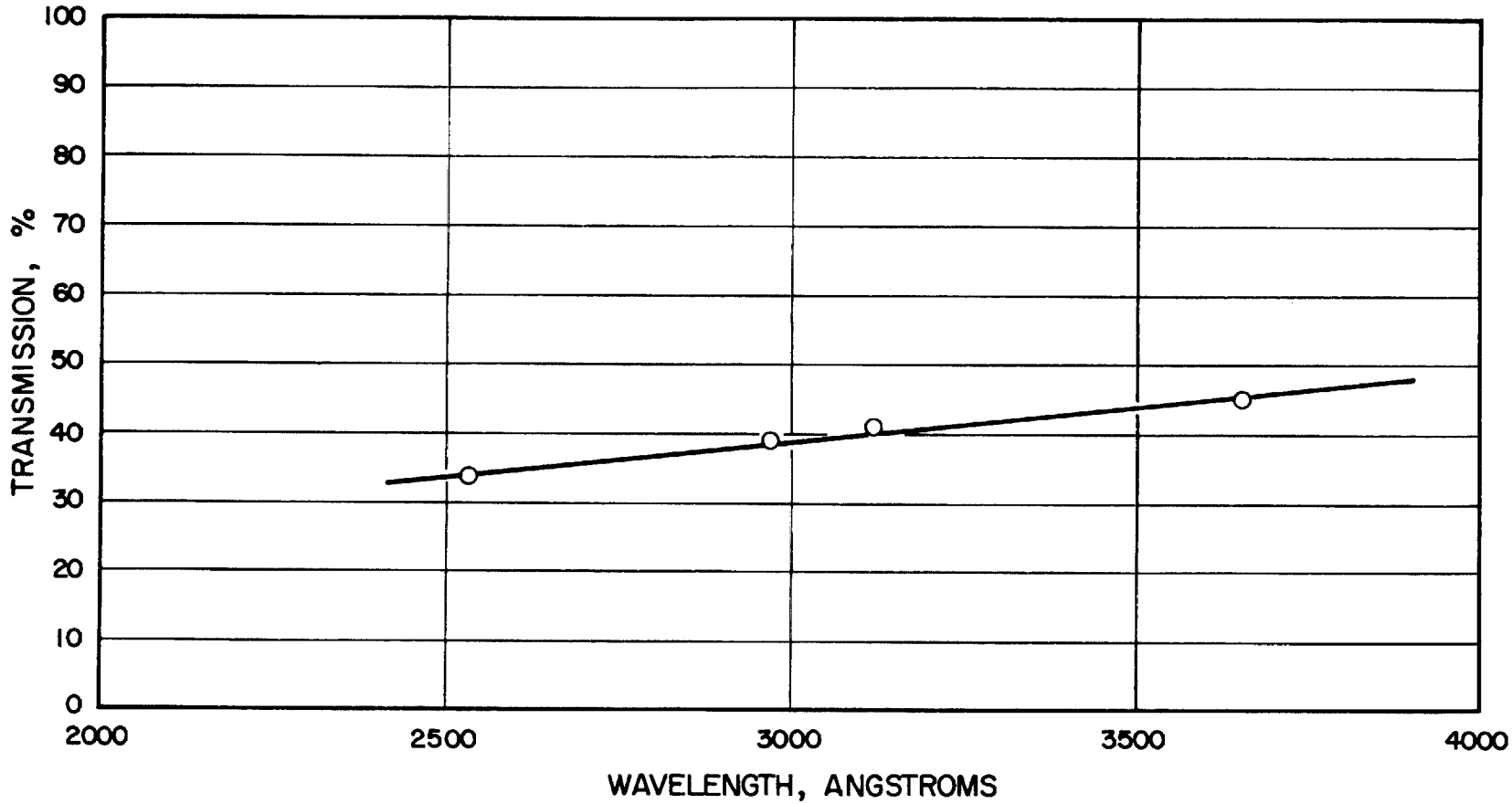


Figure 44. Measured Spectral Transmission of Inconel

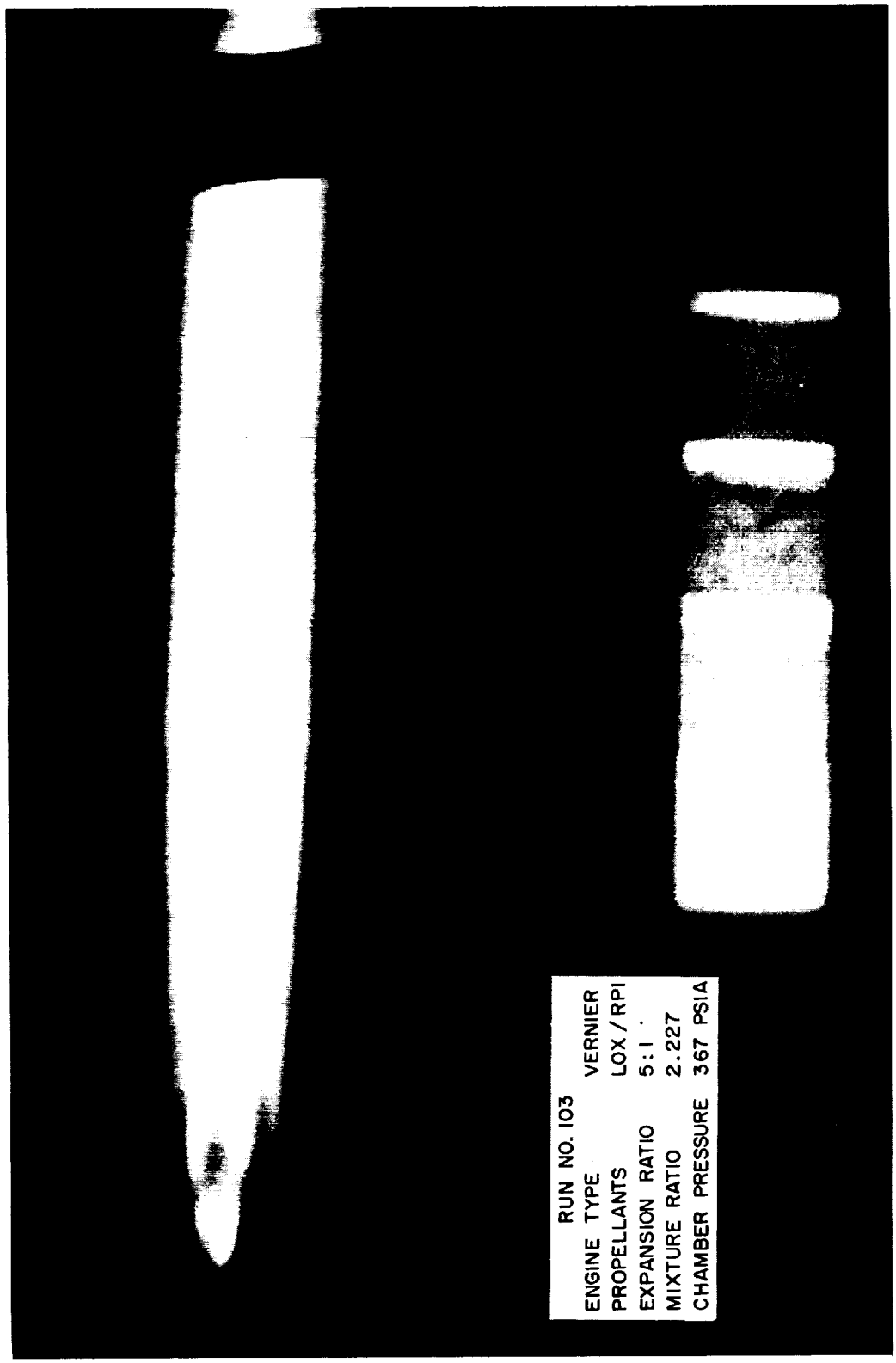


R-6288 **Figure 45.** Ultraviolet Pyrogram of Atlas Vernier Exhaust

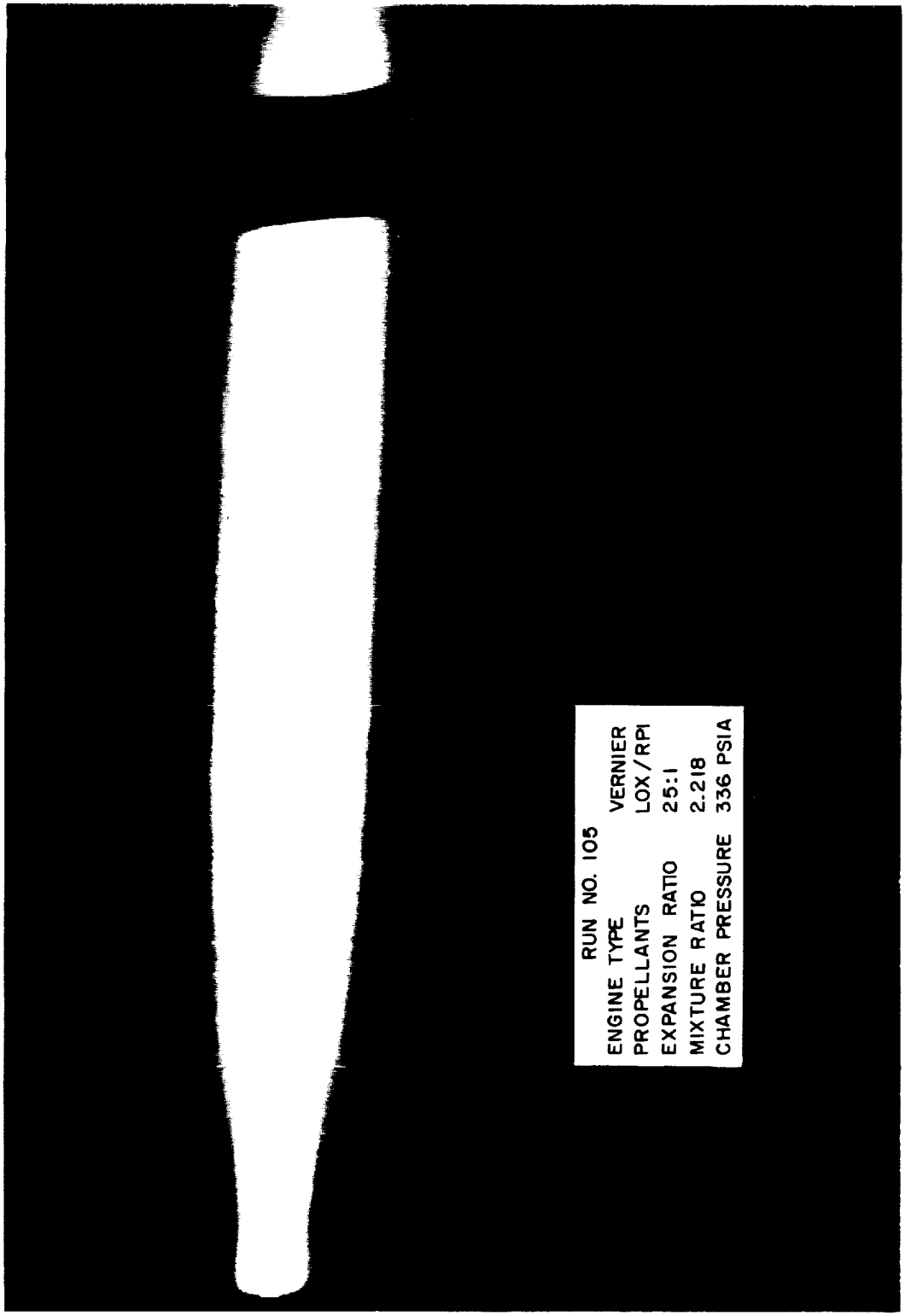


Figure 46. Ultraviolet Photograph of Modified Atlas Vernier Exhaust

104-7

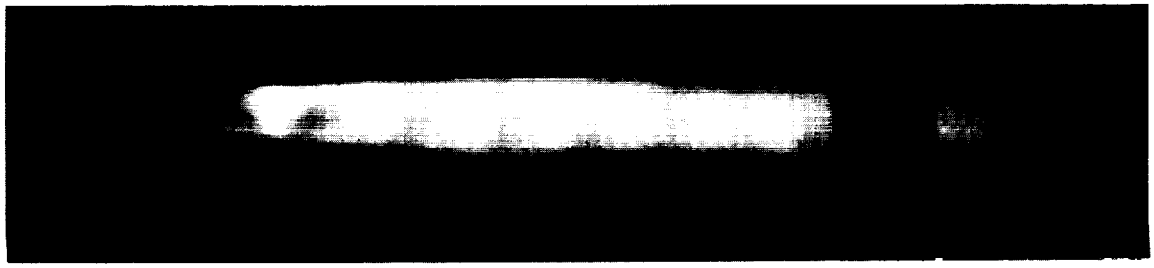

104-8

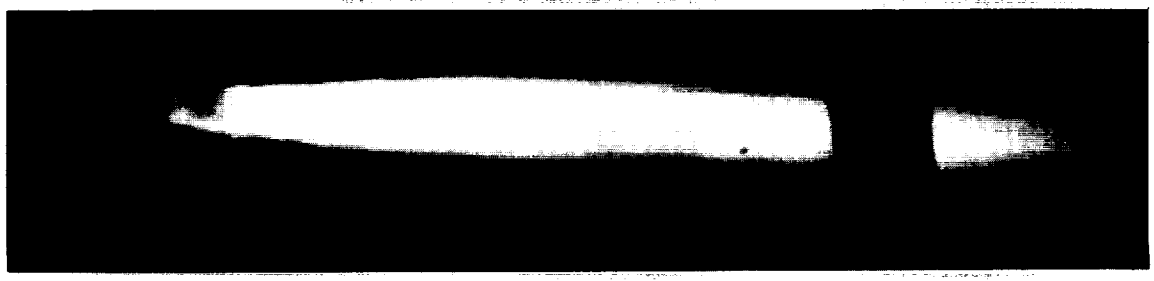

104-9

| RUN NO. 104 | |
|---|---|
| ENGINE TYPE | VERNIER |
| PROPELLANTS | LOX / RP1 |
| EXPANSION RATIO | 5:1 |
| MIXTURE RATIO | 2.23 |
| CHAMBER PRESSURE | 350 PSIA |

Figure 47. Sequence of Ultraviolet Photographs of Atlas Vernier During Injector Failure

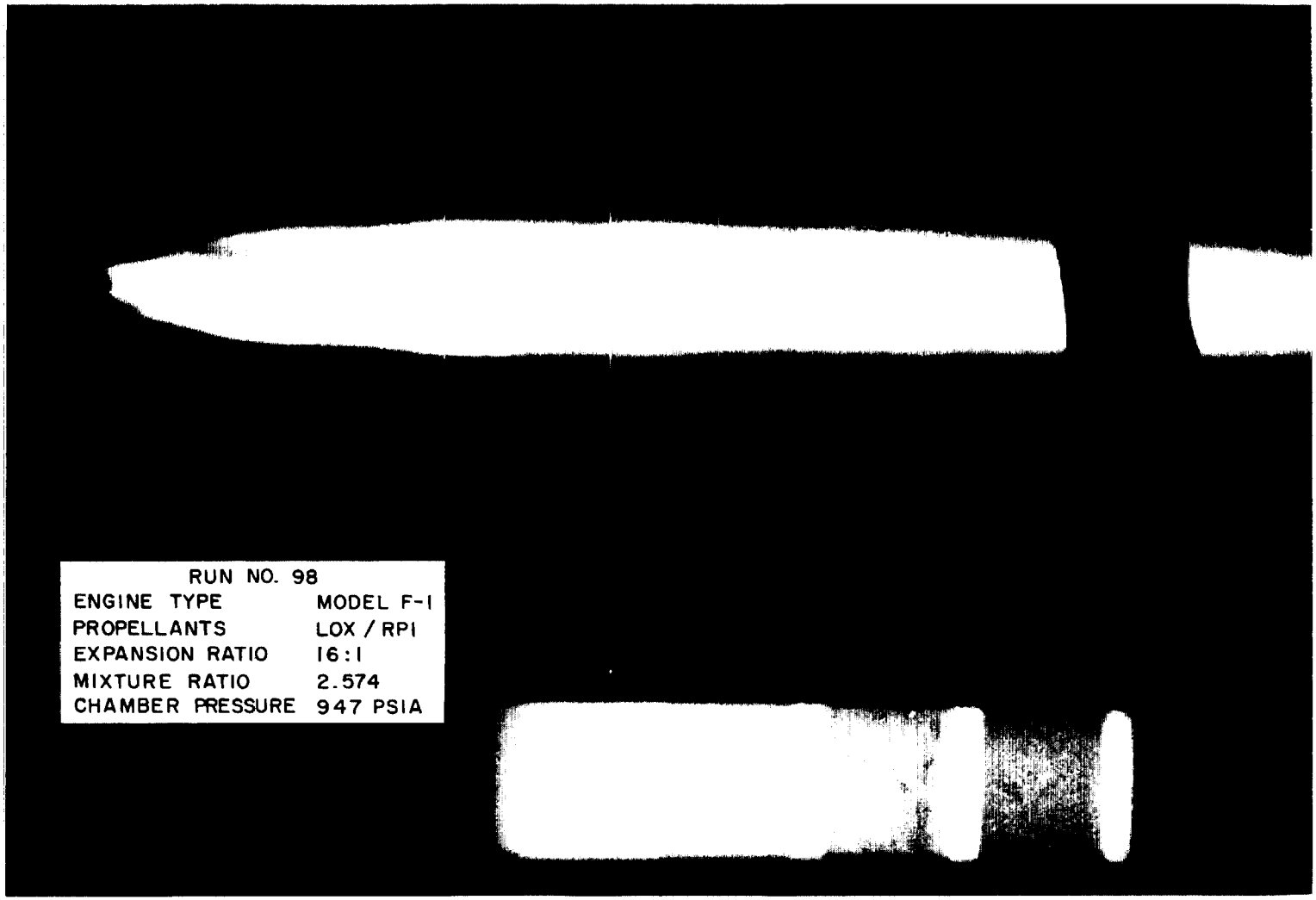


Figure 48. Ultraviolet Pyrogram of Model F-1 Exhaust

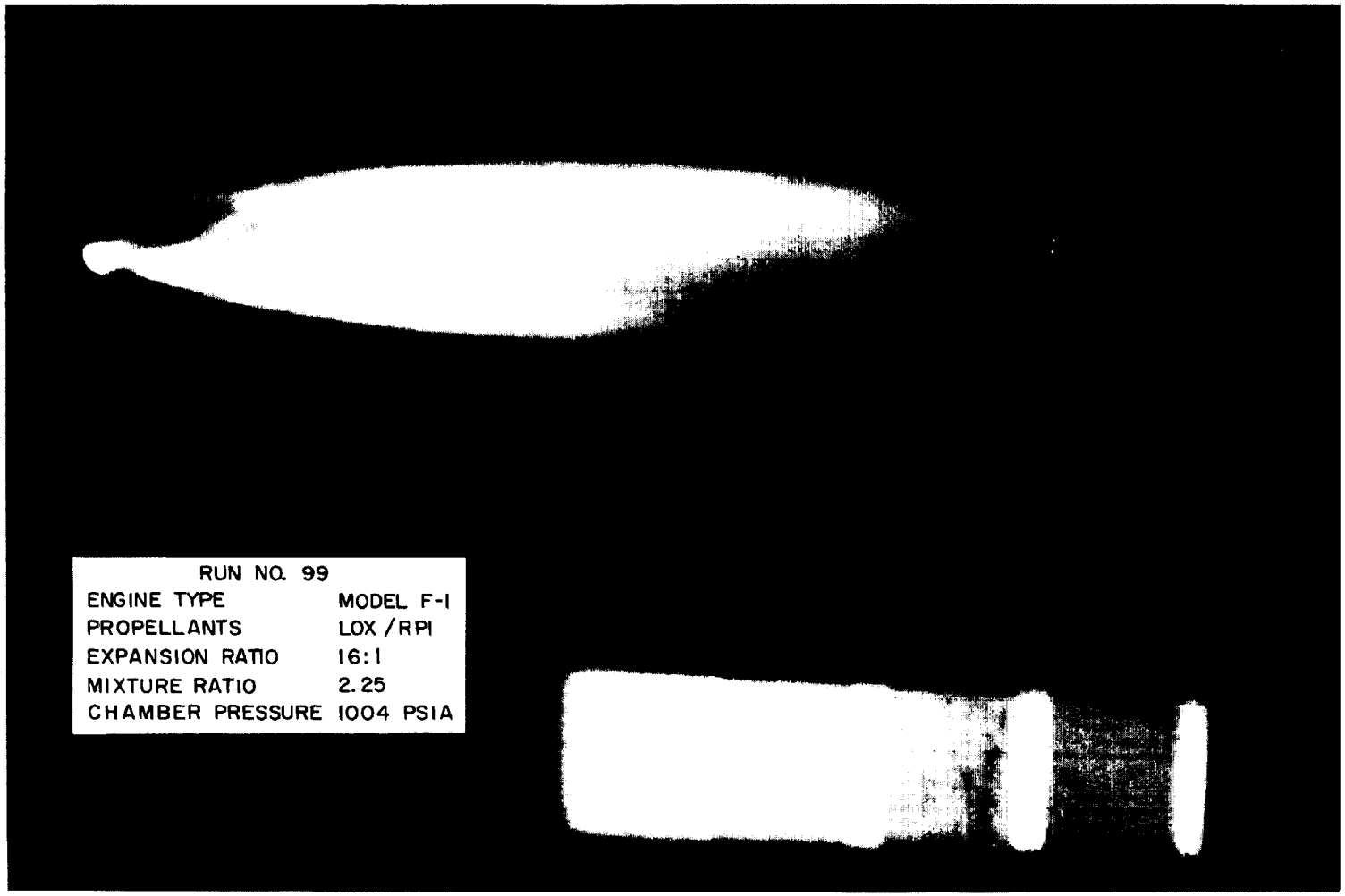


Figure 49. Ultraviolet Pyrogram of Model F-1 Exhaust with Sampling Probe

Figures 45 and 46 are representative ultraviolet photographs of the Atlas vernier exhaust at two different expansion ratios. Figure 45 shows the exhaust of the Atlas vernier with an exit area to throat area expansion ratio of 5:1. The exhaust of the modified vernier with an extension skirt and an expansion ratio of 25:1 is pictured in Figure 46. This nozzle is overexpanded at sea-level ambient pressure, and flow separation occurs within the nozzle.

The outer afterburning mantle and the shock structure of the inner core, typical features of low altitude plumes, can be discerned in Figure 45. Afterburning commences downstream of the nozzle exit near the first shock. Note that the brighter part of the mantle surrounding the first shock nodes is at the periphery and that there is a darker region adjacent to the inner core. This observation suggest that there is greater afterburning intensity (hence greater OH radiation) at the periphery. This is consistent with the idea that afterburning occurs in the mixing region, which must commence at the periphery of the exhaust. As the mixing region broadens downstream of the exit then the afterburning intensity should correspondingly proceed to greater depths in the exhaust. It is apparent from Figure 45 that the width of the brighter region of the mantle increases as the exhaust gases travel downstream.

Figure 46 indicates different conditions of afterburning for the over expanded nozzle. Flow separation has taken place within the rocket nozzle and mixing with the atmosphere has begun before the exhaust gases leave the nozzle. The afterburning mantle can be seen to commence at or possibly before the nozzle exit.

Figure 47, starting at the top, is a series of three UV photographs taken in succession during the unstable operation of a vernier with a 5:1 expansion ratio. The injector failed on this occasion and the resulting disruption of the exhaust structure is evident. The asymmetry of the afterburning mantle near the nozzle exit suggests an uneven distribution of propellants during the injector failure.

The exhaust of the model F-1 engine with a 16:1 expansion ratio is pictured in Figure 48. Again, the inner core and outer, afterburning mantle can be seen. For this type of exhaust, too, the brighter region at the mantle periphery is in evidence as the afterburning begins.

A firing of the model F-1 with the exhaust sampling probe in place was also monitored with the UV photographic pyrometer. The result is shown in Figure 49. The bright spot at the left in the plume is located just below the bend in the sampling probe. Shock waves due to the probe's presence in the supersonic exhaust gases are seen as a pattern of bright streaks obliquely traversing the exhaust.

Densitometer traces of selected directions through Figure 45 are presented in Figures 50, 51, and 52. Figure 50 is a trace made by scanning the image of the step attenuator. Figure 51 shows a scan of the plume image. This trace was made by scanning along the exhaust axis, the left edge of the trace corresponding to the nozzle exit plane. In Figure 52 are shown three traces made by scanning perpendicularly to the exhaust axis. Proceeding from left to right the traces represent scans made between the 1st and 2nd shock nodes, 2nd and 3rd shock nodes, and 3rd and 4th shock nodes respectively.

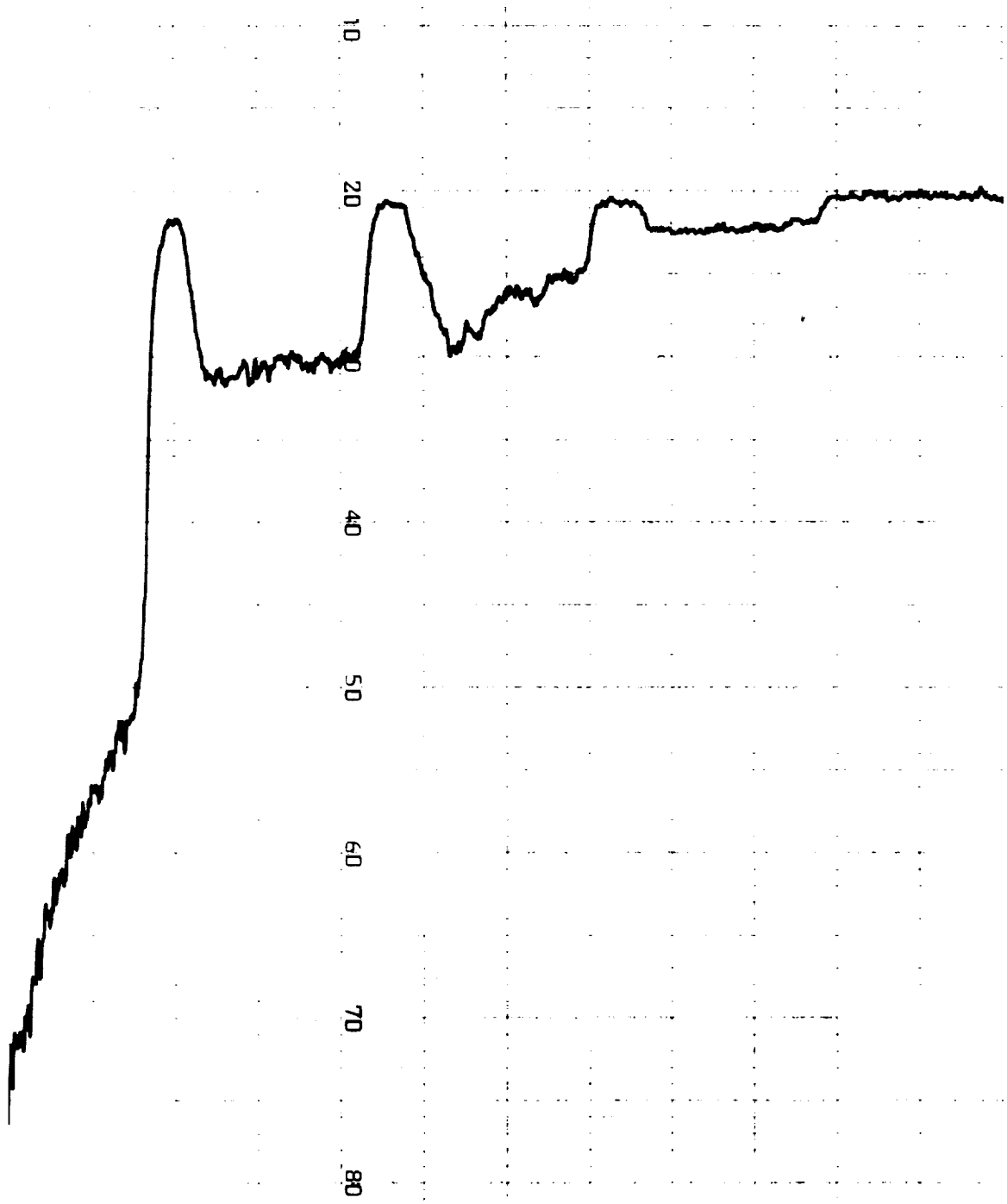


Figure 50. Densitometer Trace Across Step Attenuator Image

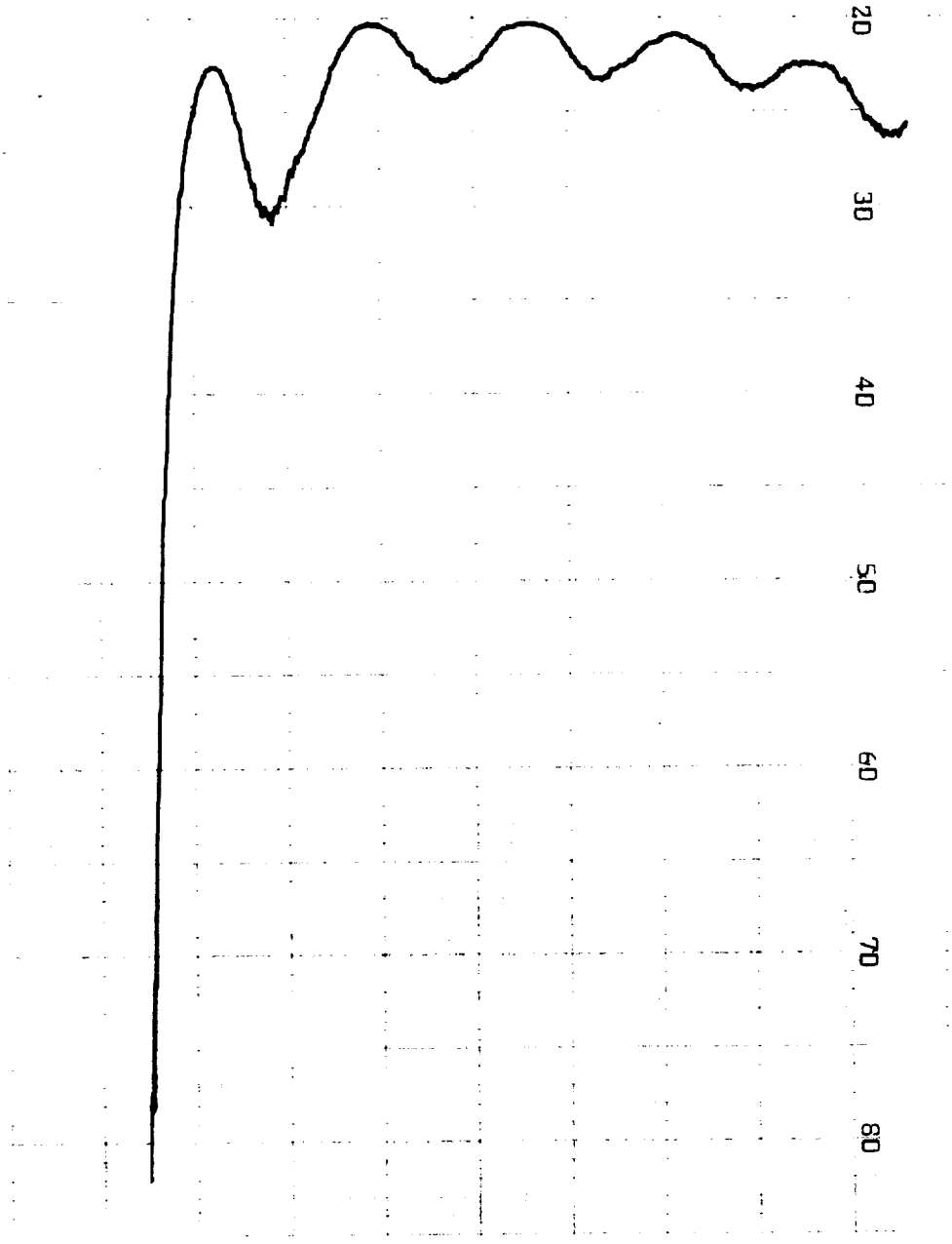


Figure 51. Densitometer Trace Along Axis of Plume Image

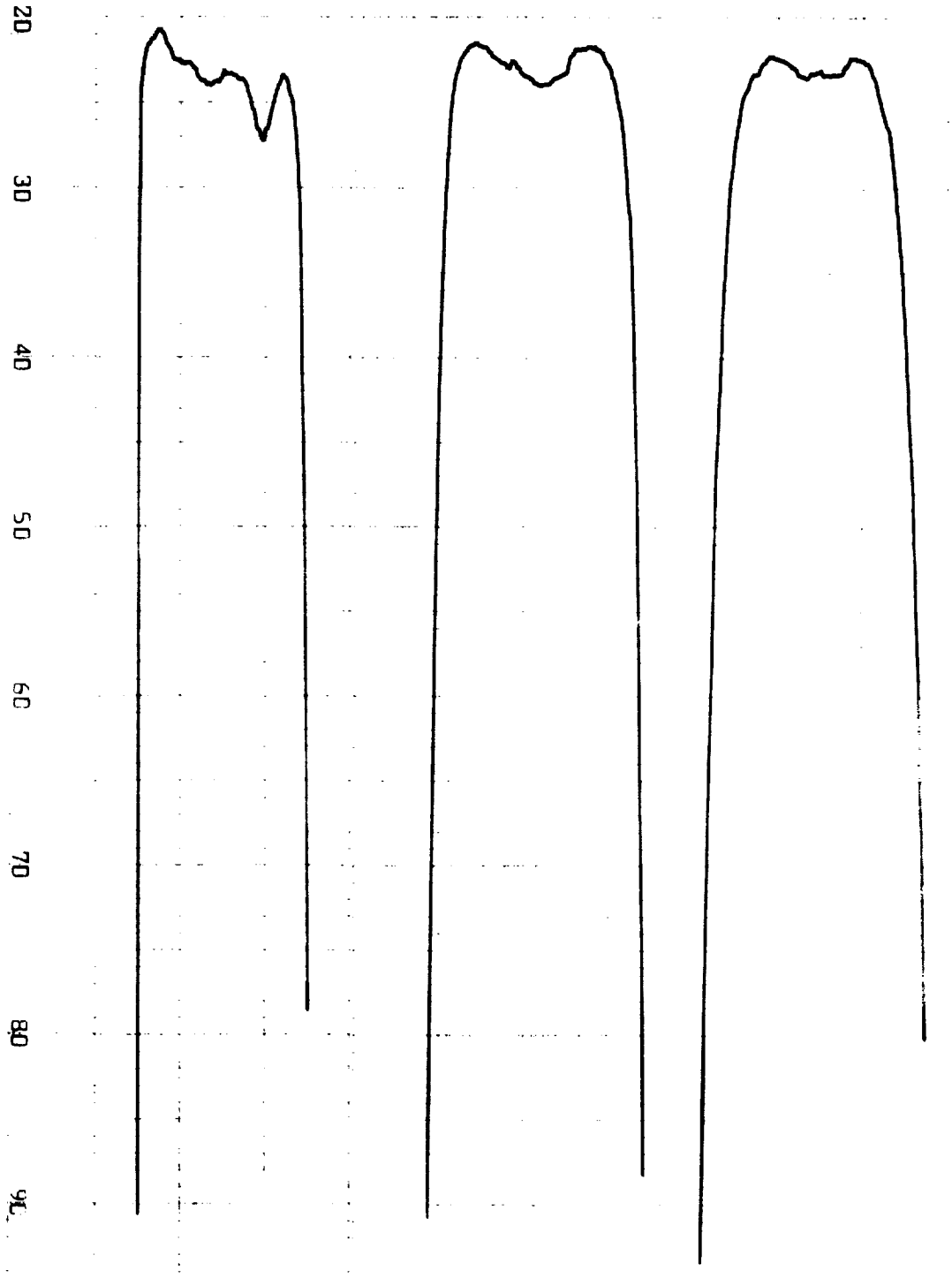


Figure 52. Densitometer Traces Across Plume at Three Positions

Modifications to the Photographic Pyrometer. It has been found that a wide range of intensities are exhibited in the plume during a single firing. For a photographic instrument, operating under the limitations of film sensitivities, this means that, in general, only a part of the plume can be quantitatively reduced for each camera setting. In order to acquire more information per motor firing, it is desirable to alter the apparent plume intensities, and thus the plume image film densities, by inserting an additional attenuator plate in the path of radiation originating at the plume.

A one quarter inch thickness of Ultraviolet Transmitting Plexiglas II (manufactured by the Rohm and Haas Company of Philadelphia) attenuates the plume intensity, in the spectral region of interest, by approximately 50%. Transmission characteristics of this material are shown in Fig. 53. These data are reproduced from Rohm and Haas publications.

Such an attenuator plate can be installed on the instrument so that it is fixed in the path of radiation from the exhaust plume to the camera for the first half of the motor test run and then released (by means of an electrically operated switch) for the remainder of the test.

The existing step attenuator is about 33mm long and divided into five transmission zones of approximately equal width. In the present configuration the five zones span the entire filament length of the tungsten calibration lamp, that is, the outside zones receive radiation from the ends of the filament and the inner zones from the center of the filament. There exists, however, a noticeable temperature gradient along the filament length, so that each zone is actually receiving radiation of an intensity slightly different from the other four. Comparison of the

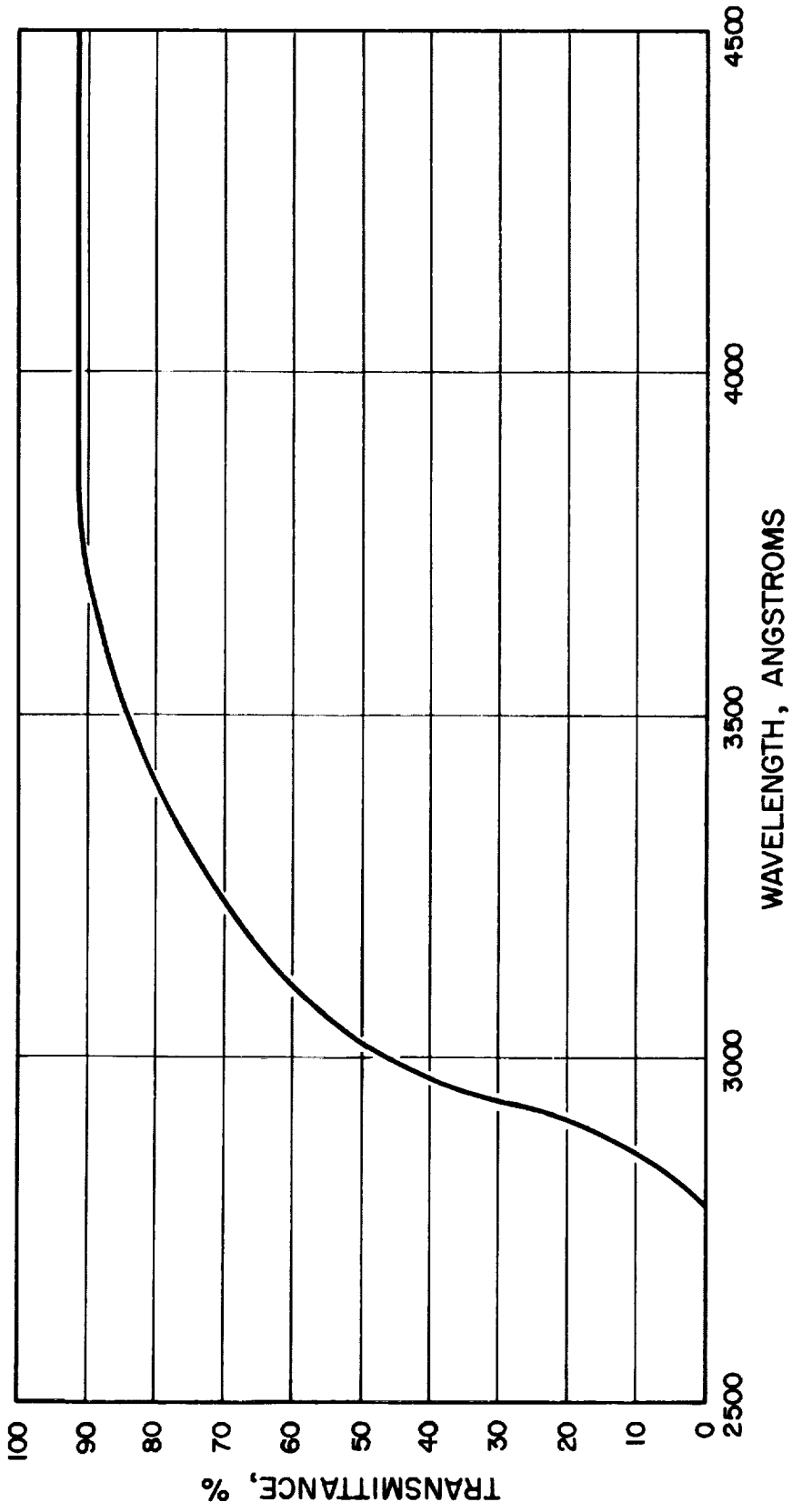


Figure 53. Spectral Transmission of UVT Plexiglass, Type II

different zones for purposes of intensity calibration, therefore, requires that each zone be read with an optical pyrometer for each lamp current setting. This is a very costly, time-consuming procedure.

With advanced coating techniques it will be possible to reduce the zone widths from 5 or 6mm to one mm each, a dimension which is compatible with the data reduction equipment. All five zones can then be located at the position of the central zone (of the present attenuators), and all will transmit radiation from the center of the tungsten filament; i.e. from a filament region of constant temperature. That area of the quartz plate not coated with aluminum or inconel will be blackened to minimize stray light.

Ultraviolet and Visible Telespectrograph

A spectrograph equipped with telescopic entrance optics was employed to record quantitative plume emission spectra in the ultraviolet and visible spectral regions. A schematic diagram of the telespectrograph is presented in Fig. 54. The radiation from the plume is collected by a 4 inch diameter, 48 inch focal length off-axis paraboloidal mirror and is brought to a focus forming a primary image in a plane which intersects the plane of the preslit, a small, vertical aluminum stripe deposited on the surface of a flat glass plate. Light striking the aluminum stripe is reflected into the quartz condensing lens which forms a secondary image on the slit of the spectrograph. The remainder of the light from the primary image passes through the transparent portion of the preslit plate and is imaged on the film or view finder in a camera. The image in the view-finder is used to boresight the telespectrograph, while the image on

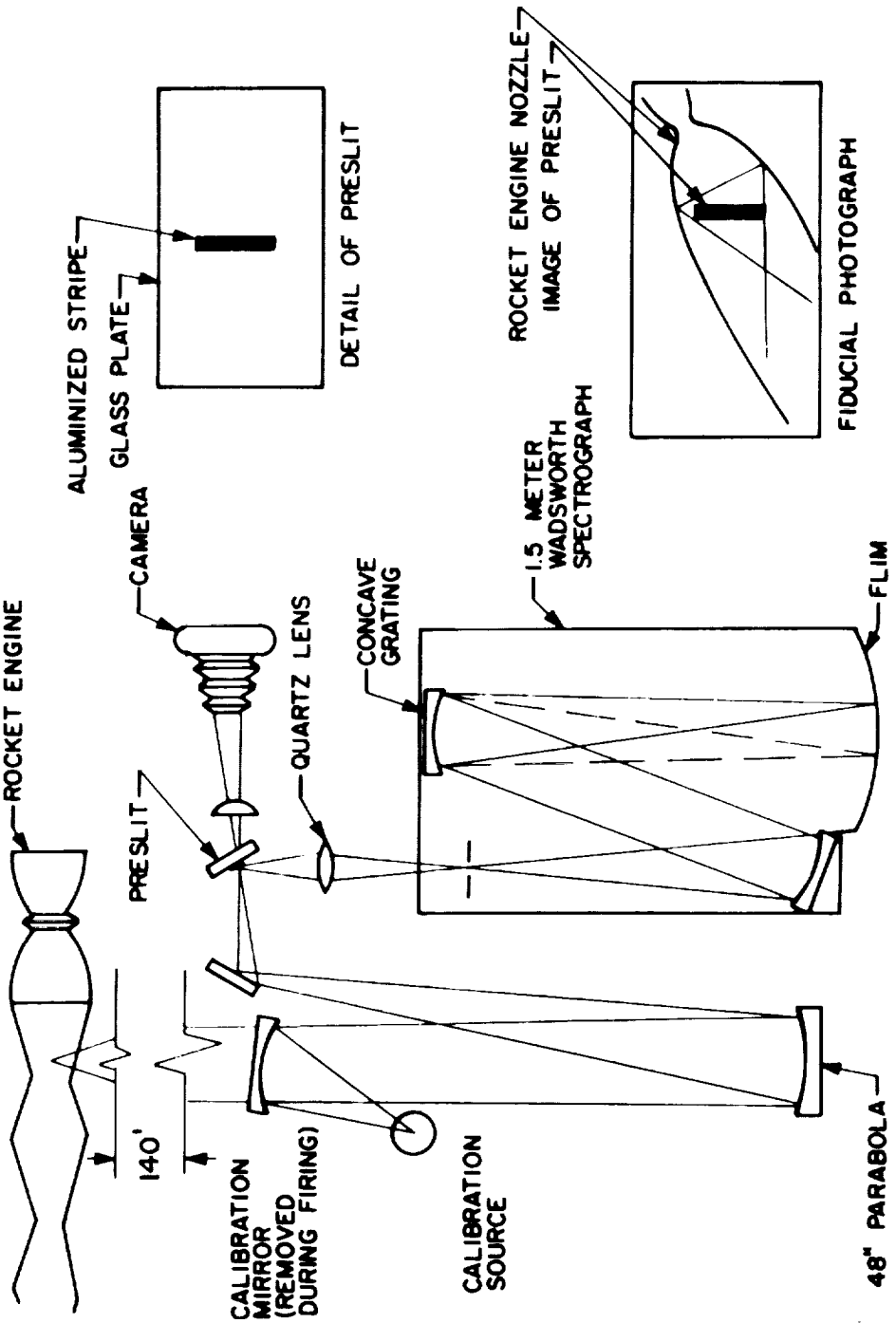


Figure 54. Optical Schematic of Telespectrograph

the film produces a fiducial photograph. A noteworthy feature of the entrance optics is that light from only a small, well-defined portion of the plume enters the spectrograph via the preslit and the slit, while the optical arrangement allows light from the larger portion of the plume to enter the fiducial camera, where an image of the plume and the superimposed shadow of the preslit is recorded. The shadow of the preslit in the fiducial photograph thus locates the region of the plume from which the radiation enters the spectrograph. Figure 55 shows a fiducial photograph taken before a firing with the model F-1 engine.

The spectrograph is a 1.5 meter Wadsworth mounting grating instrument. It can record spectra from 2500 to 8000 Å on a horizontal 20 inch length of 35mm film. The film has a useful width of about 25mm for recording spectra, and the film holder is arranged to move vertically so that several spectra can be recorded on one film.

Wavelength and Intensity Calibration

Wavelength calibration is accomplished by recording the spectrum of a mercury arc lamp at three different positions on each film strip. Several prominent lines of this mercury spectrum (in both first and second orders) are used as wavelength references.

In addition to the three mercury wavelength calibration spectra and, of course, the spectrum of the engine firing, five spectra of an intensity calibration source are recorded on each film strip. The exposure time of these five intensity calibrations is set by an automatic timing mechanism to equal the exposure time of the engine firing spectra. The

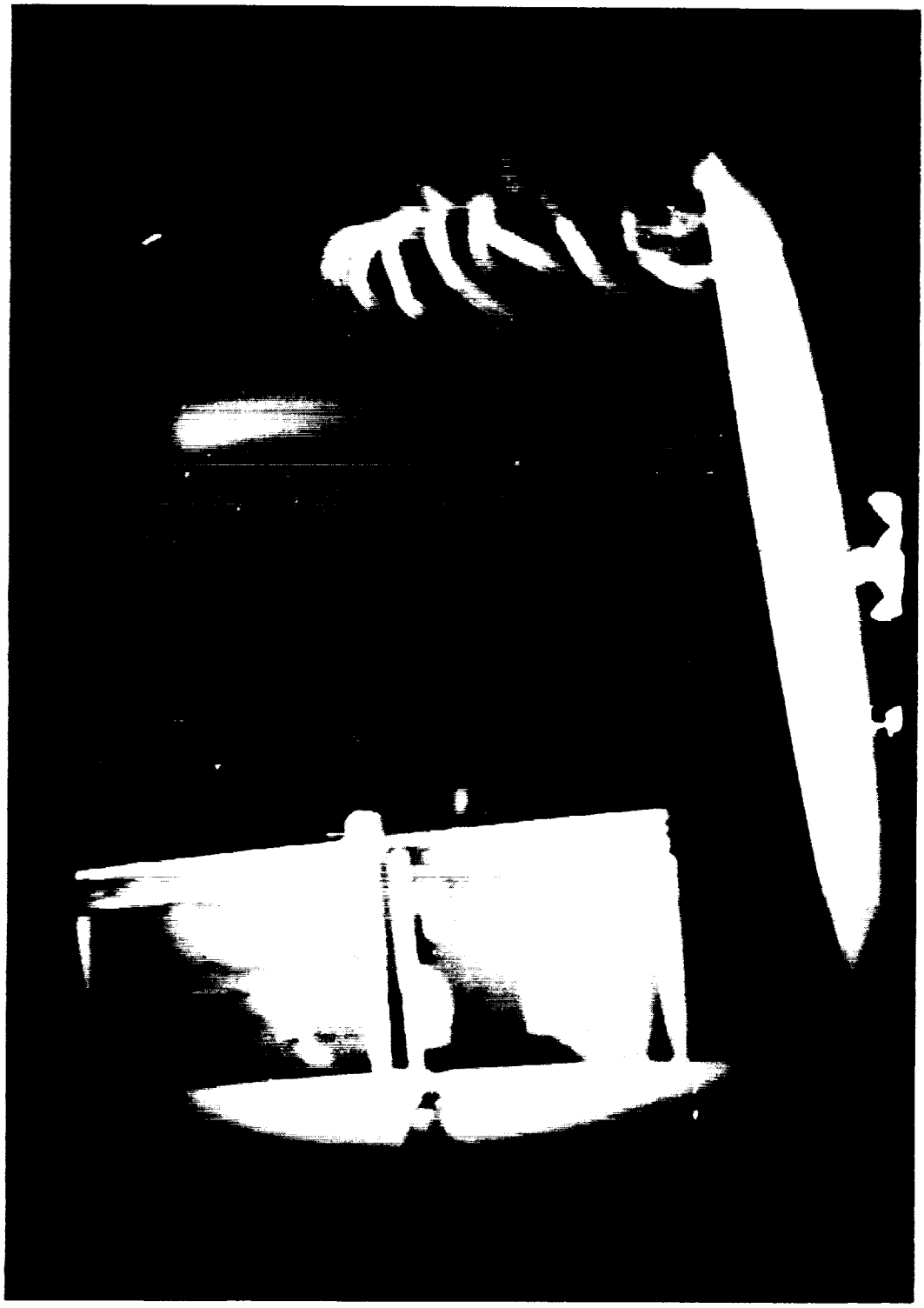

Figure 55. Fiducial Photograph Before Model F-1 Firing

intensity calibration source is a tungsten ribbon filament lamp with a quartz window. This lamp is calibrated against an optical pyrometer, which, in turn, is calibrated against an NBS certified lamp. The settings of the tungsten standard lamp are chosen so that for any given spectral region of interest the resulting radiances span that of the rocket exhaust.

Data Reduction

A Jarrell-Ash Model 2310 recording microdensitometer with a Bristol strip chart recorder is used to produce densitometric traces from the completed spectrograms. Every film is run through the densitometer six times, this producing one trace of the engine exhaust spectrum and one trace of each of the five tungsten lamp intensity calibrations. On each of these traces, the positions of the mercury wavelength calibration lines are indicated. The densitometer trace is effectively then a graph of per cent transmission of the film vs wavelength.

The essential step in the actual quantitative reduction of the data is the construction of the characteristic response curve of the film at each wavelength selected. This is necessary because the transmission of the film is not a linear function of the amount of radiation it receives and, also, because the response curve varies with the wavelength of the incident radiation. The construction of a response curve is accomplished as follows: the transmission, T read from the 0 - 100% scale on the densitometer trace is converted to photographic density, D, according to the relationship

$$D = \log_{10} \frac{1}{T}$$

This is done for all five traces of the tungsten standard lamp settings at some fixed value of wavelength. The corresponding spectral radiances of the tungsten lamps are computed from the relationship using the known information about the tungsten temperature and spectral emissivity. The value of the tungsten filament radiance at the given wavelength, corrected by a suitable factor for various transmission and reflection losses, is denoted by the symbol E. When the five values of D are plotted against the common logarithms of the corresponding values of E, the result is the characteristics curve of the film at the selected wavelength. An example of such a curve is shown in Fig. 56. Characteristic curves all display this general sigmoid shape.

Once the characteristic curve is obtained for a particular value of wavelength, the density, $D_f$, of the engine exhaust spectrum at that wavelength is calculated from the plume spectrum densitometer trace. The radiance of the plume is then obtained from the value of $\log_{10} E$ which corresponds to the intersection of the characteristic curve with the value of $D_f$ (see Fig. 56). In practice, much of the computation, including curve-fitting and interpolation, can be performed by an electronic computer.

## Ultraviolet Spectra

Figure 57 presents typical spectrographic data from a firing of a model F-1 engine burning LOX/RP-1 propellants. Figure 55 is a fiducial photograph taken before the run. Figure 58 is a fiducial photograph taken during the run indicating observed area of the exhaust. In each of the fiducial photographs the nozzle exit of the motor can be seen

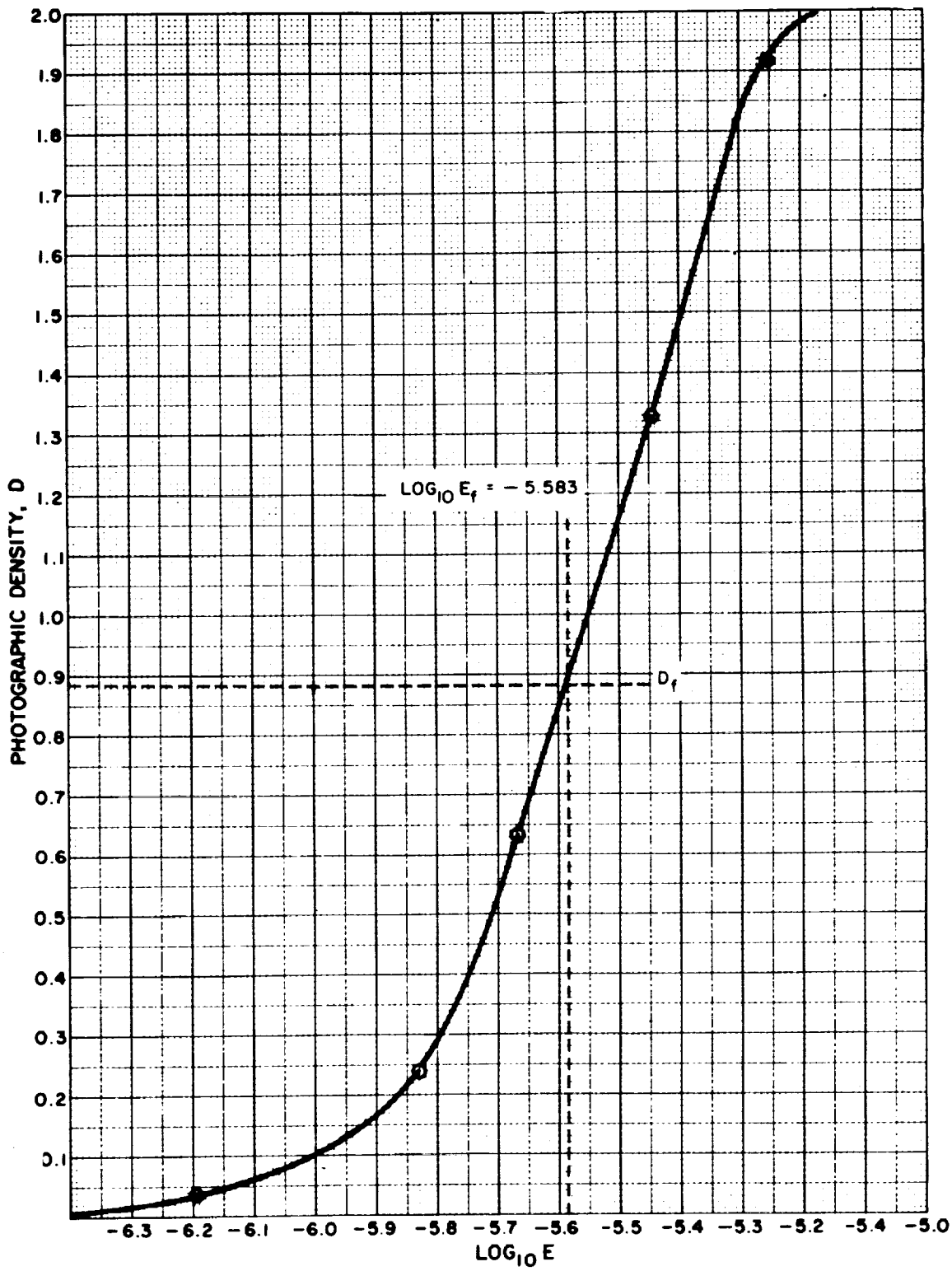


Figure 56. Film Responsivity Curve

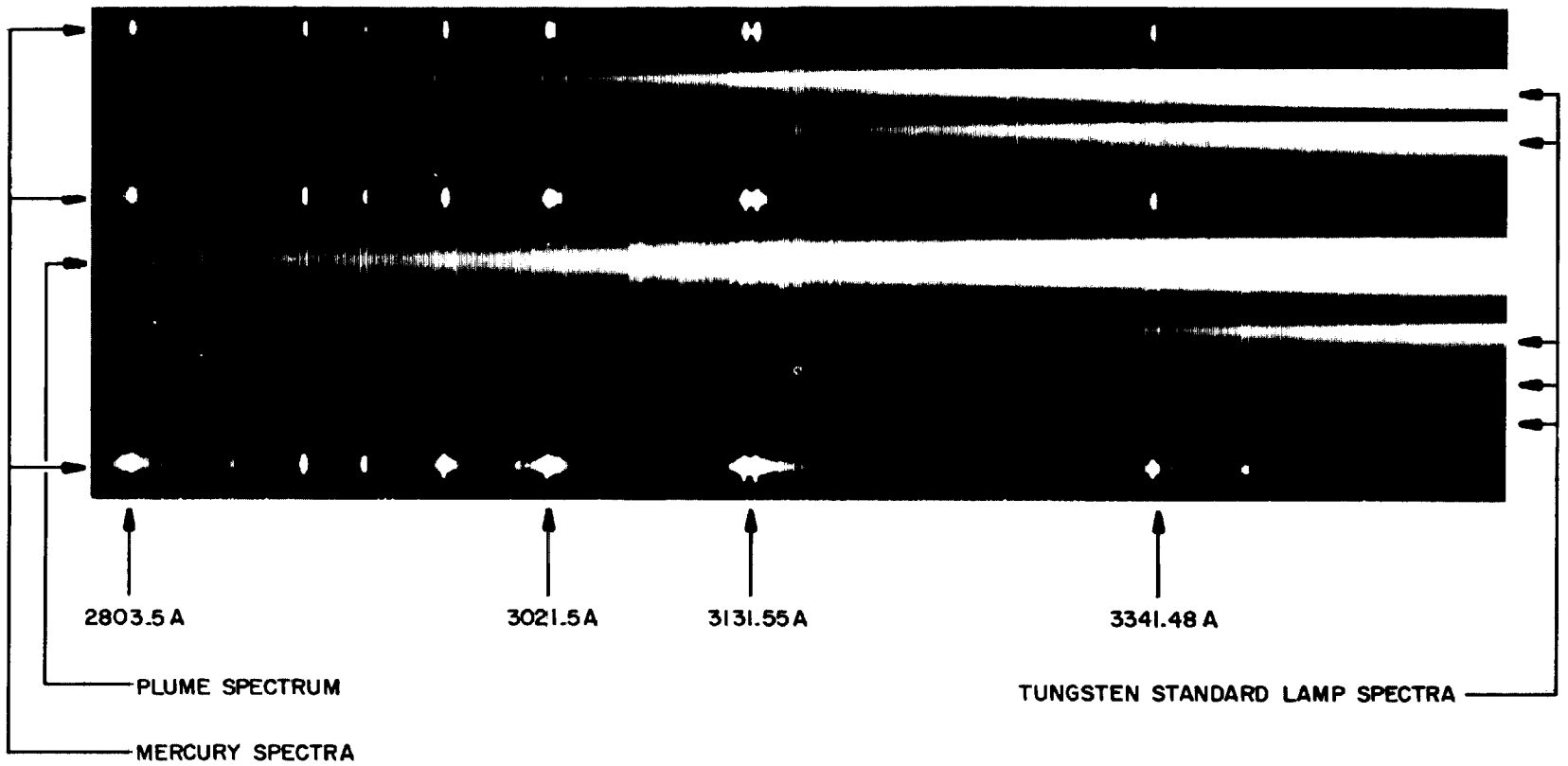


Figure 57. Ultraviolet Spectrogram of Model F-1 Exhaust Radiation

Figure 58. Fiducial Photograph During Model F-1 Firing

approximately one quarter inch to the left of the preslit shadow.

The plume spectrum, the five intensity calibration lamp spectra, and the mercury wavelength calibration spectra are indicated in Figure 57. The wavelengths of some of mercury lines are also given. The complex band structure in the plume spectrum is due to the OH radiation. The most prominent bands are the 1,0 band at 2811 Å, and the 0,0 band at 3064 Å. The 0,0 band is the strongest band in the OH ultraviolet spectrum. The OH band structure is superimposed upon the continuum radiation due to the incandescent carbon particles. Toward longer wavelengths the carbon continuum increases in intensity, masking the weaker OH radiation.

## UTILIZATION OF THE INSTRUMENTATION SYSTEM

The instrumentation system described in the preceding sections will be used primarily to investigate the radiative characteristics of the model F-1 motor exhaust.

In order to assess the effects of various motor operating parameters on the radiative properties of the exhaust, the model F-1 motor is planned to be operated at a variety of parameter settings. The variations in these operating parameters include the following ranges:

L*, 25 and 50 inches

$P_c$, 750 to 1100 psia

M.R, 1 to 3

Prior to an ordered permutation of these operating parameters, however, the entire instrumentation system will be used to obtain representative data, with the model motor operated under conditions which most nearly simulate those of the actual F-1 operation. The operating parameters chosen for this initial investigation are L* = 50 inches, $P_c$ = 976 psia, and M.R. = 2.27. With the motor operating at these settings, infrared (zone radiometry) measurements will be performed on the nozzle exit region of the exhaust and at other selected regions downstream. This will be accomplished by moving the model motor backwards (in an upstream direction) relative to the stationary spectrometer tunnel and greybody. The ultraviolet telespectrograph will monitor the nozzle exit region of the exhaust, and, when the motor is repositioned, will monitor other regions as far downstream as 3 exit diameters. Similarly, the ultraviolet photographic pyrometer will continue to view the major and significant length of the exhaust plume. The sampling probe will be positioned at several radial and axial stations within the exhaust plume.

In this way, information will be acquired on the history and distribution of the exhaust plume carbon particles, for the fixed set of model motor operating parameters.

In addition to the use of the entire instrumentation system at the Rocketdyne Plume Studies Laboratory, a second plume sampling system will be fabricated and used in attempts to sample the exhaust of an F-1 engine during static test at Edwards Rocket Base. If possible, samples of the F-1 exhaust will be extracted from the exhaust core and from the sheath of turbine exhaust which surrounds the core in the region occupying the first several feet downstream of the nozzle exit.

The radiometric and sampling systems constitute a powerful tool for acquiring data on a variety of rocket exhaust configurations which can be accomodated at the Rocketdyne Plume Studies Laboratory. An example of this is a multiple motor configuration, arranged so that the plume impingement region can be controlled and varied, observed with the radiometric apparatus, and appropriately sampled for analysis of radiative species.

Further complexities in rocket exhaust radiation processes can be conveniently and economically studied by the unique flexibility and versatility of this system.

## REFERENCES


1. DeBell, A. G. and B. P. Levin: "Ultraviolet and Infrared Spectral Radiance of Rocket Exhaust Plumes," Proc. of AMRAC, Vol. 5, Part 1, November, 1961, SECRET. Also Rocketdyne, Research Report No. RR 61-30, November, 1961, SECRET.
2. DeBell, A. G. and E. W. Speiser: "Infrared Spectral Radiance of Large Liquid Propellant Rocket Engine Exhaust Plumes," Rocketdyne, Report No. R-2019, on Contract No. AF19(604)-3499, Air Force Cambridge Research Center Report No. AFCRC-TR-60-226, April 1960, SECRET.
3. DeBell, A. G., F. S. Simmons, and B. P. Levin: "Spectral Radiances and Emissivities of Rocket Exhaust Plumes," Rocketdyne, Report No. R-3216, on Contract No. AF19(604)-5701, December 1961, SECRET.
4. Herget, W. F., E. Suarez-Alfonso and B. P. Levin: "Infrared Radiances and Spectral Absorption Coefficients of Rocket Exhausts at Simulated Altitudes." Proc. of the Infrared Information Symposia, Vol. 9, No. 4, Jan. 1965, also Rocketdyne Report No. R-5218 on Contract AF04(695)-48, SECRET.
5. Nestor, O. H. and H. N. Olsen: SIAM Review 2, 200 (1960).
6. Gooderum, P. B., and G. P. Wood: NACA Technical Note 2173 (August 1950).
7. Freeman, M. P. and S. Katz: JOSA 50, 826 (1960).
8. Tables for the Spectral Radiant Intensity of a Blackbody, (Rocketdyne, Canoga Park, Calif., 1959) Report No. 59-32.
9. Wilkins, R. L. and J. D. Weiher: "Propellant Performance Manual", Rocketdyne Report R-669, 1 February 1959.
10. Tempelmeyer, K. E. and G. H. Sheraden: "Compressible Flow Tables for Gases with Specific Heat Ratios from 1.10 to 1.28", AEDC-TN-58-9, Arnold Engineering Development Center, USAF, March 1958 (Also available as ASTIA Document AD-152 041).

11. Hill, K. W.: "Analysis of the F-1 Nozzle Contour by the Method of Characteristic," North American Aviation, Inc. Internal Letter LAP 63-805, 16 Dec. 1963.
12. Personal communication from H. L. Burge, Dept. 991-361, Rocketdyne.
13. Personal communication from E. Talmor, Dept. 991-361, Rocketdyne.
14. Dewey, C. F., Jr.: "A Correlation of Convective Heat Transfer and Recovery Temperature Data for Cylinders in Compressible Flow," Int. J. Heat and Mass Transfer, 8, 245-252, Feb. 1965.
15. Svekla, R. A.: "Estimated Viscosities and Thermal Conductivities of Gases at High Temperatures", NASA TR R-132, 1962.
16. Hines, W. S.: "Experimental Evaluation of the Limitations of the Commonly Used Connection Correlations for Prediction of Heat Transfer to Liquids at Very High Heat Fluxes and Flow Rates," Paper presented at A.I.Ch.E. Meeting in Los Angeles, Calif., Feb. 1962.
17. Shapiro, A. H.: The Dynamics and Thermodynamics of Compressible Fluid Flow, The Ronald Press Co., N.Y., 1953, Vol. 2, p. 886.
18. Ambrosio, A. and A. Wortman: "Stagnation-Point Shock-Detachment Distance for Flow Around Spheres and Cylinders," ARS Journal, Vol. 32, No. 2, Feb. 1962.
19. Katekaru, J.: "Analysis of Products in Sample Chamber," North American Aviation Internal Letter AC-991-65-16, 28 July 1965.
20. Sloan, R. D. and W. E. Gardner: "The Electron Microscopic and X-Ray Diffraction Studies of Several Specimens of Rocket Exhaust Soot," Sloan Research Industries, Inc. Report No. 567270, 27 July 1965.
21. Dieke, G. H. and H. M. Grosswhite: "The Ultra Violet Bands of OH, Fundamental Data," The Johns Hopkins University, Bumblebee Report No. 87, November 1948.

22. Levin, B. P. and A. G. DeBell: "Ultraviolet Spectral Radiance of Large Liquid Propellant Rocket Engine Exhaust Plumes," Rocketdyne Report No. R-3514, on Contract No. AF33(616)-8026, Air Force Aeronautical Systems Division Report No. ASD-TR-62-547, March 1962, SECRET.

23. Haas, G. and J. E. Waylonis: J. Opt. Soc. Am., Vol. 51, 1961, 719-722.